FINAL REPORT

BRIDGE SCOUR IN BED MATERIALS OTHER THAN COHESIONLESS SEDIMENTS

WPI No. 0510817
STATE JOB No. 99700-3578-119
CONTRACT No. BB-276
UPN No. 97050891
ACCOUNT No. 4511 345 12
CONTRACT PERIOD 9/8/97 – 6/30/00

PRINCIPAL RESEARCHER

D. MAX SHEPPARD
COASTAL AND OCEANAGRAPHIC ENGINEERING DEPARTMENT
UNIVERSITY OF FLORIDA
GAINESVILLE, FLORIDA

June 2000

TABLE OF CONTENTS

LIST OF FIGURES

1. INTRODUCTION

1.1 Problem Statement

The soil at many bridge sites in the state of Florida is composed of materials other than cohesionless sediments (i.e. other than sand, loose shell, etc.). This includes cohesive materials (such as muds and clays), combinations of cohesive and cohesionless sediments, and harder materials such as limestone and coquina. The erosion characteristics of these materials are quite different from those of cohesionless sediments and yet (due to our lack of understanding of their erosion characteristics) they are treated as cohesionless sediments in current design scour prediction equations in HEC-18 (1993). Since the "erodibility" of these sediments can vary widely, the present approach could be overly conservative in some cases while for other cases scour depths could be under predicted. There is a clear need to improve our ability to predict design local and contraction scour depths in these types of materials.

1.2 Objective

The long-term objective of the work in this study is to provide a means of predicting aggradation and degradation, contraction, and local (structure-induced) sediment scour at bridge sites for the range of bed materials encountered in Florida. It is envisioned that either measurements of the bed material properties at the site or a laboratory analysis of bed material samples from the site would provide the necessary information for predicting the rates at which the material would erode as a function of flow conditions. Then, knowing the predicted design flow conditions (water velocities, depths, etc.) at the site, design scour depths can be estimated. As stated above, the bed material to be investigated includes cohesive sediments (and mixtures of cohesive and cohesionless sediments), and different types of limestone and coquina. The objectives of the present study can be summarized as follows:

1 Construct the laboratory apparatus designed in an earlier study (Part 1 of this study). Due to the wide range of materials being considered in this investigation it will be necessary to design and construct two test facilities. The design of these facilities will be one of the products of the work performed in Part 1 of this study. The instrumentation needed to both, control the apparatus and to measure the rates of erosion will be constructed, assembled and installed.

2 Calibrate and test the apparatus. The facility will be tested and calibrated using materials with "known" erosion rates and modifications made to the apparatus and/or instrumentation as needed.

3 Using samples of standard cohesive sediments, measure rheological properties and erosion rates to verify correlations reported in the literature.

4 Obtain field samples of coquina and limestone. Measure rheological properties and correlate with erosion rate characteristics for these materials. Measure

erosion rates of these samples using either the apparatus used for cohesive sediments or one designed specifically for these harder (composite) materials.

1.3 Scope and Purpose

The study was divided into two parts (Parts 1 and 2). The scope of Part 2 consisted of the following tasks:

- Construction of rotating cylinder test apparatus
- Calibration and testing of rotating cylinder test apparatus
- Construction of prototype enclosed flume device
- Measurement of rheological properties and erosion rates of standard cohesive sediments
- Measurement of rheological properties and erosion rates of coquina and limestone
- Proposed approach to classifying rock materials and erosion rates in Florida

This report summarizes those activities that were completed during Part 2. Section 2 describes the details for the construction of the rotating cylinder test apparatus. Section 3 describes the calibration and testing of the apparatus. Section 4 presents the details for the prototype enclosed flume device. Section 5 describes the testing of standard cohesive sediment samples and measurement of their rheological properties and corresponding erosion rates. Section 6 presents the data for the testing of the coquina and limestone samples. Section 7 of this report details an approach to classifying rock materials and erosion rates in Florida as well as an example.

2. CONSTRUCTION OF ROTATING CYLINDER TEST APPARATUS

The preliminary design of the rotating erosion device from part 1of this study was evaluated the construction details are given below:

2.1 Design Layout

The design and details of the rotating erosion test device are given in Sections 3.1 – 3.6 of Appendix A. Figure 1 shows the basic layout of the design. A photograph of the testing device is shown in Figure 2.

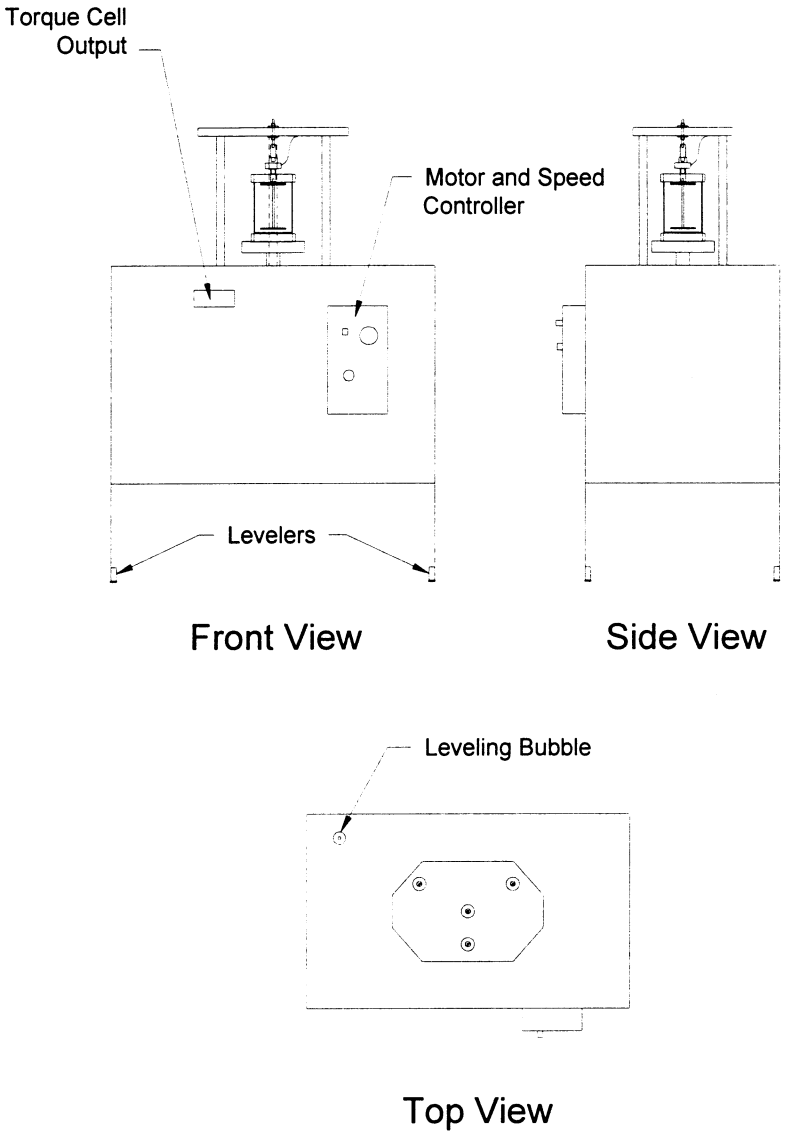

Figure 1. Design Schematic of Rotating Cylinder Test Apparatus

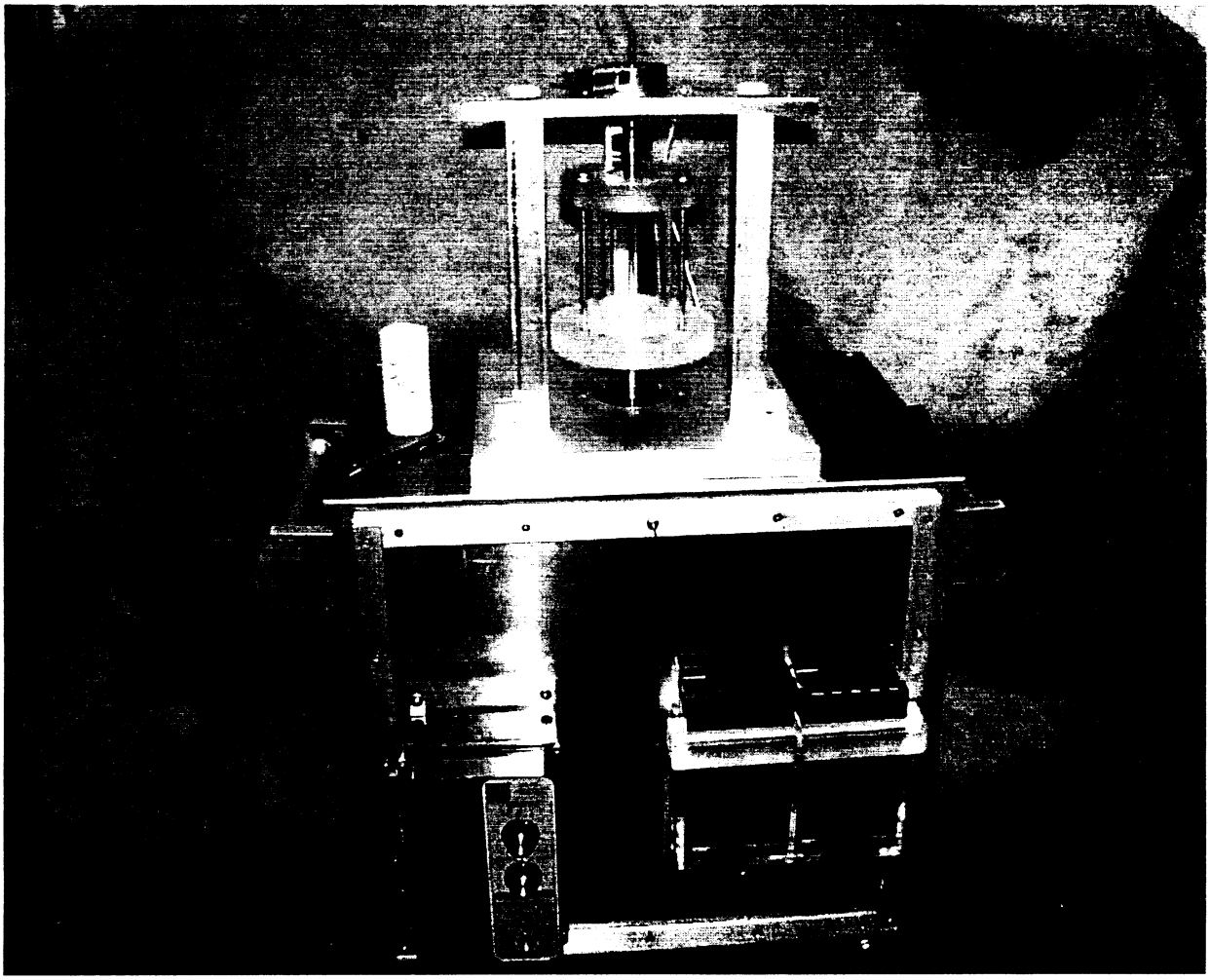

Figure 2. Photograph of the rotating rate of erosion apparatus.

3. CALIBRATION AND TESTING OF ROTATING CYLINDER TEST APPARATUS

The following section describes calibration and testing of the rotating cylinder erosion apparatus.

3.1 Calibration

The details of the calibration are given in Section 3.6.2 of Appendix A and Section 3 of Appendix B. The table below presents the data from a standard calibration test. Figure 3 shows the plot of the measured versus calculated torques.

Mass (g)	Torque-Measured (N*mm)	Torque-Calculated (N*mm)
0	0	0.000
10	11.6	11.527
15	17.6	17.290
20	23.6	23.054
25	29.7	28.817
30	35.5	34.580
50	58.8	57.634
20	23.6	23.054
5	5.8	5.763
2	2.3	2.305

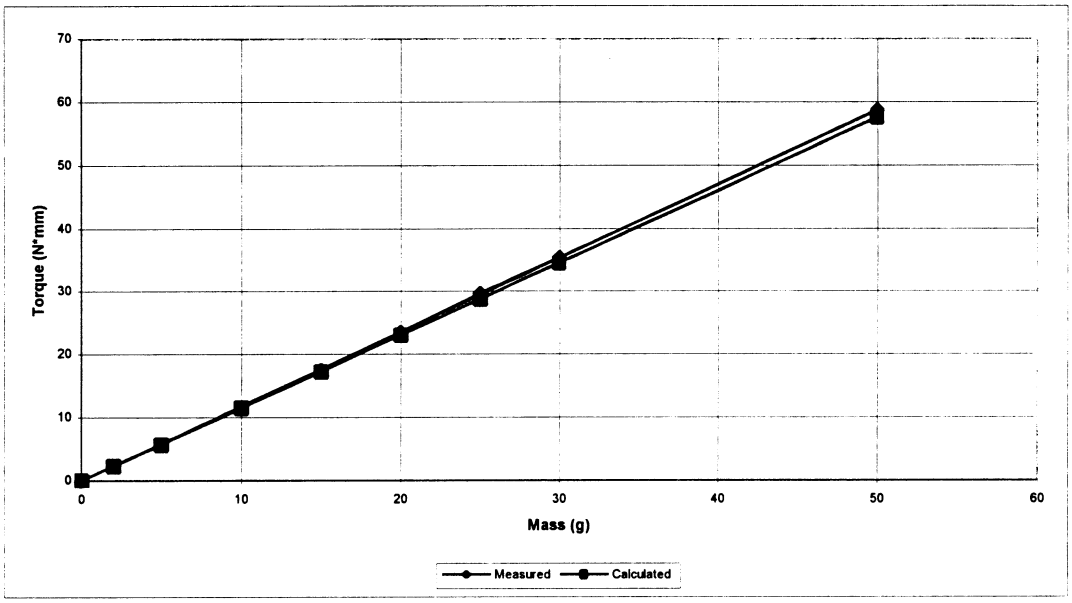

Figure 3. Anticipated and Measured Torque Values for Torque Cell Calibration

3.2 Testing

Testing of the device is given in full in Sections 3.6.3 – 3.7.3 of Appendix A and Section 4 of Appendix B.

4. CONSTRUCTION OF PROTOTYPE ENCLOSED FLUME DEVICE

This section of the report presents the design specifications for the enclosed flume device.

4.1 Design Layout

A methodology for the prediction of contraction and local scour depths has been developed. Using the background information from this methodology, the required measurements necessary for input into the model were formulated. These measurements include the erosion rate and the shear stress being applied to the rock samples. In order to use this methodology an instrumented flume device is needed to measure the rate of erosion and the bed shear stress. This device must be capable of measuring these criteria with precision and repeatability. Field conditions were modeled in order to approximate the bed shear stress that is present during a storm event. A channel geometry and velocity for the field model were assumed and the shear stress was estimated to be 2.358 lb/ft^2. The design of the hydraulic flume device began with the sizing of a channel that would create the required shear stress at a reasonable flow condition. A channel having a 2-in height and an 8-in width was chosen, shown in Figure 4, and a flow rate of approximately 1000 gpm was calculated to produce the required bed shear stress. The length of the flume was determined by the development of a boundary layer that would create a constant velocity profile over the sample as shown in Figure 5. A prototype was constructed with the above design criteria and has been tested for structural stability under the calculated test pressure and checked for leakage and flow problems.

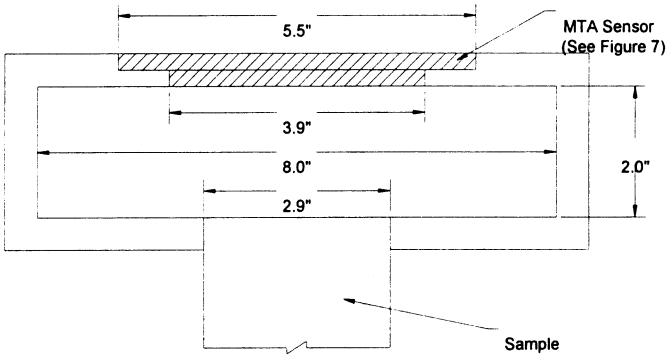

Figure 4. Flume Channel Layout

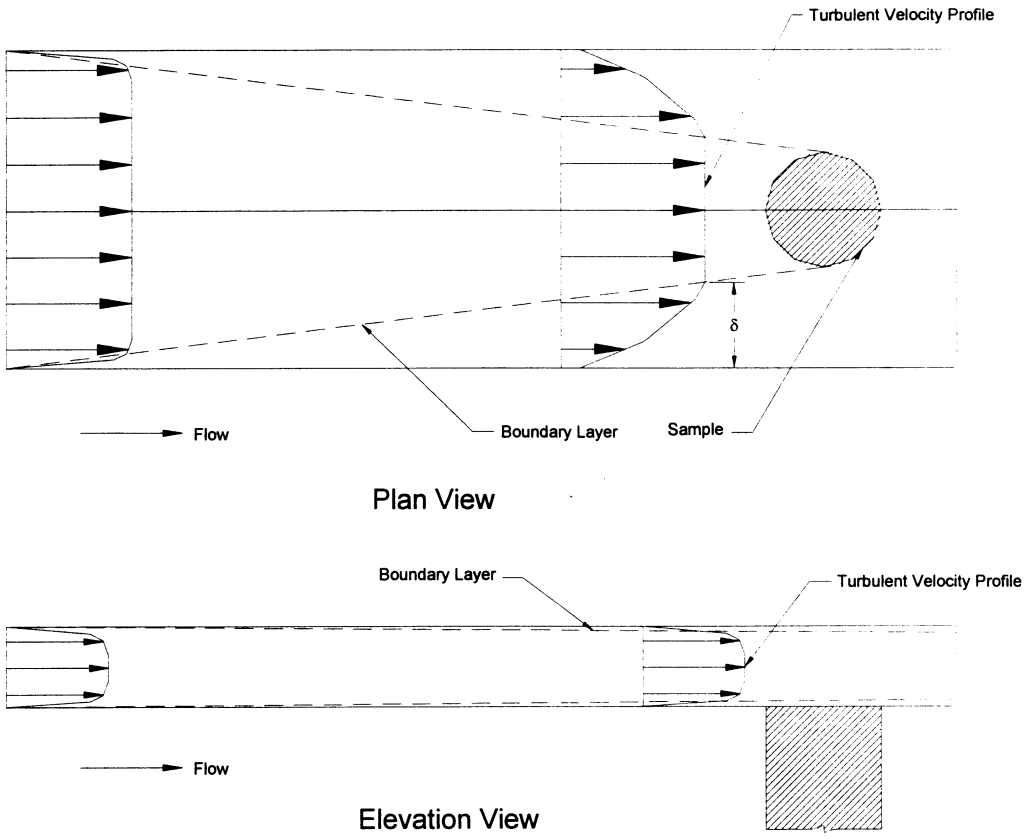

Figure 5. Boundary Layers and Velocity Profiles

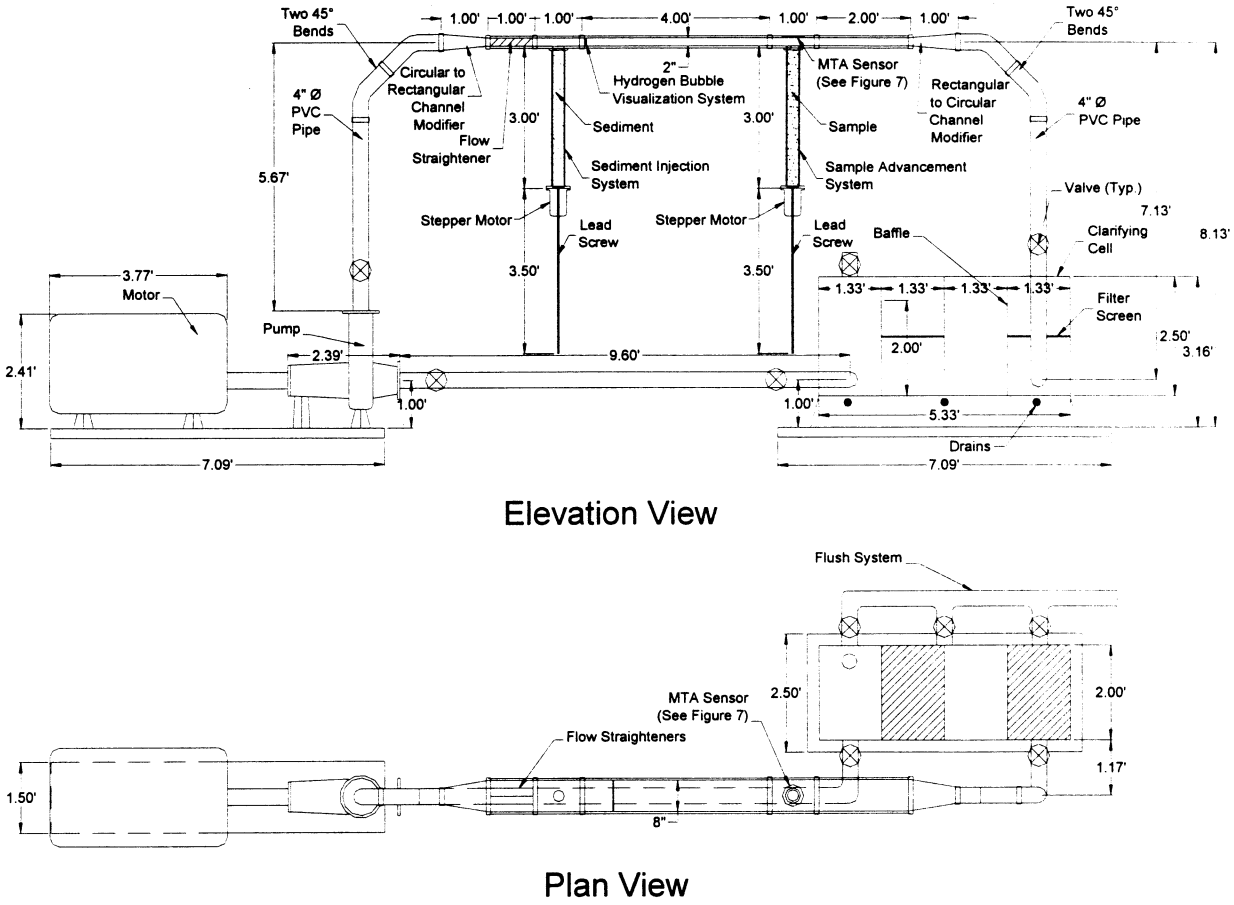

Figure 6. Flume Device Layout

A complete design was done of the modeling system shown in Figure 6. The major components of the flume are as follows:

- Data Collection System (Multiple Transducer Array (MTA) with computer controlled feedback system)
- D-824 Ingersoll Dressor Pump 6 x 4 x 11 F with 9.6-in impeller trim
- TEFC, 30 Hp, 1800 RPM Motor
- Clarifying Cell
- Sample Advancement System (LA42BLKL-6 Stepper Motor with 700 lb force piston linked to computer controlled feedback system)
- Differential Pressure Manometer (Shear Stress Sensor)
- Sediment Injection System (LA42BLKL-6 Stepper Motor with 700 lb force piston with constant rate injection)
- Hydrogen Bubble Visualization System

The conveyance system is constructed of 4-in PVC pipe. A transition between circular and rectangular is accomplished with a channel modifier. Flow straighteners (honeycomb filter) are placed at the transition region in order to reduce the creation of secondary flows. The rectangular section is fabricated out of clear PVC. The data collection system is comprised of the MTA, as shown in Figure 7, linked to a CPU with

LABVIEW software. The MTA is a short-range depth sensor that can accurately measure to 0.05 cm. The sample advancement system is comprised of a stepper motor with lead screw attached to a CPU with digital control unit and motion control card connected to LABVIEW software. The computer system allows for a control feedback loop between the MTA and the motion of the stepper motor for the advancement of the sample. The stepper motor is linked to a microstep unit which allows for a precision of 0.00005-in / step. The data collection system will record the erosion of the surface of the sample and in turn relay the required amount to advance the sample to the stepper motor controller. The differential pressure manometer will measure the pressure change from the beginning of the test section to the end. The shear stress will be calculated from this pressure drop.

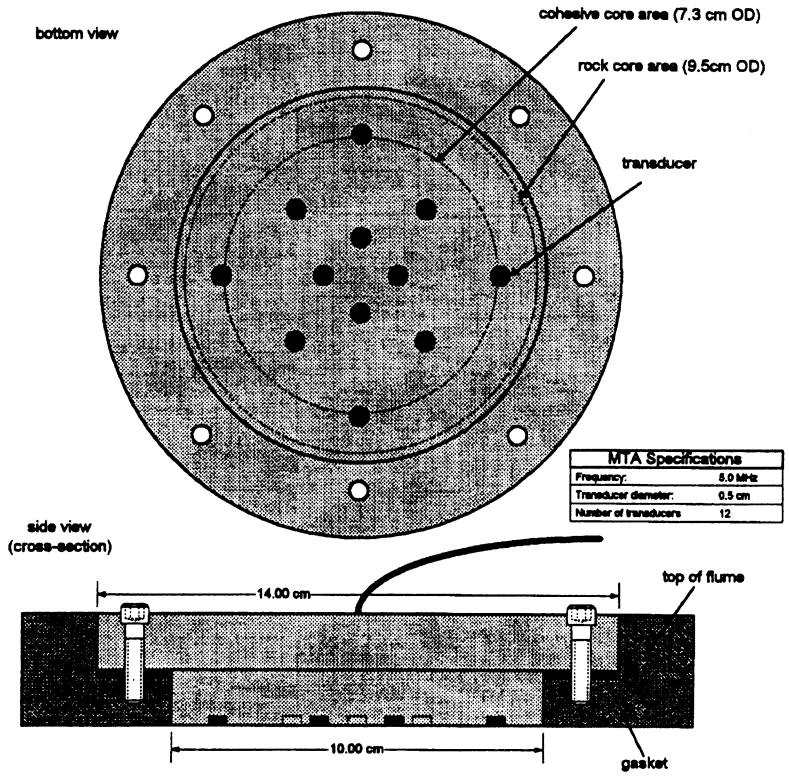

Figure 7. Multiple Transducer Array (MTA) Layout

The sediment injection system consists of a stepper motor and lead screw that is linked to a constant rate control unit. A rate is inputted into the system in order to achieve a desired concentration of sediment in the flow. The clarifying cell is comprised of a series of baffles and screens that filter out the sediment and eroded particles from the experiment. The hydrogen bubble visualization system generates a visible velocity profile by using electrical current pulsating through a wire producing a series of bubbles in the flow stream.

5. MEASUREMENT OF RHEOLOGICAL PROPERTIES AND EROSION RATES OF STANDARD COHESIVE SEDIMENTS

The following section describes the testing done on samples of standard cohesive sediment. The data outlined includes the material's properties, erosion rates, and verification of the test data to known correlations.

5.1 Rheological properties and erosion rates

Section 4 of Appendix B presents the testing of the standard cohesive samples and their respective compositions. Section 5 of Appendix B describes the results of the tests

5.2 Verification of data

The data from the tests on standard cohesive sediments was checked for accuracy and correlation with calculated models. The result of this analysis is given in Section 6 of Appendix B.

6. MEASUREMENT OF EROSION RATES FOR COQUINA AND LIMESTONE

This section describes how the field samples were obtained and a description of the procedure used to measure their properties. A correlation between sample properties and erosion rates was also investigated.

6.1 Field samples and properties

Field samples of limestone found in Florida water have been obtained from the Florida Department of Transportation's (FDOT) Materials Testing Laboratory in Gainesville, Florida. Specifically, samples have been obtained from the 17th Street Causeway Bridge in Ft. Lauderdale, Florida (District 4) and the Buckman Bridge (District 2). Preliminary tests have been performed on these samples as a possible parameter to correlate with the rates of erosion. Specifically, the tests that we performed are ASTM D 5240-92, "Testing Rock Slabs to Evaluate Soundness of Riprap by use of Sodium Sulfate or Magnesium Sulfate", and ASTM D 5313-92, "Durability Test of Rock under Wetting/Drying Conditions". Preliminary experiments were performed on two limestone samples to establish the testing procedure and required drying times. It is envisioned that the results of this standard test may correlate with results obtained from the rotating cylinder device and ultimately quantify the influence of micro-cracks on the rate of erosion.

In addition, boring logs and geotechnical testing data have been received from various FDOT Districts. A representative of the University of Florida traveled to the FDOT's District 2 Offices in Lake City, FL to review geotechnical engineering reports that contained technical data regarding the properties of rock materials located within the District. This information has been evaluated to determine the ranges of cohesive soil and rock properties for the specific types of conditions in Florida. Preliminary estimates are also being performed to evaluate the stress state surrounding bridge piles placed in rock.

Upon review of the information obtained and through discussions with faculty from the University of Florida's Geology Department, a proposed method for classifying and categorizing the rock materials in Florida has been proposed. The proposed method follows in Section 7 of this report.

6.2 Rheological properties and erosion rates

The details and results of the experimental testing done on the coquina and limestone samples are given in Section 4 of Appendix A. An example of typical test data and plots is given below. A series of tests on a dark tan sandstone sample were done using the rotating erosion device. The test sample description and testing results are detailed on the next page.

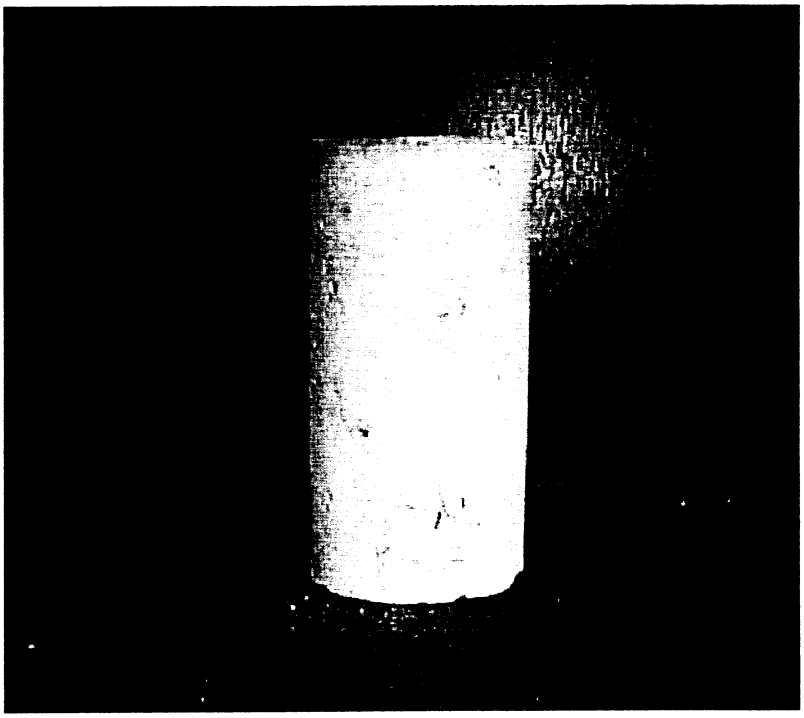

Above: Picture of Dark Tan Sandstone Sample

Sample Characteristics

Dark Tan Sandstone Sample

Dry Mass (g)	234.27
Diameter (cm)	4.62
Height (cm)	7.32
Volume (cm^3)	110.00
Density (g/cm^3)	2.13
Surface Area (cm^2)	106.24

Calculations

This section explains the calculations that were made from measurements collected during the experiments. The calculations consisted of determining the mass lost during an erosion test, the shear stress acting on the surface sample and the rate of erosion. The calculations are as follows:

1. Mass Lost (g) = Sample dry mass (g) – Sample dry mass after experiment (g)
   – mass lost from hydration (g)

2. Shear Stress (Pa) = $\dfrac{\dfrac{\text{Torque (N – mm)}}{\text{Sample Radius (mm)}}}{\text{Sample Surface Area (m}^2\text{)}}$

3. Erosion Rate (cm/min) = $\dfrac{\dfrac{\dfrac{\text{Mass Lost (g)}}{\text{Dry Density (g / cm}^3\text{)}}}{\text{Sample Surface Area (cm}^2\text{)}}}{\text{Experiment Duration (min)}}$

4. Convert to mm / hr and plot Erosion Rate (mm / hr) vs. Shear Stress (Pa)

Results

Dark Tan Sandstone Results

RPMs	Torque	τ	Duration	Mass Loss	Erosion Rate e
	(N-mm)	(Pa)	(min)	(g)	(mm/hr)
1780	1.2	4.9	4340	0.13	7.94E-05
2070	2.1	8.6	4325	0.18	1.10E-04
2230	2.6	10.6	3905	0.21	1.43E-04
2380	2.9	11.8	4365	0.23	1.40E-04

The results from the above table are plotted in Figure 8 and are compared with rate of erosion results from previous testing done on a loose-cemented sand sample in Figure 9.

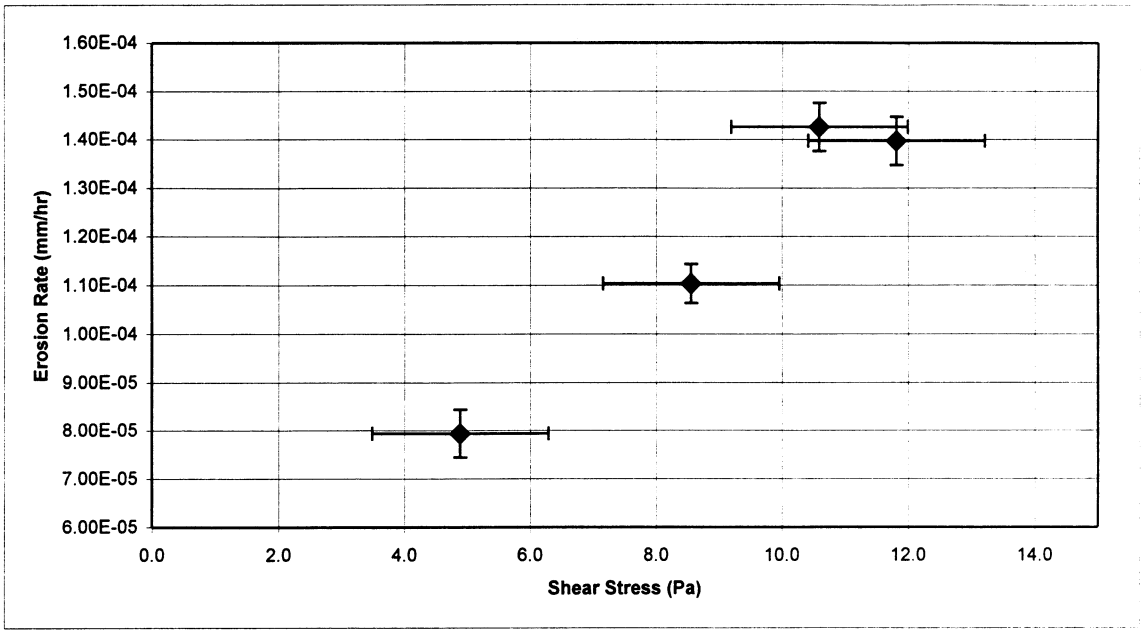

Figure 8. Erosion Rate vs. Shear Stress for Dark Tan Sandstone Sample

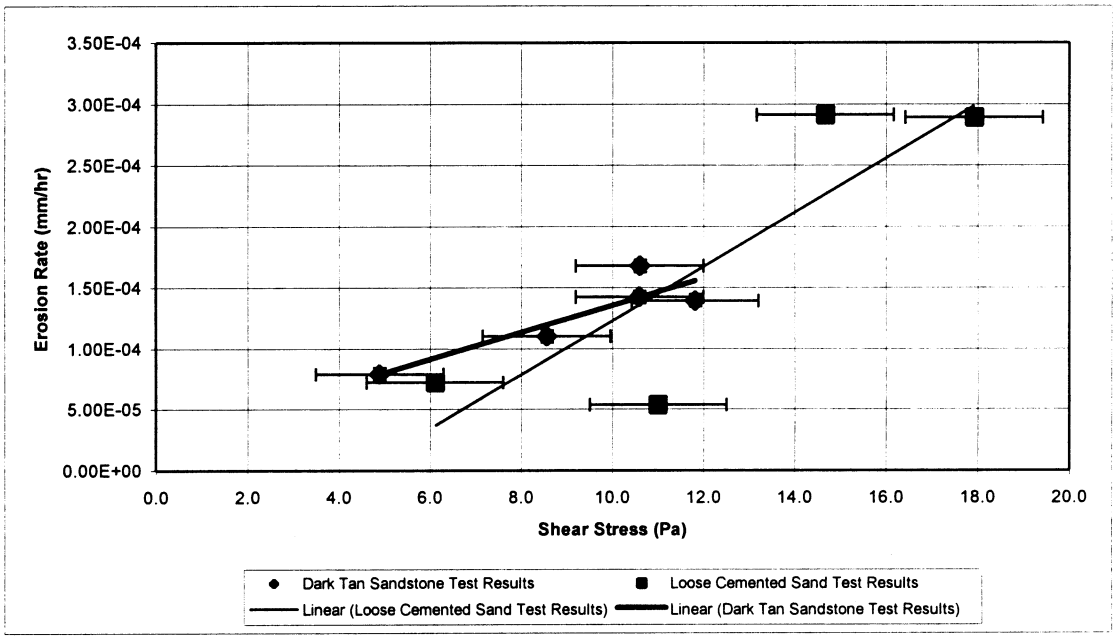

Figure 9. Erosion Rate vs. Shear Stress for Dark Tan Sandstone and Loose Cemented Sand Samples

7. PROPOSED APPROACH TO CLASSIFYING ROCK MATERIALS AND EROSION RATES IN FLORIDA

This section summarizes the proposed approach to classifying and categorizing the rates of erosion for the different types of rock materials found in coastal waters and rivers in Florida in which bridge piers are to be located. The rates of erosion for the different types of rock materials will be determined from testing equipment that is currently being constructed by the University of Florida as part of this contract. Once determined, the rates of erosion may be used to estimate the depth of contraction scour for a given flow scenario. The purpose of classifying the rock materials and their respective rates of erosion is to provide hydraulic engineers with an efficient database to estimate the erodibility of rock.

The proposed method for classifying the rock materials is described below. An example is then presented of how the proposed method would be used in practice.

7.1 Proposed Method

The goal of the proposed approach is to provide hydraulic design engineers with a system to estimate the rate of erosion for a specific type of rock identified from geotechnical borings. The first step in this approach is to identify the type of rocks that may be encountered at a proposed bridge location. Therefore, the different types of rocks that could be encountered at bridge sites must be identified and categorized. In discussion with Florida Department of Transportation (FDOT) engineers, it was discovered that a uniform system for identifying and labeling rock materials in boring logs across the state does not exist at this time. It is necessary to locate another database. Through discussions with faculty from the Geology Department and Geotechnical Engineering Department at the University of Florida, a set of maps was identified which described and summarized the geology across the state. These maps are *Physiographic Divisions* and *The Geology of Florida* developed by Dr. H.K. Brooks at the University of Florida in 1981. The Institute of Food and Agricultural Science (IFAS) publish these maps at the University of Florida. These maps divide the state into specific regions and identify the types of rocks that make up the specific region. For example, the southeastern portion of the state (from approximately Palm Beach to the Florida Keys) is identified as the Gold Coast and Florida Bay District and the types of rock materials located within the district are oolitic limestone, coquina, and coral rock. It is proposed that the districts and materials used in this map be the basis for the general identification of the different rock materials within the state. This will provide, on a general basis, a description of what type of rocks may be found in a particular location within the state.

Secondly, to further define the specific individual types of rocks found within the districts described above, it is proposed that a range of geotechnical properties for these rock materials be used. Since the types of rocks and their properties may vary within a region, the geotechnical testing data may provide a more detailed description as to the rocks characteristics. It is anticipated that the geotechnical properties that will be used are the

Uniaxial Compressive Strength, Tensile Strength, L.A. Abrasion Test, and Sulfate Soundness Test. Results from some of these tests are available from existing FDOT projects and geotechnical reports. In addition, it is anticipated that the tests will also be performed on the samples that are being tested for erosion, which is being conducted as part of this contract to evaluate if there is a correlation between the rates of erosion and geotechnical properties of the rock. At this time, the exact ranges and categories have yet to be determined.

The rates of erosion for the various rocks in Florida will then be determined from the erosion testing apparatus being constructed at the University of Florida. The ranges of erosion rates will be compiled and assigned to the corresponding rock based on its district and geotechnical engineering properties. For example, a sample of rock was sent from a bridge site in Miami, FL. This sample is from the Gold Coast and Florida Keys District. Geotechnical tests will then further categorize the rock within the district. The sample will be tested for erosion and the appropriate rate of erosion will be noted for this type of rock. It should be noted that the ranges of erosion rates database would be developed over time as more samples are collected from bridge sites and experiments are conducted.

This is the proposed classification system to relate the experimental erosion rates to the rocks found in Florida. The attached figure shows a possible district and type of rock within the district. Presented below is an example of the how this classification example may be used in practice.

7.2 Example

A bridge is to be constructed near Miami, FL. The hydraulic engineer locates the site and district (Gold Coast and Florida Keys District). Within the district, he finds that the typical type of rocks found in that area are limestone formed as oolitic carbonate shoals. Geotechnical borings are completed in the proposed location and Uniaxial Compressive Test results that the rocks are "weak" for strength purposes. For the weak limestone found in this area of the state, the erosion rates range between X and Y. The hydraulic engineer can then choose to either use the worst case result or if he feels that the value may be too conservative, he can have samples collected and test the samples to establish the actual erosion rates. A diagram with the classification table is shown on the next page.

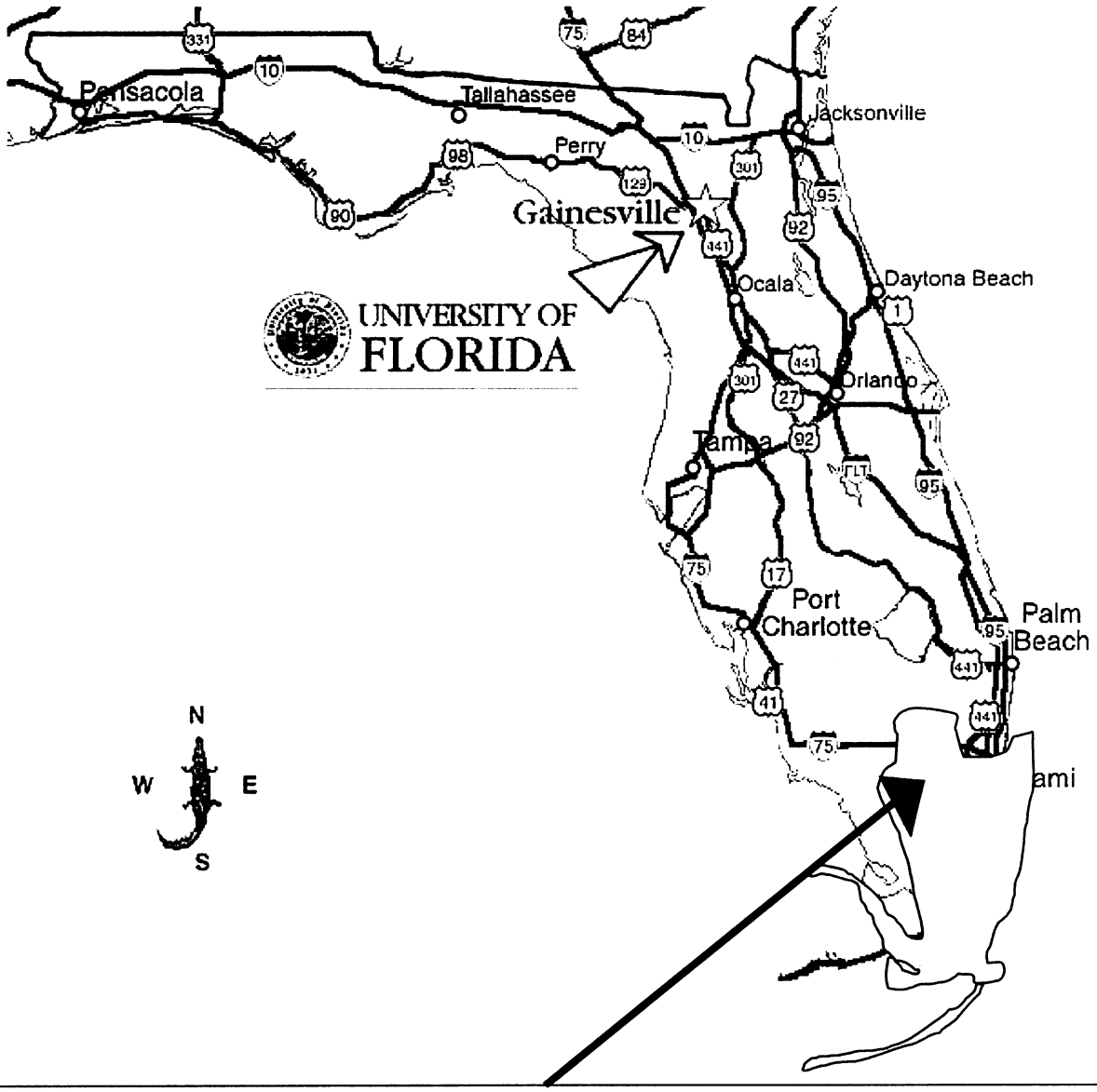

GOLD COAST and FLORIDA BAY DISTRICT

Subdivision	Rock	Qu Range	Description	Erosion Rates
2a4	Limestone (Oolitic carbonate shoals)	0.25 -1 MPa 1-5 MPa 5-25 MPa	Extremely Weak Very Weak Weak	A - B C - D X - Y

Figure 10. Example of Rock Erosion Database

A LABORATORY METHOD TO EVALUATE THE RATES OF WATER EROSION OF NATURAL ROCK MATERIALS

By

MATTHEW R. HENDERSON

A THESIS PRESENTED TO THE GRADUATE SCHOOL
OF THE UNIVERSITY OF FLORIDA IN PARTIAL FULFILLMENT
OF THE REQUIREMENTS FOR THE DEGREE OF
MASTER OF SCIENCE

UNIVERSITY OF FLORIDA

1999

APPENDIX A

ACKNOWLEDGMENTS

I would like to thank Dr. Max Sheppard, my advisor and supervisory committee chairman, for his help and support during my research and Dr. Dave Bloomquist for his help in the design and construction of the testing device. Thanks also go to the staff of the Coastal & Oceanographic Engineering Laboratory and the Civil Engineering Laboratory. Special thanks go to Danny Brown and Vernon Sparkman for their efforts in the construction of the testing device. None of this would be possible without their help.

I would also like to thank Dr. Robert Dean and Dr. Ashish Mehta for serving on my supervisory committee. My appreciation also extends to Dr. Nick Cristescu and Dr. Oana Cazacu for their assistance in helping me understand the behavior and mechanics of rocks.

I am grateful to Mr. Shawn McLemore, P.E., of the Florida Department of Transportation, for his financial support and professional interest. I am also grateful to Dr. Dave Horhota of the Florida Department of Transportation for providing us with rock samples to test. Thanks go to Dr. Rob Nairn, of Baird & Associates, and Dr. Andrew Cornett, of the Canadian Hydraulics Center, for providing me with information about the Northumberland Strait Crossing Bridge and the rock erosion experiments that they performed.

Many thanks go to my classmates and friends, especially Al, Greg, Judy, Joel, Adam, Eduardo, Jennifer, Wendy, Tom, Bill, Becky, Justin, Ed, Lisa, and Thanasis – all of whom acted as sounding boards and lent encouragement when necessary.

Finally, I would like to thank my family and especially my wife, Beth, who have always supported me in my endeavors.

TABLE OF CONTENTS

page

LIST OF TABLES

LIST OF FIGURES

LIST OF SYMBOLS

d	width of gap between rotating and fixed cylinders
$\dot{e}$	erosion rate
J_s	relative ground structure number
J_n	joint set number
K_b	particle/block size number
K_d	discontinuity or inter-particle bond strength
K_h	material's resistance to erosion
k_s	Nikuradse Roughness Length
L	unit length of channel
l	length of thin horizontal crack
M_s	mass strength number
m	bending moment in the rock above crack
N	rotational speed
P	Stream Power
P_1	pressure outside thin horizontal crack
P_2	pressure outside think horizontal crack
q_u	unconfined compressive strength
Re_{cr}	critical Reynolds number for the onset of Taylor vorticies
R_e	external radius of rotating cylinder

R_i	internal radius of fixed cylinder
S_f	slope of energy grade line
t	height of thin horizontal crack
Ta	Taylor number
$\overline{U}$	depth average velocity
$\overline{u}_*$	friction velocity
u_1	steady flow velocity outside thin horizontal crack
u_2	flow velocity inside thin horizontal crack
V_e	peripheral velocity of outer rotating cylinder
X	variable being measured
ΔX	unit error
α	ratio of external to internal radius
γ	unit weight of water
μ	dynamic viscosity
ν	kinematic viscosity
ρ	fluid density
σ_{max}	maximum axial stress
$\overline{\tau}$	average shear stress
$\overline{\tau}_0$	average shear stress on a bed

Abstract of Thesis Presented to the Graduate School
of the University of Florida in Partial Fulfillment of the
Requirements for the Degree of Master of Science

A LABORATORY METHOD TO EVALUATE THE RATES OF WATER EROSION OF NATURAL ROCK MATERIALS

By

Matthew R. Henderson

August 1999

Chairman: D. Max Sheppard
Major Department: Coastal & Oceanographic Engineering

This thesis discusses the design and testing procedures developed to evaluate the rate of water erosion of natural rock material. A laboratory testing device – the rotating cylinder erosion testing apparatus – previously used for testing rates of erosion of cohesive soils was modified and improved to accept intact rock samples. Laboratory testing procedures and methods were developed for conducting erosion experiments using this apparatus on rock samples. Preliminary experiments were performed on samples of rock collected in Florida.

The results indicate that there are potential relationships between rock erosion rates and applied bed shear stress. In general, as the shear stress applied to the sample was increased, the erosion rate increased. The relationship between the shear stress and erosion rate appears be linear or similar to the relationships previously identified in cohesive soils. Even though the results have the anticipated trend, a number of additional

tests are needed before the variability of the samples and the locus of highest values can be established. Recommendations for additional testing and further design improvements are also provided.

CHAPTER 1
INTRODUCTION

It is a common engineering practice to support bridges over water with piles or footings that rest on individual piles. This design allows for water to continuously flow underneath the bridge and reduces the hydraulic force acting on the structure. One of the most important factors in the design of the supporting piles is the depth the piles must be installed in the river or sea bed to provide adequate support capacity for the structure.

However, in many cases, the bed can be eroded due to the action of flowing water. This process is known as scour. Scour, in turn, can reduce the support capacity of the bridge piers. It is therefore imperative to have accurate and dependable design equations that engineers can use to estimate the depth to which piles must be installed.

Scour at a bridge pier can cause the bridge to fail. The most common cause of bridge failures is floods, with the resulting scouring of bridge piles and foundations being the most common cause of flood damage to bridges (Richardson and Davis, 1995, p. 2). Such bridge failures can have tragic results. On April 5, 1987, the Schoharie Creek Bridge (part of the New York State Thruway System) collapsed. Four cars, a truck, and 10 lives were lost as a result (Shepard and Frost, 1995, p. 9). The failure was attributed to the loss of support capacity of the bridge footings due to scour. More recently, on March 10, 1995, the Arroyo Pasajero Twin Bridges (part of Interstate 5) near Coalinga in southern

California collapsed due to floodwaters. This resulted in the death of 7 people (Bobb, 1995).

The damage to bridges from scour has been documented to be widespread. For example, 17 bridges were destroyed or damaged in New York and New England during the floods that occurred in 1987. In 1985, floods in Pennsylvania, Virginia, and West Virginia destroyed 73 bridges. More recently, the 1993 flood in the upper Mississippi basin caused 23 bridge failures for an estimated damage of $15 million (Richardson and Davis, 1995, p. 2). Also, flooding from the storm Alberto in Georgia caused damage due to scour to over 500 state and locally owned bridges (Richardson and Davis, 1995, p. 2). It is evident from these figures that even the non-fatal failures can give rise to excessive costs.

It is clear from the situations described above that it is imperative to have an understanding of flood–related scour, as such damage to bridges can present a danger to the public that frequently use these bridges. Since the failure of the Schoharie Creek Bridge, the Federal Highway Administration (FHWA) has taken a proactive approach to the evaluation of bridges susceptible to scour and provided guidance on designing new bridges for scour (Pagan-Ortiz, 1998, p. 2). The guidance document currently used in practice by hydraulic engineers to evaluate and design for scour conditions is the FHWA Hydraulic Engineering Circular No. 18, "Evaluating Scour at Bridges," which is known as HEC-18.

To understand the scour process, it is first important to provide explanations of scour, the different types of scour that occurs at a bridge site, and the current guidance document used by practicing hydraulic engineers to estimate the depth of scour at these

bridge sites. The definitions and explanations presented below are those that are currently used by hydraulic engineers and contained in HEC-18.

1.1 Types of Scour

The FHWA defines scour in HEC-18 as

> Erosion or removal of streambed or bank material from bridge foundations due to flowing water, usually considered as long-term bed degradation, contraction, and local scour. (Richardson and Davis, 1995, p. xxiii)

The total scour at bridge sites consists of three specific types of scour: long-term aggradation and degradation, contraction scour, and local scour. A description of these different types of scour is provided below.

1.1.1 Long-term Aggradation and Degradation

FHWA describes this process in HEC-18 as

> Aggradation and degradation of a river or tidal water body involves the long term streambed elevation changes due to natural or man-induced factors that can affect the reach of a river on which the bridge is located. (Richardson and Davis, 1995, p. 6)

Aggradation is defined as "The general and progressive buildup of the longitudinal profile of a channel bed due to sediment deposition" (Richardson and Davis, 1995, p. xiii). Degradation is defined as "A general and progressive lowering of the channel bed due to scour" (Richardson and Davis, 1995, p. xvi).

Some examples of factors that affect long-term bed elevation changes include: dams and reservoirs, changes in watershed land use, changes in downstream channel base level, diversion of water, natural lowering of the fluvial system, tidal ebb and flood, littoral drift (Richardson and Davis, 1995, p.7).

1.1.2 Contraction Scour

Contraction scour is defined in HEC-18 as "Scour in a channel or floodplain that is not localized at a pier, abutment, or other obstruction to flow" (Richardson and Davis, 1995, p. xvi).

In a channel, contraction scour results from the contraction of streamlines and usually affects all or most of the channel width (Richardson and Davis, 1995, p. 8). Contraction scour can occur when the flow area of a river or stream at flood stage is reduced, either by a natural contraction or a bridge, or when overbank flow is forced back to the channel by roadway embankments at the approaches to a bridge (Richardson and Davis, 1995, p. 8). Contraction scour is based on the continuity equation. That is, as the flow area decreases, the average velocity in the channel section increases. As a result, the bed shear stress through the contraction increases. The increase in shear stress causes an increase in sediment transport. As sediment is transported and the bed is lowered, the shear stress decreases, eventually to a magnitude where sediment is no longer transported and equilibrium is reached.

However, in coastal areas subjected to tidal flow, as the cross-sectional area increases, the discharge from the ocean may increase. If that occurs, the velocity and shear stress may not decrease. As a result, equilibrium may not be achieved. In this situation, the contraction scour may result in a continual lowering of the bed, similar to long-term bed degradation (Richardson and Davis, 1995, p. 8).

1.1.3 Local Scour

Local scour is defined in HEC-18 as "Scour in a channel or on a floodplain that is localized at a pier, abutment, or other obstruction to flow" (Richardson and Davis, 1995, p. xx).

Local scour is caused by the formation of vortices at the base of either a pier or abutment. This vortex, known as a "horseshoe vortex," causes the bed material to be removed from the base of the structure (Richardson and Davis, 1995, p.14).

HEC-18 presents methods for estimating and designing for long-term bed aggradation and degradation, contraction scour, and local scour. The methods and equations presented within the guidance document were based upon laboratory studies that were conducted with beds consisting of cohesionless sediments (sand). It has been discovered by hydraulic and geotechnical engineers, utilizing the equations in HEC-18 to design and construct bridges, that these equations provide reasonable estimates of scour depths for small structures in cohesionless sediments. However, the HEC-18 equations overpredict the scour depths for larger or complex structures and for structures located in bed materials other than the cohesionless sediments. Currently, several researchers are investigating and attempting to improve on the design equations for larger and complex structures presented in HEC-18.

The current approach used in calculating the scour depths around structures located in bed materials other than sand is to apply the equations provided in HEC-18 with the assumption that the bed materials will erode to the same depths, given sufficient time, as cohesionless sediments (Annandale et al., 1996, p. 59). The limitation of this approach is that it ignores the ability of materials such as rock to offer more resistance to scour than

sand (Annandale et al., 1996, p. 59). The sea or riverbeds at many bridge sites in the State of Florida are composed of materials other than cohesionless sediments (that is, other than sand or loose shells). This includes harder materials such as limestone and coquina. The erosion characteristics of these materials are quite different from those of cohesionless sediments. However, due to the current lack of understanding of their erosion characteristics, these rock materials are treated as cohesionless sediments in the current design scour prediction equations in HEC-18. Since the erosion of the rock materials can vary from cohesionless sediments, the present approach can be overly conservative in the prediction of scour depths. It is estimated by Florida Department of Transportation (FDOT) engineers that such overdesigns can lead to excessive costs on the order of millions of dollars for bridges. There is a clear need to improve the ability to predict design local and contraction scour depths in rock materials.

It should be noted that this problem is not limited to Florida, but applies to all states where bridges are located in erodible rock materials. For example, the Kentucky Transportation Center conducted a study that included on-site inspection of bridges with footings located on rock. An assessment was made of the validity of the FHWA guidance for assessing the scourability of piers and abutments founded on rock (Froehlich et al., 1995, p. 977). Scour hazards were assessed at 366 Kentucky bridges having at least one pier founded on rock. Analysis of the preliminary data collected during the on-site inspection found the scour hazard to be high at 8.5 percent of the bridges, moderate at 12.1 percent, and low at 79.4 percent of the structures (Froehlich et al., 1995, p. 979).

Along the same lines, on the Yellowstone River in Montana, a 50-year storm event caused a significant shift in the channel angle of attack on the Burlington Northern

Railroad Bridge piers. This resulted in severe scour at the piers and abutments. These piers were founded in a weathered shale, which is a rock material (Lewis, 1993, pp. 2255-2257).

There has been very little research performed in the area of the scour of rock materials. Chapter 2 of this thesis presents a description of rock materials found in the State of Florida and provides a summary of the previous experimental and engineering work that has been conducted on rock erosion and scour. It also presents a summary of the current state of knowledge of rock erosion as it relates to the scour process.

1.2 Purpose and Scope

1.2.1 Purpose

The scour at a bridge pier is a complex process, involving long-term aggradation and degradation, contraction scour, and local scour. Since extensive research into the rock scour process has been lacking as compared to research with cohesionless sediments, the goal of the work performed in this thesis was to develop a method for evaluating the rates of erosion of rock materials found in the State of Florida. By determining the erosion rate of a rock formation, estimates can be made about the amount of material that would be removed during the design life of a bridge. This information would be beneficial in estimating the long-term degradation and contraction scour at a bridge site located in rock in Florida. Local scour, which is the next step in the design process, in rock formations will need to be addressed in future research.

1.2.2 Scope

The scope of the research that was conducted as part of this thesis involved:

- The design and construction of a laboratory apparatus to test the erosion rate of rock materials from samples collected from bridge sites;
- Development of procedures to perform the testing;
- The measurement of erosion rates for rock samples collected at bridge sites in Florida.

Chapter 3 of this thesis presents a description of the design and construction of the rock erosion testing apparatus and describes the procedures developed for and the results of rock erosion experiments. Chapter 4 presents the results and analysis of the experimental data. Chapter 5 provides a summary of the analysis and the conclusions that were drawn from the experiments. Chapter 6 also presents recommendations for further research to be conducted in the field of rock erosion and scour.

CHAPTER 2
BACKGROUND AND LITERATURE SURVEY

This chapter presents a detailed description of the rock erosion process and a summary of the research that has been conducted in this field. It provides general descriptions of rock and the erosion process as well as the current methods used by practicing engineers to estimate scour in rock materials. It is important to note that the scope of this work does not include a detailed description of the geology of Florida or the rock formation processes. However, a brief description of the geology is included to provide some level of understanding of the rock materials that were evaluated. A detailed description of Florida's geology may be found in *The Geology of Florida* (Randazzo and Jones, 1997).

2.1 What is Rock?

Before a description of the rock erosion process can be undertaken, it is first important to provide a definition and description of rock. The definition or interpretation of rock can vary depending on the level of detail required for the application. Simply stated, rock is an assemblage of minerals (Judson et al., 1987, p. 6). A more detailed geologic definition of rock is "...any naturally occurring aggregates of minerals or mass of mineral matter, whether or not coherent, constituting an essential part of the earth's crust" (Jumikis, 1983, p. 37). However, to the civil engineer, in particular the geotechnical engineer, rock is considered to be a firm and coherent or consolidated substance that can

not be excavated by manual methods alone. The physical and strength properties of rocks are of primary concern to the engineer (Jumikis, 1983, pp. 37-38).

A simple concept of rock has been presented in Jumikis (1983):

> Rock is a granular material composed of "grains and glue." There is nothing else involved. The "glue" may be ferroginous, calcareous, argillaceous, or siliceous material which cements the grains. (Jumikis, 1983, p. 38).

Rock is often assumed to be a homogeneous and isotropic medium for design purposes. However, in actuality, most rocks are not entirely sound, they are neither homogeneous nor isotropic (Jumikis, 1983, p. 38). Rock is a heterogeneous and anisotropic material, having preferred particle and crystal orientation. In addition, rocks typically have a great number of pores and microcracks that may open, close, or even multiply when a loading is applied (Cristescu, 1989, p. 1). Rocks react differently to forces in different directions, depending on the degree on anisotropy. In summary, rock is a multiple-body system and an extremely complex material difficult to work with (Jumikis, 1983, p. 39).

2.2 How is Rock Classified?

Rocks are typically classified according to several different principles. Jumikis (1983) lists some of these classification systems:

- By origin or genesis,
- Geological or lithological classification,
- Engineering classification of intact rock on the basis of rock strength, or
- A combination of the above items.

A brief description of each of these types of classifications is provided below.

2.2.1 Origin or Genesis

Rocks can be classified based upon the physical process by which they were formed. The three broad groups in which rocks can be placed are:

- Igneous rocks,
- Sedimentary rocks, and
- Metamorphic rocks.

Igneous rocks are formed from the solidification of magma – the hot molten silicate material from within the earth's crust. Sedimentary rocks are formed from the solidification of deposited and accumulated sediments of other rocks, plant remains and animal remains that have been weathered by wind or water at the earth's surface (Jumikis, 1983, p. 45). These are the primary types of rocks that are found in Florida's surface geology. The specific types of sedimentary rocks that are found in Florida will be discussed in Section 2.3 in further detail. Metamorphic rocks are formed when either igneous, sedimentary, and even metamorphic rocks undergo a change in mineralogy or texture due to application of heat, pressure and chemical reaction (Judson et al., 1987, p. 114).

The scope of the work of this thesis deals with sedimentary rocks, as these are the rocks primarily found in the state of Florida at the depths in which bridge piers will be located.

2.2.2 Geological or Lithological Classification

Lithology is the study of the physical character of rocks, such as its mineralogical composition and texture together with a descriptive term from some accepted rock classification system (Jumikis, 1983, p. 62). Examples of a lithologic classification would be limestone or coquina. From an engineering perspective, the geologic descriptions are

not adequate for classifying rocks based on their engineering properties (such as strength). This is due to the fact that a specific type of rock, limestone, for example, could exhibit varying strength characteristics.

2.2.3 Engineering Classification of Intact Rock

Engineering classification systems are based upon the material properties of the rocks. These include geomechanical engineering properties such as uniaxial compressive strength or the Modulus of Elasticity. Standard laboratory tests and examinations can evaluate these properties. An example of an engineering classification system is the rock strength classification system adopted by the International Society of Rock Mechanics (ISRM).

2.3 Types of Rocks in Florida

As described above, the predominate type of rocks that are found in the Florida at shallow (surface) depths are sedimentary rocks. Specifically, the types of rocks are limestone, coquina, sandstone, and coral rock. A description of each of these types of rocks is presented below:

2.3.1 Types of Sedimentary Rocks

As stated above, sedimentary rock is formed from accumulations of sediment, which may consist of rock fragments of various sizes, remains or products of animals or plants, products of chemical action or of evaporation, or mixtures of these (Judson et al., 1987, p. 465). Sedimentary rocks or metamorphic rocks derived from them constitute approximately 75 percent of the rocks exposed at the surface of the earth (Judson et al., 1987, p. 90). Sedimentary rocks are generally distinguished in two groups – detrital and

chemical. Detrital sedimentary rocks are formed from accumulations of minerals and rock fragments derived either from the erosion of existing rock or from the weathering products of these rocks (Judson et al., 1987, p. 91). Chemical sedimentary rocks are produced from chemical processes (Judson et al., 1987, p. 91). However, many sedimentary rocks are combinations or mixtures of the two different groups (Judson et al., 1987, p. 91).

Sedimentary rocks may be composed of a variety of minerals. The detrital sedimentary rocks are accumulations of igneous rocks (consisting of quartz, feldspar, ferromagnesian silicates) together with precipitated mineral matter that serves to cement the grains together (Judson et al., 1987, p. 93). In addition, sedimentary rocks may contain clays, quartz, and calcite (the most common cementing material in the coarse-grained sedimentary rocks).

Sedimentary rocks are further described based on the texture and particle size of the grains. In the case of chemical sedimentary rocks, they are described further based on the origin of the sediment – inorganic or biochemical. Sandstone, which is considered a detrital sedimentary rock, is formed by the consolidation of grains of sand size between 1/16 (0.06) mm and 2 mm in diameter (Judson et al., 1987, p. 98). Sandstone is found in Florida's geology and is described in greater detail below.

Chemical sedimentary rocks that are of biological origin include limestone, coquina, and coral rock. These rocks are explained in much greater detail below. It is important to know that limestone can also be formed from inorganic processes. Table 2.1 presents a classification of sedimentary rocks.

Table 2.1. Classification of Sedimentary Rocks (Excluding Pyroclastic Rocks) (Judson et al., 1987, p.97)

Origin	Texture	Particle Size or Composition	Rock Name
Detrital	Clastic	Granule or larger	Conglomerate (round grains) or Breccia (Angular grains)
		Sand	Sandstone
		Silt	Siltstone
		Clay	Mudstone and shale
Chemical: Organic	Clastic or Nonclastic	Calcite, $CaCO_3$	Limestone
		Dolomite, $CaMg(CO_3)_2$	Dolostone
		Halite, NaCl	Salt
		Gypsum, $CaSO_4 *2H_2O$	Gypsum
Chemical: Biochemical	Clastic or Nonclastic	$CaCO_3$ shells	Limestone, chalk, coquina
		SiO_2 diatoms	Diatomite
		Plant remains	Coal

2.3.2 Limestone

Jumikis (1983) provides a general description of limestone:

Limestone is a bedded carbonate rock and consists predominately of calcium carbonate ($CaCO_3$) which has been formed by either organic (biologic) or inorganic processes. If of biologic origin, limestone is formed from accumulation of lime shells from shellfish. Limestone responds to the hydrochloric acid test, i.e., limestone effervesces in diluted HCL-acid.

> The color of limestones vary from white through varying shades of gray and black.
>
> Most limestones have a clastic texture, but crystalline textures are common. The carbonate rocks, dolomite and limestone, constitute about 22% of the sedimentary rocks exposed above sea level.
>
> Limestones vary greatly in porosity, some being very impervious, some very porous, hence, pervious. Because carbonate rocks are relatively soluble, solution cavities in limestones may be abundant. One refers here to Karst topography. In limestone areas are solution cavities and hence ready permeability should always be suspected until contrary evidence is obtained. (p.52)

Figure 2.1 shows a sample of limestone from a FDOT rock core collected at a bridge location in Fort Lauderdale, Florida. The boring log accompanying this rock core describes this sample as "Gray Limerock, Soft with Intermittent Layers of Hard Limerock."

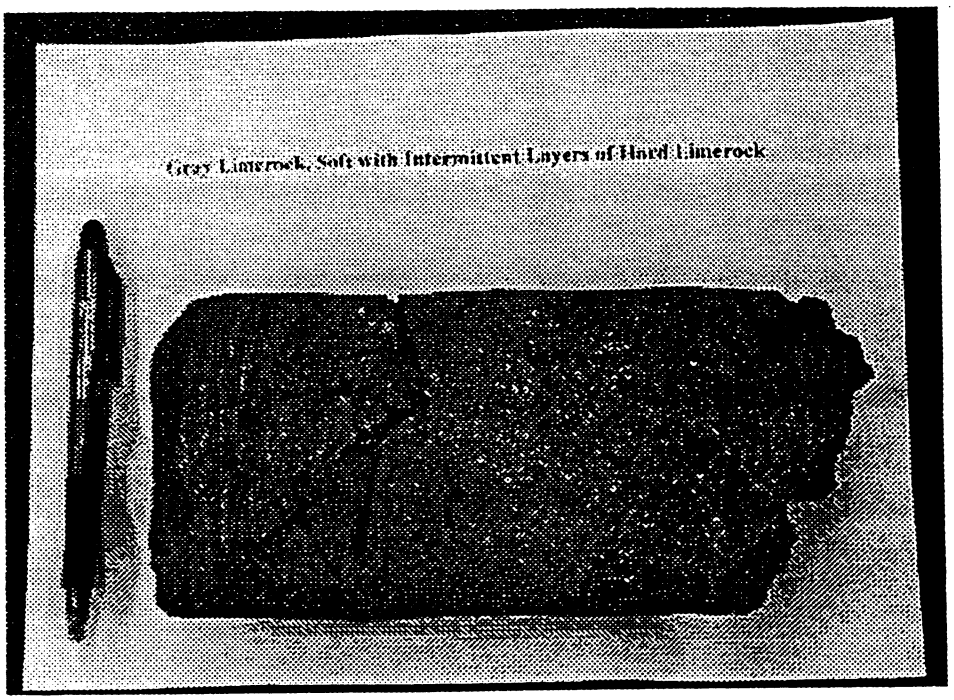

Figure 2.1. Gray Limerock, Soft with Intermittent Layers of Hard Limerock

Specific descriptions of the locations of the limestone within Florida are presented in Section 2.3.6.

2.3.3 Sandstone

Jumikis (1983) provides a general description of sandstone:

> Sandstone is a consolidated, porous and pervious rock composed mainly of sand particles – quartz grains – cemented together by clayey, siliceous, calcareous or limonitic material which fills the spaces between the grains.
>
> A sandstone which is rich in quartz is stable over a wide range of temperature and pressure. A siliceous cement usually produces the strongest sandstone.
>
> Calcareous cement may dissolve, and can be detected by means of the hydrochloric acid test upon which test the calcareous material will effervesce.
>
> The flaking off of the sandstone at free surfaces, known as "spalling" occurs in course of time. (pp. 52-53)

Figure 2.2 shows a sample of sandstone from a FDOT rock core collected at a bridge location in Fort Lauderdale, Florida. The boring log accompanying this rock core describes this sample as "Gray Sandstone."

It should be noted that in the surficial depths in Florida, sandstone is found in layers intermixed in the limestone rock formations.

2.3.4 Coquina

Coquina is a coarser type of limestone composed of organic remains and is characterized by the accumulation of many large fragments of shells (Judson et al., 1987, p. 100). The name coquina derives from the Spanish for "shellfish" or "cockle". These are biochemical rocks, as described above, since they are a direct result of the

accumulation of shells, plant fragments and other organisms. Figure 2.3 shows a sample of coquina.

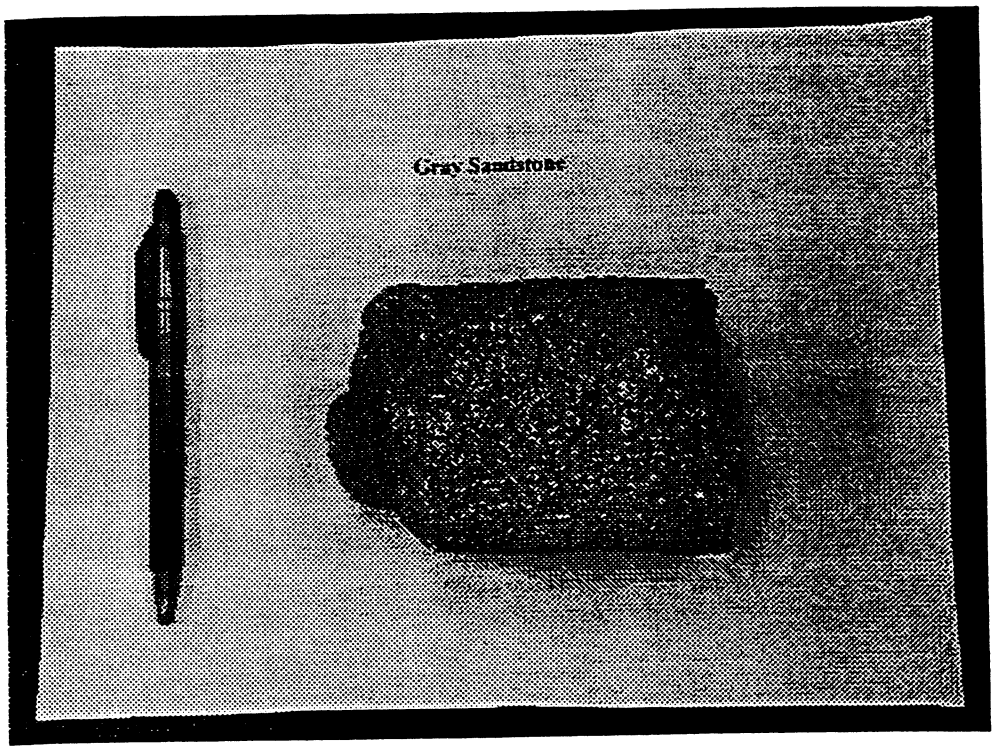

Figure 2.2. Gray Sandstone

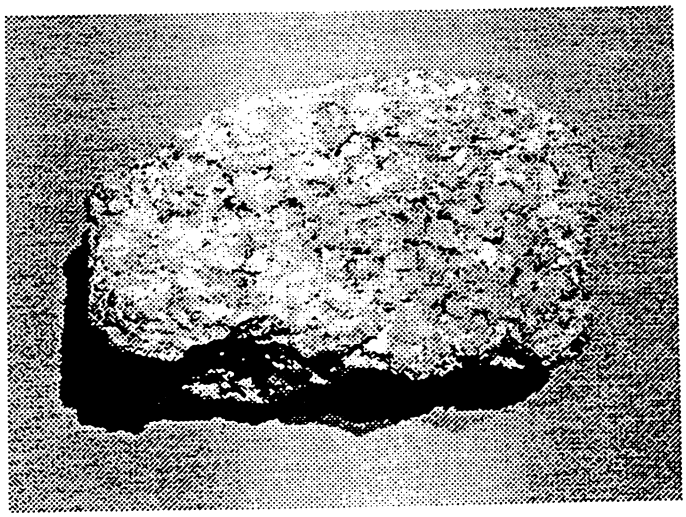

Figure 2.3. Coquina (from http://index.ecu.edu/geology/harper/sedimentary/display)

Specific descriptions of the locations of the coquina within Florida are presented in Section 2.3.6.

2.3.5 Coral Rock

Coral rock is a biochemical limestone that is created by the action of plants and animals that extract calcium carbonate from the water in which they live. The calcium carbonate may be either incorporated into the skeleton of the organisms or precipitated directly. When the organism dies, it leaves behind a quantity of calcium carbonate. Large deposits of this material may be built up over long periods of time (Judson et al., 1987, p. 100). Reefs are examples of such accumulations. In Florida, the rock formed from such accumulations is described as coral rock. Figure 2.4 shows a sample of coral rock found in Florida (the exact location is not known).

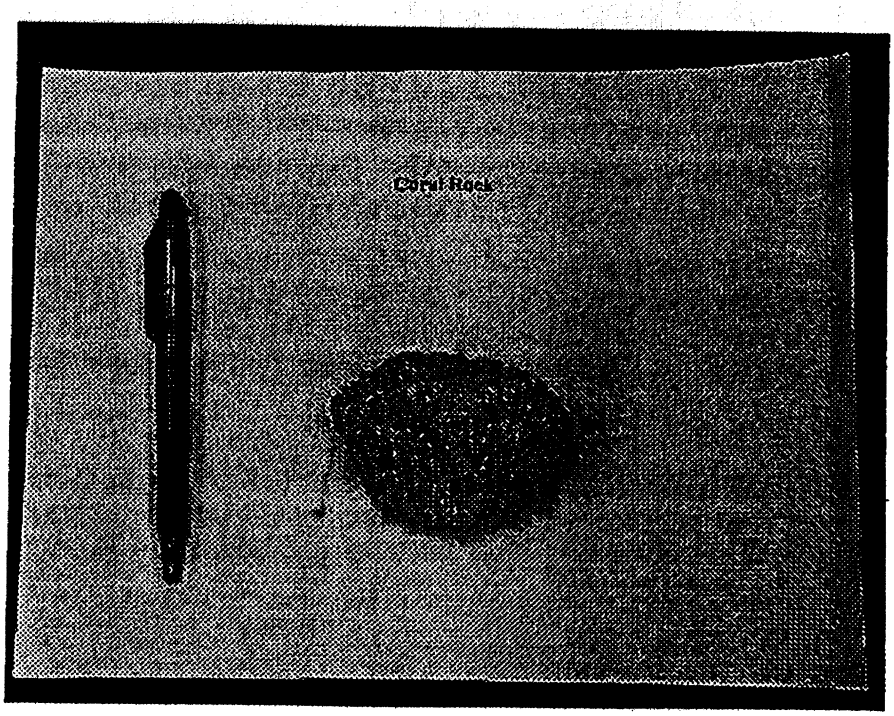

Figure 2.4. Coral Rock

In should be noted that in tropical regions such as Florida Bay and the Florida Keys, there are virtual limestone "factories." These are shallow-water continental shelf regions, with warm climates and warm surface water temperatures that appear to be supersaturated with calcium carbonate, dominated by lime muds and lacking in terrigenous detritus (Judson et al., 1987, p. 100).

Specific descriptions of the locations of the limestone within Florida are presented in Section 2.3.6.

2.3.6 Locations of Rocks in Florida

This section describes the locations where the different types of rocks listed above may be found in Florida and is based on the work performed by Dr. H.K. Brooks for the Institute for Food and Agricultural Sciences at the University of Florida. Brooks (1981a, 1981b, 1981c) characterized the natural features of Florida based on rock and soil types, geologic structure of the underlying rock, geomorphic process that constructed or sculpted the landscape, and relief. Brooks (1981a, 1981c) developed maps, titled the "Physiographic Divisions of the State of Florida" and the "Geologic Map of Florida," that identify the various types of rocks that are located at the surface throughout the state.

Brooks subdivided the state into the following districts:

- Sea Island District,
- Eastern Flatwoods District,
- Gold Coast – Florida Bay District,
- Southwestern Flatwoods,
- Central Lake District,
- Ocala Uplift District,
- Tifton Upland District,
- Dougherty Karst District,
- Apalachicola Delta District, and
- Southern Pine Hills District.

Figure 2.5 shows the approximate locations of the boundaries of these districts. The exact boundaries are shown on the "Physiographic Divisions of the State of Florida" Map. Detailed descriptions of these areas and the rocks that may be found within them are presented below.

In most locations in Florida, the solution of limestones have influenced the landscape and courses of the creeks and rivers (Brooks, 1981b). It is important to stress that this is an overview and a general description of the type of rocks found in Florida. More specific and detailed information may be available on a site by site basis. To assist in the identification of the areas, the counties that are covered within the districts are presented.

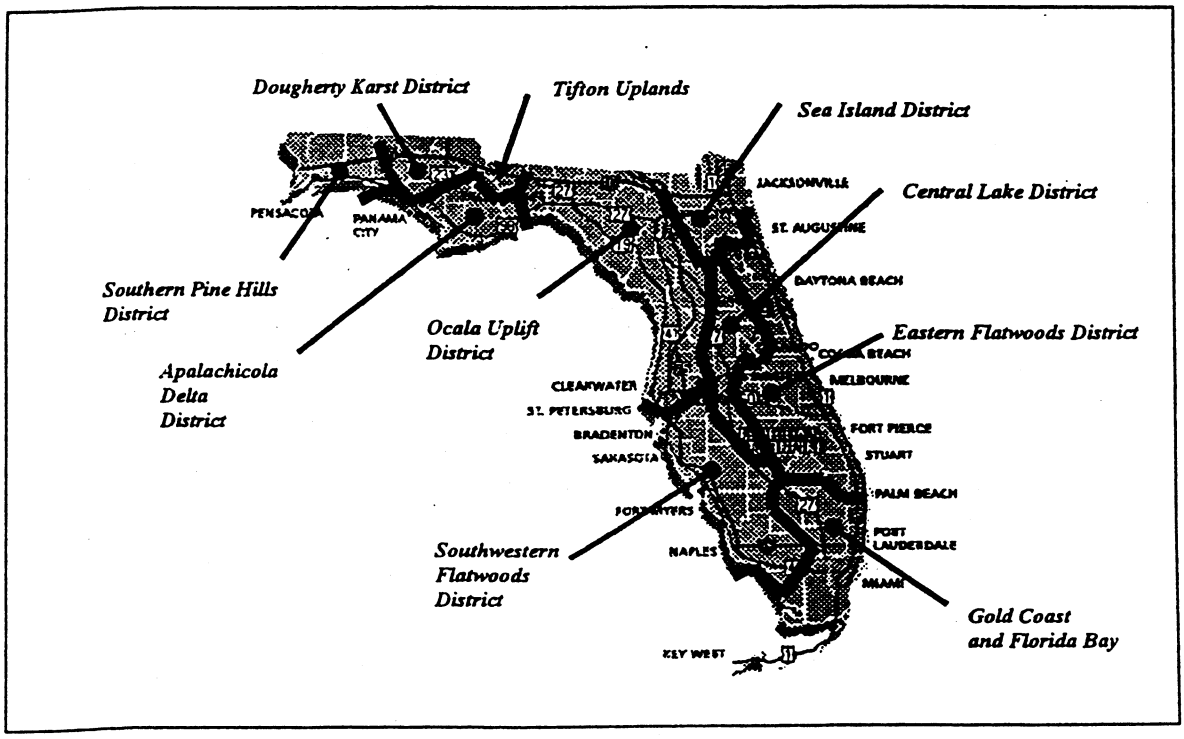

Figure 2.5. Physiographic Divisions of Florida (after Brooks, 1981c)

2.3.6.1 Sea Island District

The Sea Island District is located in the northeast corner of the state. The district encompasses the counties of Nassau, Duval, Baker, and parts of Hamilton, Columbia, Union, Bradford, Clay, St. Johns, and Alachua Counties. The rock type present here is limestone, specifically Ocala Limestone. However, in most places, the Ocala Limestone is covered by an overburden too thick to influence the landscape or drainage. Outcrops of limestone occur along the St. Johns River in some locations (Brooks, 1981b).

2.3.6.2 Eastern Flatwood District

The Eastern Flatwoods District extends from St. Johns County south along the Atlantic Ocean coast of Florida to Martin County. Limestone and coquina are the rock types present in this district. Ocala Limestone is present at or near the surface in the vicinity of Cresent Lake in Flagler County. Coquina is present along the coast from St. Augustine, southeast past Cape Canaveral to Juno Beach (Brooks, 1981b).

2.3.6.3 Gold Coast – Florida Bay District

This district located in the southeastern part (Palm Beach, Broward, Dade, and Monroe Counties) of the Atlantic coastline of Florida, extending from West Palm Beach south to the Florida Keys. The District includes the Everglades and Florida Bay. The rock types present within this district include limestone, coquina, and coral rock (Brooks, 1981b). The Atlantic coastal ridge is no longer underlain or influenced by coquina deposits in this district, as was the case with the Eastern Flatwoods District. However, the offshore barrier island in the vicinity of Palm Beach is perched upon coquina. Limestone formed as oolitic carbonate shoals are located in the vicinity of Miami. The

Florida Keys are islands of limestone or carbonate sand and mud. They are comprised of Coral Reef Keys containing coral rock and Oolitic Keys composed of oolitic limestone (Brooks, 1981b).

2.3.6.4 Southwestern Flatwoods District

This district includes the southwestern portion of Florida's coastline along the Gulf of Mexico. It includes the counties of Collier, Hendry, Lee, Charlotte, Glades, De Soto, Hardee, Sarasota, Manatee, Pinellas, and portions of Hillsborough County. It extends from St. Petersburg, along the Gulf Coast, south past Naples. The rock type that may be encountered within this district is limestone (Brooks, 1981b).

2.3.6.5 Central Lake District

Located within the central part of the state, this district is the region of most active collapsed sinkhole development. This district is located between the Sea Island District, the Eastern Flatwood District, the Southwestern Flatwoods District, and the Ocala Uplift District. Limestone is the type of rock that may be encountered within this district. In certain areas, the limestone is very near the surface (Brooks, 1981b).

2.3.6.6 Ocala Uplift District

The Ocala Uplift District extends along the northwest Gulf Coast up to but not including the Panhandle. It extends from Tampa northeast to Apalachee Bay. Limestone is at or near the surface in most places within this district (Brooks, 1981b). Ocala Limestone is present within this area. Brooks (1981a) describes the Ocala Limestone as "limerock," consisting of the skeletons of fossils in a silt to sand size matrix, skeletons originally as argonite are now molds, 93-96% $CaCO_3$, usually soft porous and friable, with

massive chert nodules occurring near the top and lower portion being rubbly where very small spheroidal fossils are dominant.

2.3.6.7 Tifton Upland District

This district is located on the border of Florida and Georgia and includes Gadsden County. Thick residual silty and clayey soil support a mixed forest in this area (Brooks, 1981b).

2.3.6.8 Dougherty Karst District

The Dougherty Karst District is located on the panhandle section of the state along the Florida and Alabama border. It includes Holmes, Jackson, and Washington Counties. The rock type present in this area is limestone. The limestone in this area is near enough to the surface to have influenced the landscape development (Brooks, 1981b).

2.3.6.9 Apalachicola Delta District

This district is located in the Panhandle along the Gulf Coast. It extends from Apalachee Bay west to Choctawhatchee Bay. This district has a clastic terrain with no karst, which is atypical of the Florida Section (Brooks, 1981b).

2.3.6.10 Southern Pine Hills District

This district is located on the western portion of the Panhandle on the Florida-Alabama border. It includes Escambia, Santa Rosa, Okaloosa, and portions of Walton County. This district contains clastic sediments and rocks that are very thick (Brooks, 1981b).

The Florida Geologic Survey (FGS) is currently publishing two new maps – "The Geologic Map of Florida" and "The Geomorphic Map of Florida." These maps may include updated or refined information from the maps and information presented above.

2.4 Current Methods for the Prediction of Rock Scour

Based on the previous section, it has been demonstrated that rock materials are present at surficial depths throughout the State of Florida. Bridge piers are being founded within these materials. Therefore, it is necessary to estimate the depths of scour in rock materials in Florida. This section describes the current methods used by hydraulic engineers to estimate the scour of rock materials for bridge piers.

2.4.1 HEC-18

Chapter 3 of HEC-18 titled Designing Bridges to Resist Scour describes the approach for placing footings on erodible rock once the total scour for the worst case condition as been estimated (Richardson and Davis, 1995):

> Weathered or other potentially erodible rock formations need to be carefully assessed for scour. An engineering geologist familiar with the area geology should be consulted to determine if rock or soil or other criteria should be used to calculate the support for the spread footing foundation. The decision should be based on analysis of intact rock cores, including rock quality designations and local geology, as well as hydraulic data and anticipated structure life. An important consideration may be the existence of a high quality rock formation below a thin weathered zone. For deep deposits of weathered rock, the potential scour depth should be estimated (steps 4 and 5) and the footings placed below that depth. Excavation into weathered rock should be made with care. If blasting is required, light, closely spaced charges should be used to minimize overbreak beneath the footing level. Loose rock pieces should be removed and the zone filled with clean concrete. In any event, the final footing should be poured in contact with the sides of the excavation for the full designed footing thickness to minimize water intrusion below footing level. Guidance on the scourability of rock formations is given in FHWA

memorandum "Scourability of Rock Formation" dated July 19, 1991. (p. 21)

A summary of the FHWA memorandum referenced in HEC-18 is presented below.

2.4.2 Scourability of Rock Formations Memorandum

As described above and in recognition that bridge foundation failures have occurred due to scour of rock or rock-like materials, FHWA developed an interim guidance to assess rock scourability using empirical methods and testing procedures (Gordon, 1991). These procedures were provided until the results of ongoing research would permit more accurate evaluation procedures.

The empirical methods presented in the interim guidance are commonly used by geotechnical engineers and geologists to determine rock mass engineering properties (Gordon, 1991). The guidance recommends that designers use a combination of the methods presented as no single index property correctly assesses the potential for scour. Several properties contribute to the quality, bearing capacity and soundness of rock (Gordon, 1991). The guidance recommends the following 7 methods to assess the scourability of rock:

- Subsurface Investigation;
- Geologic Formation/Discontinuities;
- Rock Quality Designation (RQD);
- Unconfined Compressive Strength;
- Slake Durability Index;
- Soundness; and
- Abrasion.

A description of these items is presented below.

2.4.2.1 Subsurface investigation

The purpose of a subsurface investigation for shallow foundations on rock is to identify rock types, determine the discontinuity frequency, and recover high quality rock cores for testing and evaluation (Gordon, 1991). The guidance recommends the number of rock cores and type of cores to collect to obtain quality data.

2.4.2.2 Geologic formation/discontinuities

The type of rock and the number of discontinuities have a significant impact on the engineering properties (Gordon, 1991). Whether the rock is igneous, sedimentary, or metamorphic can impact a rock resistance to scour. In general, harder and more sound rock is less susceptible to scour (Gordon, 1991).

The spacing of discontinuities is an indication of overall rock quality and is measured as the perpendicular distance between parallel discontinuities (Gordon, 1991). High fracture frequency (5 or 6 fractures per foot in a drill core) would indicate a poorer quality rock which would be considerably weaker and more susceptible to scour (Gordon, 1991).

2.4.2.3 Rock Quality Designation (RQD)

The RQD value is a modified computation of percent rock core recovery that reflects the relative frequency of discontinuities and the compressibility of the rock mass. It is determined by measuring and summing all the pieces of sound rock in a 10.2 cm or longer length of core run, and subsequently dividing this by the total core run length. Rock with a RQD value less than 50% should be assumed to be soil-like with regard to scour potential (Gordon, 1991).

2.4.2.4 Unconfined compressive strength

The unconfined compressive strength (q_u), as determined by American Society of Testing and Materials (ASTM) D2938, is the primary intact rock property of interest for foundation design (Gordon, 1991). In general, samples with unconfined strengths below 1724 kPa (250 psi) are not considered to behave as rock (Gordon, 1991). There is only a generalized correlation between between unconfined compression strength and scourability – as unconfined compressive strength increases, bearing capacity generally increases and scourability decreases (Gordon, 1991).

2.4.2.5 Slake Durability Index (SDI)

The International Society of Rock Mechanics (ISRM) SDI test is used on metamorphic and sedimentary rocks such as slate and shale. SDI values less than 90 indicate poor rock quality. The lower the SDI value, the more scourable and less durable the rock material (Gordon, 1991).

2.4.2.6 Soundness

The laboratory test for soundness (based on AASHTO T104) uses a soaking procedure in magnesium or sodium sulfate solution. The samples are soaked for a total of 5 cycles with a duration of 16 to 18 hours per cycle. In general, the less sound the rock, the more susceptible to scour the rock will be. Loss rates of 12% (for the sodium sulfate solution) and 18% (for the magnesium sulfate solution) for the test duration can be used as an indirect measure of scour (Gordon, 1991).

2.4.2.7 Abrasion

The Los Angeles Abrasion Test (AASHTO T96) is an empirical test to assess the abrasion of aggregates. A rock sample is added with 12 steel balls in a rotating steel cylinder. The cylinder is rotated for 1000 revolutions at 30 to 33 revolutions per minute (RPMs). Rock with loss rates greater than 40% should be considered susceptible to scour (Gordon, 1991).

2.4.3 Geotechnical Data Comparisons for Rock Materials in Florida

The FHWA rock scourability guidance memorandum recommends that design engineers perform several geotechnical tests to use as an evaluation for the susceptibility of rock to scour. The FDOT and University of Florida have conducted some of the recommended test on rock core samples to assess their values in relation to the values presented in the guidance document.

Limestone samples collected from the US 441 Bridge site over the Santa Fe River were tested for Unconfined Compressive Strength, Los Angeles Abrasion Test, and Magnesium Sulfate Soundness Test. Statistical analysis of the Unconfined compressive strength (q_u) test results indicate that the minimum q_u expected is 1430 kPa or 207 psi (PSI, 1996, p. 5). The Los Angeles Abrasion Test that was performed yielded a loss of 72.3% (PSI, 1996, p. 9). The Magnesium Sulfate Soundness Test indicated a loss of 80.0% (PSI, 1996, p. 10).

The University of Florida conducted limited geotechnical tests on limestone samples from Florida. The results from Unconfined Compressive Strength test indicated strengths ranging from 1372 kPa to 1475 kPa (199 psi to 214 psi). Magnesium Sulfate Soundness tests performed on limestone samples indicated losses from 58.7% to 91.1%.

In a review of FDOT and UF testing results, the q_u are below the 1725 kPa (250 psi) threshold value. The Los Angeles Abrasion and Magnesium Sulfate Soundness test results also indicate that the rock materials should be considered scourable. In summary, based on these geotechnical tests, the rock materials in Florida may be susceptible to scour and must be considered in the design and scour protection for bridge sites.

2.5 Previous Rock Erosion Experiments

The HEC-18 design manual recommends that rock materials either be considered "scourable" or "non-scourable", but does not provide guidance on the rates of erosion. There has been recent experimental work to evaluate the erosion of rock materials. Specifically, the National Research Council of Canada conducted experiments for the Northumberland Strait Bridge Crossing in Canada.

A series of laboratory experiments was conducted to evaluate the erosive response of sedimentary rock and glacial till at the bridge site in Canada. W. F. Baird & Associates retained the National Research Council (NRC) of Canada Institute for Marine Dynamics to investigate the erodibility of mudstone, siltstone, sandstone, and glacial till at the Northumberland Strait Bridge Crossing. The bridge is located on the Northumberland Strait connecting Prince Edward Island to New Brunswick. The experimental procedures and the results of the experiment are included in the NRC's report titled "Erosive Response of Northumberland Strait Till and Sedimentary Rock to Fluid Flow" dated September 1994. This section presents a brief overview of the tests that were performed and the results and conclusions of the experiments.

The primary goal of the experiments was to determine the critical shear stress of various materials obtained from the seabed of Northumberland Strait (Cornett et al., 1994, p. 1). For those materials that could be eroded, the secondary objective was to determine the rate of erosion of those materials. A total of 23 core samples and 5 slab samples from various locations along the bridge route were provided for testing. Two types of flows were then used to evaluate the rates of erosive nature of the seabed materials – open channel flow and flow from a submerged jet (Cornett et al., 1994, p. 2).

The samples that were tested were categorized based on their hardness and weathering (Cornett et al., 1994, p. 3). The system of rock strength classification and rock weathering classification were presented by the International Society of Rock Mechanics. The till was described as a very stiff, moist, reddish brown clayey silt containing a wide range of sand, gravel and cobbles (Cornett et al., 1994, p. 4). The mudstone was characterized as a finely graded silt or clay with mudstone gravel (Cornett et al., 1994, p. 4). The siltstone as a moderately to highly weathered, thinly laminated, reddish brown, micaceous extremely weak to very weak siltstone (Cornett et al., 1994, p. 5). The sandstone was described as a micaceous fine grained, thinly laminated sandstone with thin inter-beds of siltstone (Cornett et al., 1994, p. 5).

Tests were performed in a 12.5-m long open-channel titling flume with a 40-cm square cross-section. A false floor of PVC was installed in the base of the flume with 3 special test sections designed to receive test samples. An entrained abrasive granular material was also placed in the flow as an abrading agent to evaluate its influence on erosion. A submerged jet was placed in the flow when it was determined that the open channel flow was not sufficient to erode the more competent materials. The surface of the

test samples lay just above the floor (approximately 3 mm into the flow) of the flume (Cornett et al., 1994, p. 6). Core samples were cut and placed in a tray (containing 18 cores) to be inserted in the test sections. The shear stress exerted on the bed by the fluid was determined indirectly by measuring the vertical profile of velocity just above the bed (Cornett et al., 1994, p. 8). The velocity was measured with a laser doppler velocimeter system. Erosion of the upper surface of the test samples was measured at regular spatial intervals using an analogue dial pointer gage with an accuracy of 0.025 mm (Cornett et al., 1994, p. 13). In the core samples, the elevation was measured at one point near the core. In the slab samples, the elevation was measured in a regular grid pattern across the sample and the average elevation was calculated (Cornett et al., 1994, p. 14).

The average depth of erosion was computed as the difference in average elevation between the initial and final profile. The rate of erosion is the average vertical velocity of the material surface and was computed by dividing the depth of erosion by the duration of flow (Cornett et al., 1994, p. 15). In addition, a visual observation of the samples was used to assess the onset and extent of erosion.

The results indicated that the till and unconsolidated mudstone samples responded as cohesive soils and eroded in clear water open channel flows. However, the relation between shear stress acting on the bed and the erosion of material is complicated by the wide range of particle sizes within the material as well as the variable cohesive forces that exist between the smaller particles (Cornett et al., 1994, p. 1). For the glacial till, different components begin to erode at different shear stress values thereby making it difficult to characterize the erodibility of the material by a single shear stress value. For example, for a given flow, a sample of the glacial till may erode at a rate that decreases with time as the

easily eroded components are removed at first while the less erodible material remains as part of the sample (Cornett et al., 1994, p. 1).

The weak sedimentary rock that was tested tended to erode by breaking into pieces along fractures, bedding planes, and other internal weaknesses (Cornett et al., 1994, p. 1). This result suggests that the erosion of the material is not related to shear stress. A suggested model presented by Cornett for the rock erosion process that describes the hydraulic fracturing of the samples is presented in the next section.

It should also be noted that a research project is underway at Oregon State University to determine the relationship between the erodibility of rock materials and the Slake Durability Index (SDI) test. The results of this study were not available at this time.

2.6 Rock Erosion Process

The process of rock erosion by the action of a moving fluid is a complex one that may be influenced by several factors. On a fundamental level, rocks can be thought of as simply "grains" and "glue" (refer to Section 2.1). The energy imparted by the moving fluid breaks the grains from the glue and subsequently transports the grains downstream. This fundamental description leads to the idea that there is a certain amount of energy required to initiate erosion of rock materials. In cohesionless sediments, this concept is known as a critical bed-shear stress. This is the shear stress required to initiate motion of the sediments.

Van Rijn (1993) describes the forces acting on a sediment particle resting on a horizontal bed. The fluid forces consist of skin friction forces and pressure forces. The skin friction force acts on the surface of the particles by viscous shear. The pressure

force, consisting of a drag and lift force, is generated by pressure differences along the surface of the particle. Particle movement will occur when the moments of the instantaneous fluid forces with respect to the point of contact are just larger than the stabilizing moment of the submerged particle weight (van Rijn, 1993, p. 4.1). In rock materials, there are additional forces that act between the particles tending to keep the rock a solid body.

The erosion process in rock can be more complex than just the shear stress acting on a body. Experimental work performed at the NRC found that the weak sedimentary rock that was tested tended to erode by breaking into pieces along fractures, bedding planes, and other internal weaknesses. Cornett et al. (1994) presents a simple model for the hydraulic fracturing of rock. The erosion of the rock materials at the fracture planes was not directly related to the shear stress. The results of the study suggest that the erosion of rock may be driven by hydrodynamic pressures within fractures (Cornett et al., 1994, p.26). Cornett et al. proposed the sketch presented in Figure 2.6:

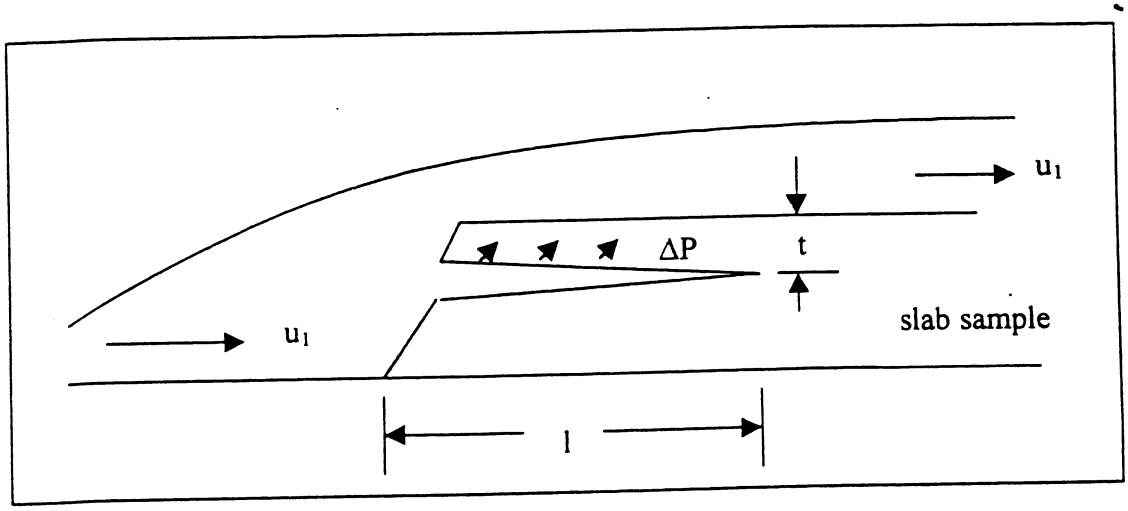

Figure 2.6. Definition Sketch for Hydraulic Fracturing of Rock (Cornett et al., 1994, p.27)

The model proposed by Cornett et al. (1994) for the hydraulic fracturing of rock is based on a thin horizontal crack in a rock sample of length l and height t that is subjected to a steady flow with velocity u_1. The crack is a point of stagnation. Through the application of the Bernoulli's equation, a pressure difference develops between the crack and the external flow, which can be expressed as:

$$\Delta P = P_2 - P_1 = \frac{\rho}{2}\left(u_1^2 - u_2^2 + 2gt\right) \approx \frac{\rho u_1^2}{2}. \qquad \textbf{Equation 2.1}$$

The pressure differential represents the velocity head of the flow that acts to open the crack. The fracture, or removal, or rock occurs when the pressure in the crack exceeds the rock strength to resist flexural failure at the base of the crack (Cornett et al., 1994, p. 26).

The bending moment M in the rock above the crack base (assuming a unit width) can be written as:

$$M = \frac{l^2}{2}\Delta P = \frac{\rho}{4} l^2 u_1^2. \qquad \textbf{Equation 2.2}$$

The maximum axial stress σ_{max} required to carry this moment is given by:

$$\sigma_{max} = 1.5\rho\left(\frac{l}{t}\right)^2 u_1^2. \qquad \textbf{Equation 2.3}$$

This representation suggests that for a fixed crack geometry, the rock strength required to resist failure is proportional to the square of external fluid velocity. Flexure failure would occur when the rock strength is exceeded by the maximum axial stress (Cornett et al., 1994, p. 27).

Annandale, who has developed a method for estimating rock erosion that will be discussed in the next section, has suggested the following framework for hydraulic erosion

of rock materials. Annandale's approach is based on a rational correlation between the rate of energy dissipation of flowing water and an erodibility classification of the materials (Annandale, 1995, p. 471). The removal of rock material occurs in three stages: jacking, dislodgment, and displacement. Figure 2.7 presents these processes.

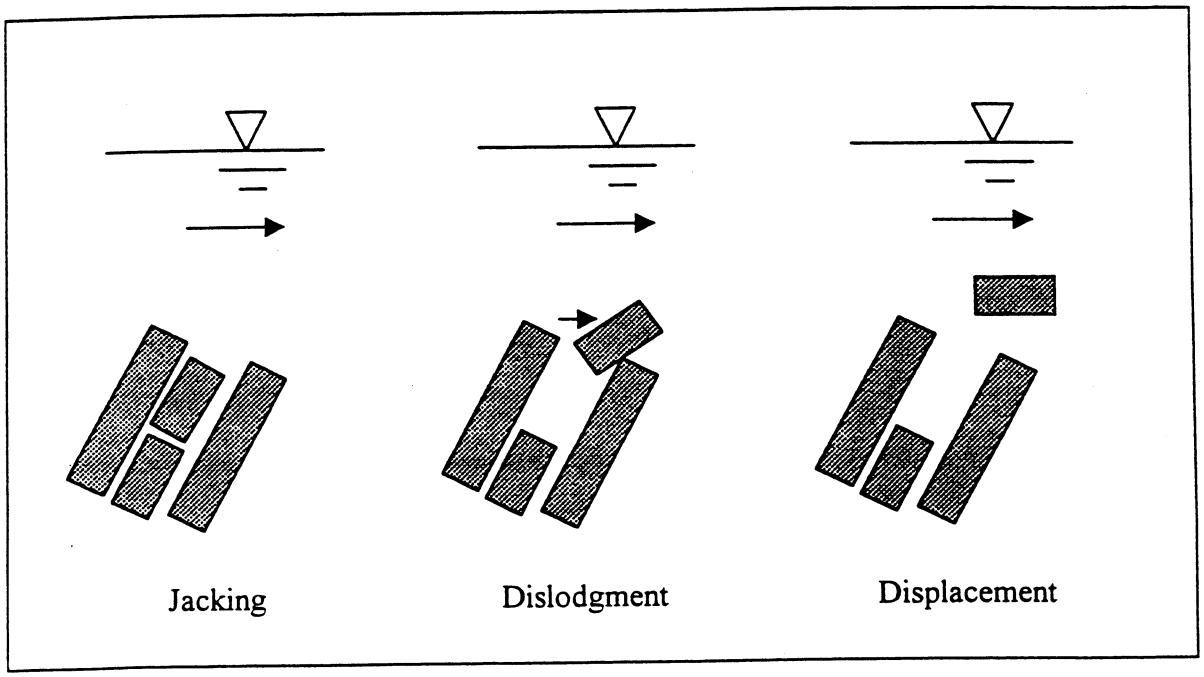

Figure 2.7. Hydraulic Erosion (Annandale, 1995, p. 473)

Flowing water is subject to turbulence which, in turn, is associated with a loss in energy. Annandale suggests that turbulence causes pressure fluctuations that result in an action that progressively jacks out material from its position. Once removed, the material is then dislodged and displaced (Annandale, 1995, p. 472). Annandale selected the rate of energy dissipation as the parameter to represent the relative strength of the fluctuating pressure disturbance. Annandale states:

> Turbulence causes both pressure fluctuations and energy loss. Increases in turbulence intensity will concurrently result in increased rates of energy

> dissipation and increases in the magnitude of fluctuation pressures. Estimates of the rate of energy dissipation should therefore represent the relative magnitude of fluctuating pressure, and thus the erosive power of water (p. 473).

Details of this method are presented in the following section.

2.7 Alternative Rock Erosion Predictive Methods

2.7.1 Erodibility Index Method

A method that has been developed for use in estimating the erosion of rock materials as well as the erosion of cohesionless and cohesive soils is the Erodibility Index method. This method, developed by Annandale (1995), compares a material's ability to resist erosion, which has been designated as the Erodibility Index, with the erosive power of flowing water. As described above, the erosive power of water has been defined in terms of the stream power. The comparison of these two values determines if a material will or will not erode. This method has been further developed for use in estimating the scour at piles for bridges, which is presented in the Interim Report by the Colorado Department of Transportation titled "Preliminary Procedure to Predict Bridge Scour in Bedrock" (Smith, 1994). A brief description of the components of the Erodibility Index method is presented below. The reader is referenced to the above mentioned report for the details of this method.

2.7.1.1 Erosive power of water

Hydraulic erosion occurs when the erosive power of flowing water exceeds a material's ability to resist erosion. The erosive power of flowing water is based on the rate of energy dissipation. In this method, the correlation between the rate of energy dissipation (P) and a material's resistance to erosion (K_h) can be expressed as

$$P = f(K_h), \qquad \textbf{Equation 2.4}$$

(Annandale, 1995, p. 472).

If $P > f(K_h)$, then the material should erode. However, if $P < f(K_h)$, then the material should not erode (Annandale, 1995, p. 472). For an open channel flow condition, the rate of energy dissipation (P) per unit width of flow (based on a unit discharge per unit width q) can be expressed as (Annandale, 1995, p. 480):

$$P = \gamma q s_f L = \gamma q \Delta E, \qquad \textbf{Equation 2.5}$$

where γ = unit weight of water,

s_f = energy slope, and

L = unit length of the channel.

2.7.1.2 Material's resistance to erosion (K_h)

As described above, K_h is the parameter used to describe a material's ability to resist erosion by water. This parameter was based on Kirsten's ripability index, which is a classification system for indexing the effort required for material excavation (Smith, 1994, p. 6). Kirsten developed a rational relationship between the flywheel power of excavation equipment and the ripability of any given earth material (Annandale, 1995, p. 481). The classification system is the product of several parameters which influence excavation and summarizes the most important variables into a single dimensionless number (Smith, 1994, p. 6).

The primary geotechnical parameters that are used in the calculation of the Erodibility Index are earth mass strength, block or particle size, discontinuity/inter-particle

bond shear strength, and the shape of material units and their orientation relative to the flow (Annandale, 1995, p. 481). The relationship is:

$$K_h = M_s K_b K_d J_s, \qquad \textbf{Equation 2.6}$$

where M_s = mass strength number,

K_b = particle/block size number,

K_d = disconitunity or inter-particle bond strength, and

J_s = relative ground structure number.

A description of these parameters is presented below. The tables containing the values for these parameters have not been reproduced in this work.

Mass Strength Number. The mass strength number represents the material strength of an intact representative sample without regard to geologic heterogeneity within the mass (Annandale, 1995. p. 482). This parameter can be determined for different earth materials such as cohesionless sediment, cohesive sediment, and rock materials.

Particle/Block Size Number. The particle/block size factor is the material parameter used to represent the rock mass quality or the median particle diameter for granular material (Smith, 1994). The larger the block and particle sizes, the greater the material will offer resistance to erosion. The particle/block size number is evaluated for rock by the ratio of rock quality designation (RQD) to the number of different joints, the joint set number (J_n).

Interparticle Bond Strength Factor. This parameter represents the relative strength of discontinuities in rock and the strength of particle bonding in granular material (Smith, 1994). It is determined by the ratio between joint wall roughness and joint wall alteration in rock material. Visual observations are required to evaluate the condition of the joint

such as tightness, alteration material and separation. Joints that are tighter and rougher with a sound alteration material within the joints will offer a greater resistance to erosion (Smith, 1994).

Relative Shape and Orientation Factor. The relative ground structure number developed by Kirsten (1982) relates the relative shape of the material particles or blocks and the orientation and spacing of the structural features to the direction of effort during excavation (Smith, 1994). For the purposes of hydraulic erosion, the direction of excavation is analogous to the direction of flowing water (Smith, 1994). This parameter can be determined from the dip angle and direction of the least favorable discontinuity relative to stream flow and the ratio of joint spacing (Smith, 1994).

2.7.1.3 Erodibility threshold

The erodibility threshold of earth materials was established by Annandale by relating the erosive power of water (stream power) and the relative ability of the earth materials to resist erosion for 150 field observations and published data on initiation of sediment motion (Annandale, 1995, p. 488). The 150 field observations were from several spillways and dams (Annandale, 1995, p. 472). A material will erode if for a given stream power and Erodibility Index is above the threshold. If it is below the threshold, it will not erode. Annandale provides graphical representations of the erodibility threshold for various earth materials that have not been reproduced here (Annandale, 1995, pp. 489-491).

2.7.2 Application of Erodibility Method

W. F. Baird & Associates applied the method in estimating the scour in cohesive soils and rock materials for the Northumberland Strait Bridge in Canada. The method was

applied by W. F. Baird & Associates in the assessment of scour protection for the 65 bridge piers for the Northumberland Strait Crossing bridge that links New Brunswick and Prince Edward Island in the Canadian Maritimes (Anglin et al., 1997, p. 89). One of the factors at this bridge location that precluded the use of standard scour prediction techniques was the presence of the highly weathered/fractured and variable bedrock seabed. An extensive literature survey was undertaken by Baird & Associates to identify scour assessment techniques that could be applied (Anglin et al., 1997, p. 92). After reviewing the available information, including HEC-18, W. F. Baird & Associates concluded that there was no acceptable technique to define scour potential for the bridge piers due to the following unique conditions:

- combined waves and currents;
- conical shape of the pier bases;
- location of some pier bases in dredged pits (up to 7 m deep); and
- highly weathered/fractured and variable bedrock seabed (Anglin et al., 1997, p. 92).

Initially, a laboratory study was performed in an attempt to characterize and quantify the erosion potential of the various seabed materials at the crossing location (Anglin et al., 1997, p. 92). The procedures and results of this study were discussed in a Section 2.5. In this experiment, the erosion process was found to be complex and it was not possible to reliably quantify the erosion of these materials as a function of either near bed velocity or shear stress (Anglin et al., 1997, p. 92).

Subsequent to these experiments, the literature review was updated. The Erodibility Index approach was identified as a potential method for estimating erosion in complex earth materials. To estimate the scour potential, both the stream power and the seabed's resistance to erosion was identified. The stream power of the ambient flow

conditions (tidal surges and currents) was identified through numerical modeling techniques. The 100-year stream power event (which considers the combined effect of waves and tidal surges/currents) was selected as the ambient design event for the project (Anglin et al., 1997, p. 94). The stream power at the bridge pier locations were evaluated and a geotechnical investigation was performed to identify the erodibility indices for the material the bridge piers were to be founded (Anglin et al., 1997, p. 97).

A pier by pier assessment was performed to assess the requirement for scour protection. A factor of safety was incorporated to address the uncertainties associated with the driving force for erosion, resisting forces, and the erosion threshold relationship. A higher factor of safety was applied at piers with a greater variation in seabed conditions or where the tolerance for scour was lower (Anglin et al., 1997, p. 99).

Currently, a monitoring program is in place to document scour which may occur around the base of the bridge piers. This is being conducted for the following reasons:

- the erodibility index method used for scour evaluation was new and had not previously been applied to bridge piers, waves, currents, or a design;
- the uncertainties associated with the estimation of the driving force for and the seabed's resistance to scour; and
- the desire to minimize seabed survey requirements around the bridge piers (Anglin et al., 1997, p. 101).

CHAPTER 3
ROCK EROSION TESTING APPARATUS

The previous chapter provides a brief overview of the current state of knowledge and practice in the field of rock erosion and scour. As can be seen from previous investigations, even though methods have been proposed for predicting water scour in rock materials, much work is still needed. To evaluate the scour of specific rock materials, it is important to examine several factors. At first, it is important to understand a materials reaction to fluid flow. A laboratory study is most suited for this type of investigation since it allows much better control of important variables and, in general, more accurate measurements. The work performed under this study consisted of the development of a methodology for the evaluation a rock's erosion reaction to fluid flow. A laboratory-testing device was required to measure and evaluate the rates of erosion of the various rock materials found in Florida.

3.1 Design Challenges

To develop a laboratory method for testing the erosion rates of rock materials, the following challenges had to be addressed.

- There are difficulties in working with rock as a matrix. First, drilling rigs are required to extract samples of rock (called cores). This is the most common method of collecting rock samples for analysis. Secondly, rock has the propensity to fracture along weak planes, leaving broken pieces of samples.

Therefore, the testing device must be able to work with limited amount of sample material and be able to utilize rock cores that are routinely collected by the FDOT as part of bridge pier design and construction.

- The laboratory-testing device must be able to simulate the action of flowing water over a bed of rock materials, similar to that found in field conditions. Specifically, the device must be able to apply a hydraulic shear stress to the rock surface.
- Along the same lines as described above, the laboratory-testing device must be able to measure the shear stress that is applied to the rock sample being tested.
- The testing device must be able to generate shear stresses at the levels that will be encountered in design storm flow conditions. Therefore, the laboratory-testing device must be able to operate at shear stresses that range from ambient to beyond design conditions.
- Based on information obtained from the literature review, rock can be highly resistant to erosion. Since the erosion rates are very low as compared with cohesionless and cohesive sediments, the laboratory-testing device must be able to measure small amounts of lost material while continuously operating for days.

An extensive literature survey was performed to evaluate the different types of devices used to measure the rates of erosion of natural earth materials with the thought that one of these devices may be able to be applied to rock materials. Based on the above described criteria, the rotating cylinder erosion testing apparatus was selected. This type of device has been used by several researchers in the evaluation of critical stress and rates

of erosion of cohesive sediments. A description of this type of device, which is similar to the viscometer used by Couette, and the improvements that have been implemented are discussed in detail below.

3.2 Previous Use of the Rotating Cylinder Testing Apparatus

Moore and Masch (1962) applied the rotating cylinder principle used in viscometers to measure the scour resistance of cohesive soils. The device was called the rotating cylinder erosion test apparatus. The apparatus consisted of a cylindrical cohesive soil sample mounted coaxially inside a slightly larger transparent cylinder. The cohesive soil sample is suspended and supported by a hollow tube. The outer cylinder is free to rotate about its axis. The annular gap between the cylinder and sample is filled with fluid. As the outer cylinder is rotated, momentum is imparted to the fluid and the fluid moves, imparting a shear stress to the face of the sample. The cohesive soil sample is stationary but mounted on flexure pivots so that the shear stress transmitted to the sample surface resulted in a slight rotation of the supporting tube. The resulting rotation was calibrated to measure the torque on the sample and, thereby, the shear stress (Moore and Masch, 1962, p. 1444).

As a shear stress was applied to the sample, material was eroded from the face of the sample. The amount of material eroded was measured and the duration that the shear stress was applied was also recorded. Therefore, the average rate of erosion could be computed for a given applied shear stress.

Several researchers including Rektorik et al. (1964), Arulanandan et al. (1973), Sargunam et al. (1973), Alizadeh (1974) and Chapius and Gatien (1986) have used similar

devices with improvements and enhancements. Akky and Shen (1973) used the rotating cylinder apparatus developed by Arulanandan to evaluate the erosion of cement-stabilized soil. In fact, Chapius and Gatien improved the testing apparatus to accept either intact or remolded cohesive soils, with improved rotation guidance, better alignment, a lower internal friction, and a reduction of the influence of end conditions on the fluid annular flow (Chapius and Gatien, 1986, p. 86). These researchers evaluated the rate of erosion of cohesive sediments with the rotating cylinder device.

3.3 Theoretical Hydrodynamic Aspects of the Rotating Cylinder Apparatus

Essentially, the rotating cylinder works along the same principle as a rotational viscometer. Rotational viscometers operate on the principle that when a cylinder is suspended and immersed in a liquid contained in a vessel which rotates at a steady speed, a balancing couple will be required to keep the cylinder at rest. This couple may be produced by the torsion of a wire from which it is suspended (Merrington, 1949, p. 30). One of the earliest types of rotational viscometers is the Couette viscometer. The outer cylinder is supported by a spindle that rotates at a fixed speed. The inner cylinder is suspended from a torsion wire (Merrington, 1949, p. 32). The fluid is contained in the gap between the two cylinders.

For a newtonian fluid, the velocity distribution increases linearly from zero at the stationary inner cylinder (no-slip condition) to the velocity of the outer rotating cylinder at the wall of the outer cylinder, as shown in Figures 3.1 and 3.2. This equates to laminar flow between two infinite parallel plates.

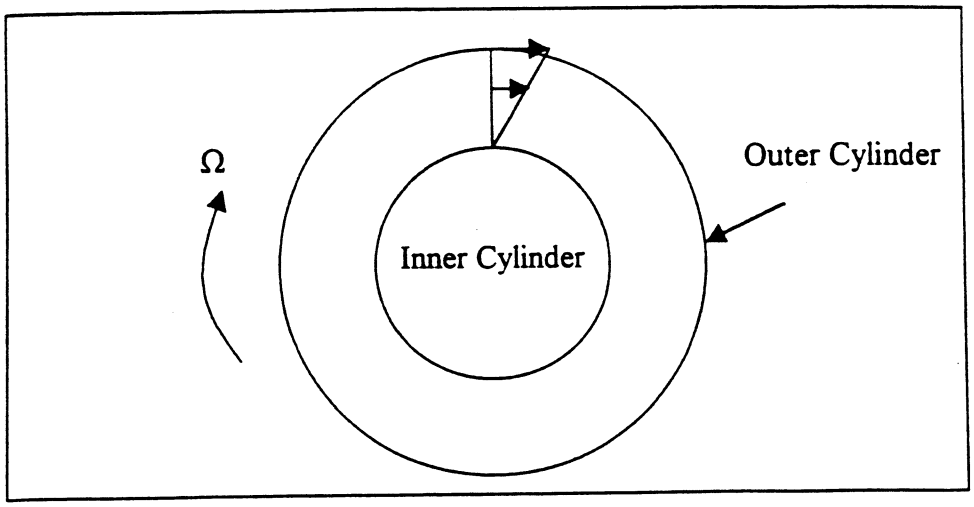

Figure 3.1. Velocity profile between two concentric cylinders

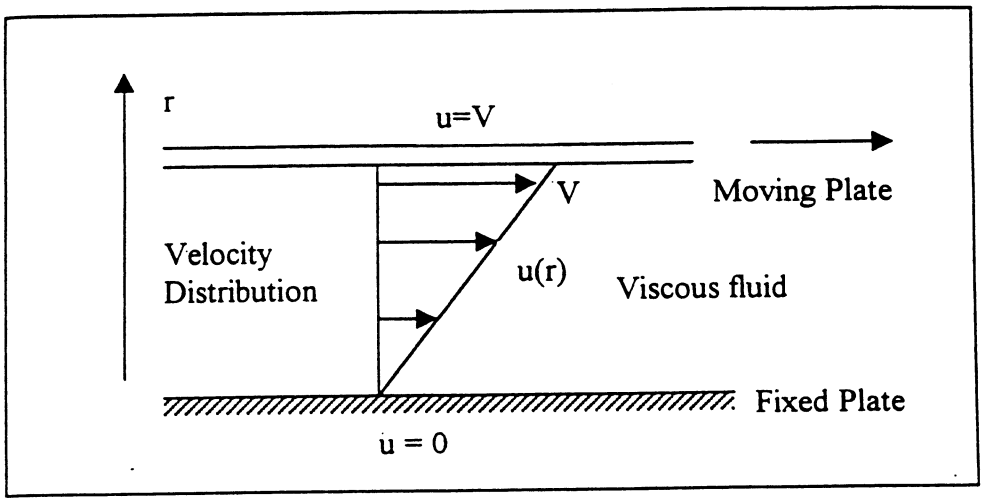

Figure 3.2. Velocity profile between two infinite parallel plates

Equating the flow to the linear velocity profile between the two concentric cylinders occurs only during laminar (tangential only) flow conditions. However, as the speed of the outer cylinder is increased (an increase in the RPMs of the motor) there are changes in the flow regime. The flow begins as a laminar flow and then, at a certain outer cylinder velocity or RPM (depending on cylinders' dimensions), the flow becomes

unstable. The instability grows until a secondary flow is achieved. The secondary flows, described by G.I. Taylor, are a succession of stable toroids or vortices, which have been termed Taylor's rotational vortices. These vorticies are well-defined counter-rotating circulation cells. As the outer cylinder speed is increased, the Taylor vortices can become unstable. Several pictures of Taylor vorticies can be found in *An Album of Fluid Motion* (Van Dyke, 1982, pp. 76-77).

Rohan and Lefebvre (1991) investigated certain hydrodynamic aspects of the rotating cylinder erosion tests. The critical Reynolds number between a laminar flow and the formation of the above mentioned Taylor vortices can be calculated by the following equation (Rohan and Lefebvre, 1991, p. 167):

$$\mathrm{Re}_{cr} = \frac{2\pi N\rho}{\mu}\ \alpha^{1.5} R_i^{\,2} > 41.3, \qquad \textbf{Equation 3.1}$$

where $N = \Omega$ (radians/s)/2π = rotational speed in cycles/s,

ρ (kg/m^3) = fluid density,

μ (Ns/m^2) = dynamic viscosity,

R_e (m) = external radius,

R_i (m) = internal radius, and

$\alpha = R_e/R_i$.

Viscous stability in the presence of three-dimensional disturbances is obtained for values of Taylor's number (Ta)

$$Ta = \frac{V_e d}{\nu}\frac{d}{R_i} < 41.3, \qquad \textbf{Equation 3.2}$$

where d = width of the gap between the cylinders,

R_i = inner radius,

V_e = peripheral velocity of the outer cylinder, and

ν = kinematic viscosity (Rohan and Lefebvre, 1991, p. 169).

In fact, there are three regimes of flow which can be distinguished based upon the calculation of the Taylor number (Rohan and Lefebvre, 1991, p. 169):

1. $Ta < 41.3$ = laminar Couette flow;
2. $41.3 < Ta < 400$ = laminar flow with Taylor vortices;
3. $Ta > 400$ = turbulent flow.

In the cases where the flow consists of secondary flows (vortices) or turbulent flow, the velocity profile is no longer a linear relationship from the wall of the stationary inner cylinder to the rotating outer cylinder.

3.4 Advantages of Rotating Cylinder Apparatus

The rotating cylinder test apparatus met several of the design criteria presented in Section 3.1. Specifically:

- a small sample quantity of rock samples can be used in this type of device as the outer cylinder can be sized to accommodate the size of the rock cores and samples,
- water can be applied to a rock sample to produce a shear stress on the sample,
- the average shear stress on the sample can be measured easily by measuring the torque that is being applied to the sample,
- small quantities of material being eroded can be measured using precision balances, and
- the apparatus can be operated for a long period of time as the outer cylinder can be driven by a continuous duty motor.

3.5 Limitations and Bias of Rotating Cylinder Apparatus

It is important to discuss the limitations of this type of testing device to understand where uncertainty and bias may be present in the results from these experiments. In the measurement of the shear stress, the shear stress is computed by measuring the torque on the sample. However, the torque being measured is the torque being applied to the entire sample. Therefore, the calculation of the shear stress results in the average shear stress over the entire sample surface. The results from the experiments assume that the shear stress is uniform across the entire surface of the sample. In actuality, the surface of rock samples can be pitted and uneven (as can be seen from the pictures presented in Section 2.3). Therefore, there may be variations in the shear stress distribution over the face.

Secondly, there may be bias in the measurement of shear stress. Rohan and Lefebvre (1991) suggest that the shear stress on the sample may be underestimated. The authors suggest that in a curved flow (such as in a curved rectangular pipe), the fluid flowing on the exterior of the curve is exposed to a centrifugal force superior to that found on the interior of the curve. This causes an external "depression" and the liquid moves toward the rotating exterior cylinder which favors helicodial flow (Rohan and Lefebvre, 1991. p. 167). In addition, Rohan and Lefebvre (1991) suggest that in the turbulent flow regime, the shear stress may be underestimated due to the fluctuations of the radial components of velocity. Authors are not unanimous in evaluating the influence of the radial component of fluctuation of velocity (Rohan and Lefebvre, 1991. p. 169). In summary, Rohan and Lefebvre (1991) suggest that in interpreting test results, the shear

stress may be underestimated due to streamline curvature and the fluctuations in the radial component of velocity (Rohan and Lefebvre, 1991. p. 170).

In essence, this indicates that the torque, and therefore shear stress, measured may be biased in the direction of underestimating the shear stress acting on the sample. In practical terms, there may be components of the flow acting on the surface of the sample in directions other than the direction in which the torque is being measured. Thus, there may be a component of shear stress which is eroding the surface of the sample that is not being accounted for in the measurements. These components are difficult to measure.

In the application of these results, the underestimation of shear stress would provide conservative estimates of the critical shear stress and rates of erosion. That is, the results would show greater erosion rates for a given shear stress. The conservative nature of these results would be appropriate for design applications. Chapter 6 provides recommendations for further research as to evaluating the magnitudes of these biases.

3.6 Rotating Cylinder Testing Apparatus for Measuring Rock Erodibility

The rotating cylinder testing apparatus used in this study was similar to the devices previously used; however, some modifications have been made. Figures 3.3 and 3.4 are schematic drawings of the rotating device used in this study and Figures 3.5 and 3.6 are photographs of the actual device itself.

3.6.1 Rotating Cylinder Testing Apparatus

This section describes the details of the rotating cylinder testing apparatus. The major components of the apparatus consist of the following:

- Bodine 1/8-hp Frame 42A motor (2500 RPMs at 50 in-oz [353 mm-N] of torque) with contoller,

- 3-in (7.62-cm) outside diameter (2.5-in [6.35-cm] inside diameter) acrylic cylinder,
- Omega digital readout, and
- Sensotec Model QWFK-8M Miniature Reaction Torque Transducer (torque cell) with a range from 0 to 25 in-oz (0 to 176.5 mm-N).

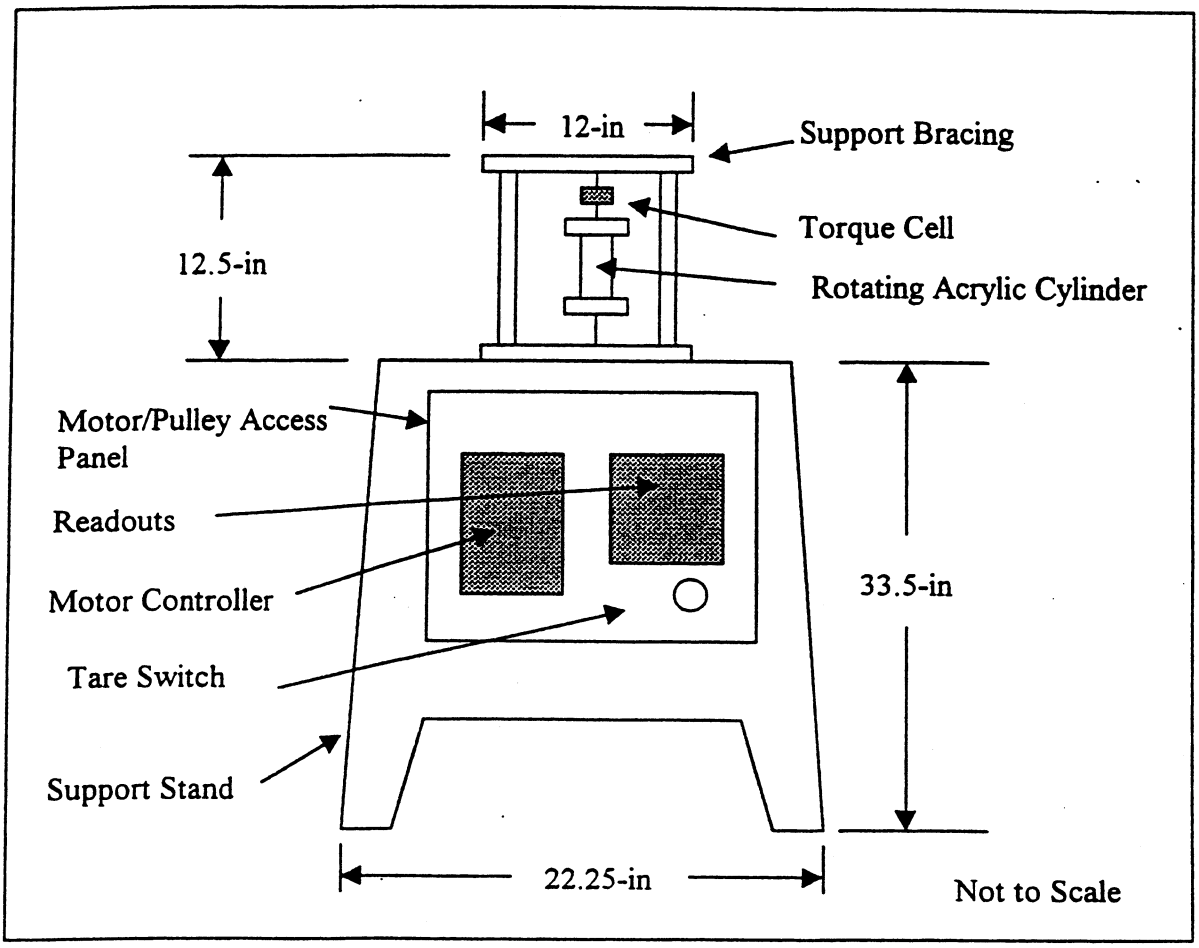

Figure 3.3. Rotating Cylinder Test Apparatus Schematic

English units are shown for equipment dimensions as they were used by the manufacturers to specify equipment sizes. The metric equivalents are also provided. The testing apparatus consists of a prefabricated metal stand with a motor access panel placed on the front of the stand. The prefabricated metal stand has adjustable feet, which is used

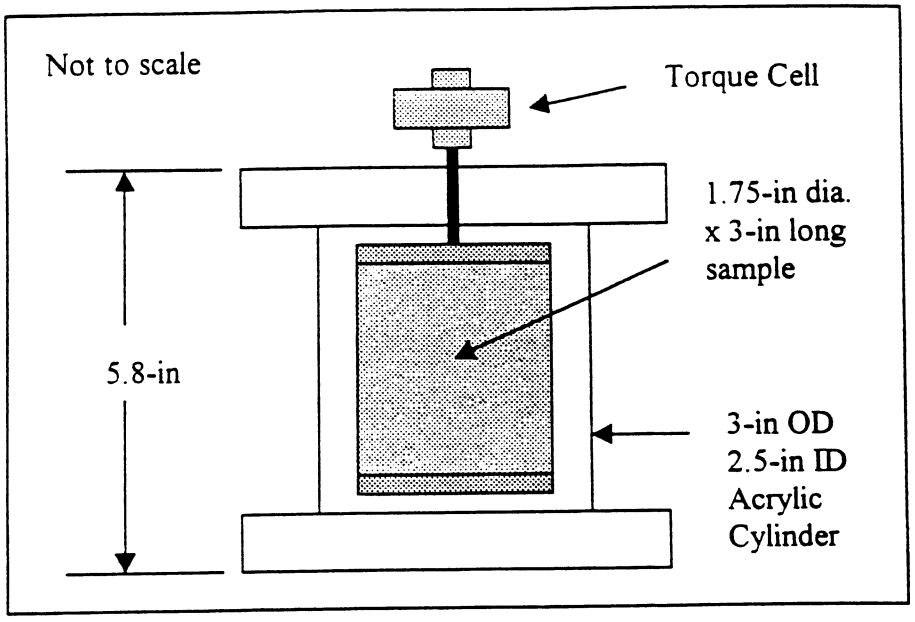

Figure 3.4. Schematic of Acrylic Cylinder and Torque Cell

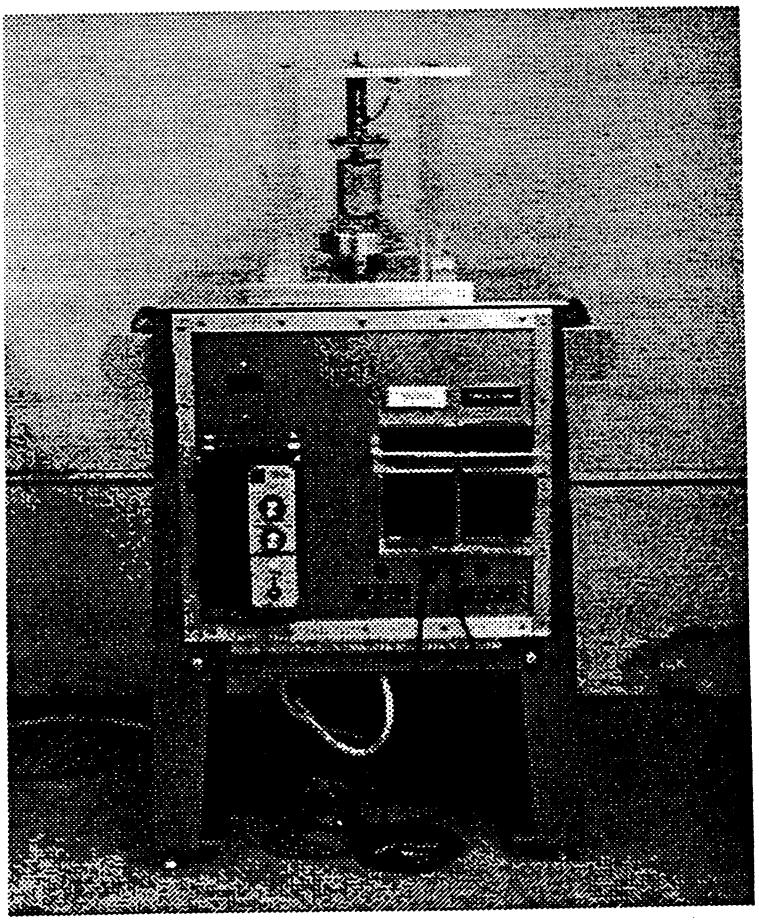

Figure 3.5. Rotating Cylinder Test Apparatus

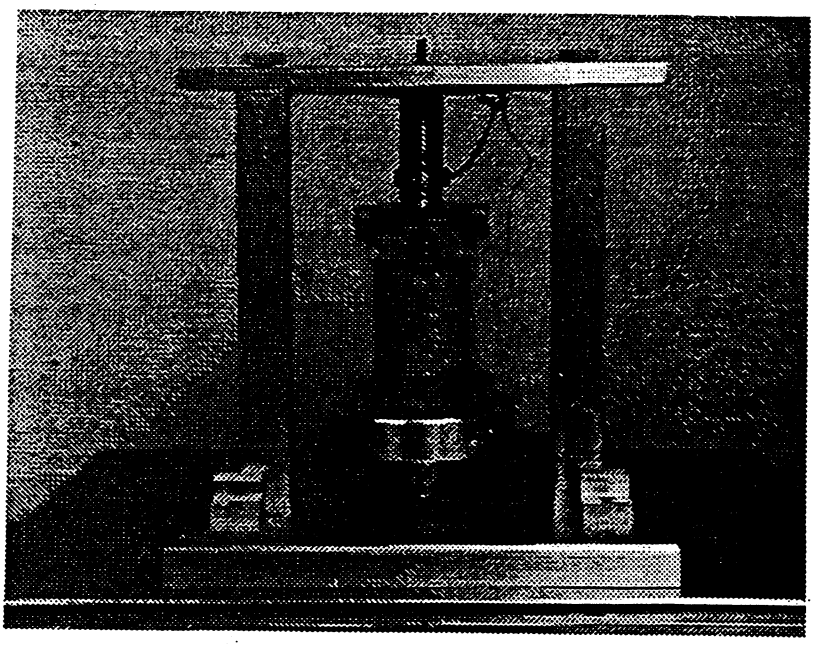

Figure 3.6. Acrylic Cylinder and Torque Cell

to level the apparatus, and handles mounted to the sides that can be used to transport the device. The motor is mounted beneath the top of the prefabricated metal stand. The acrylic cylinder is mounted to a ½-in (1.27-cm) diameter steel shaft that extends beneath the top of the metal stand. Two pulleys and a belt connect the motor and shaft. The motor controller is mounted on the outside of the access panel.

The rock sample that is being tested is fixed between 2 thin plates and is secured by a 3/16-in (0.48-cm) threaded rod placed through the center of the sample. The rock sample/rod system is connected to the torque cell, which is held stationary by the support bracing fixed directly to the apparatus. The output from the torque cell is displayed by the Omega digital readout, which was programmed (following the manufacturers' recommended procedures) to provide the torque output in mm-N. The readout is

mounted on the outside of the access panel next to the motor controller. A tare switch is connected to the readout. This allows the readout to be set to zero before a test to facilitate the torque reading. The tare switch is also mounted on the face of the access panel just below the readout.

3.6.2 Torque Cell

The addition of the torque cell is an improvement over the previous methods for measuring torque. The torque cell allows for the elimination of bearings or flexure pivots to support the sample and for the measurement of the torque contributions due to end effects. In the previous devices, the cohesive soil sample was mounted to pivots or bearings so that the shear stress transmitted to the sample surface resulted in a slight rotation of the supporting tube. The resulting rotation was calibrated to measure the torque on the sample by using either torsion wires or by a pulley and weight system. In this type of set-up, the friction within the bearings must be accounted for in the torque measurements.

The addition of the torque cell allows for the direct measurement of torque with minimal rotation of the sample. Thus the need for bearings is eliminated. One end of the torque cell is mounted to the fixed support bracing and the sample is mounted to the other end as shown in Figures 3.4 and 3.6.

To calibrate the torque cell, a moment arm was attached to the shaft where the sample would normally be located. A wire was run from the moment arm, over a pulley, to a pan where brass weights were placed. This allowed a known torque to be placed on the torque cell. The torque reading was plotted versus the expected value. Figure 3.7 shows the torque cell calibration. Notice that the cell is very linear.

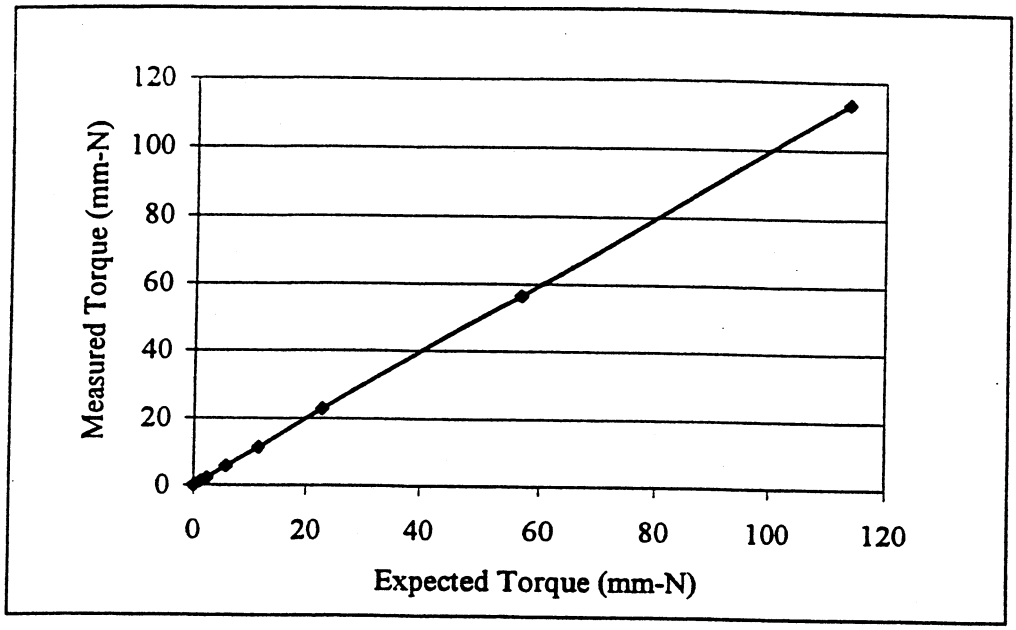

Figure 3.7. Torque Cell Calibration

The torque cell measurements agreed with the expected values, indicating that the torque cell is accurate in recording the torque.

3.6.3 Determination of End Effects

In this type of erosion testing device, the torque measurements are for the total torque exerted on the sample. Water flow over the top and bottom ends of the sample also produces a torque that is measured by the torque cell. Since the ends are protected from being eroded by thin metal plates, the torque being produced on the end of the sample must be taken into consideration. A method to evaluate the end effects with the torque cell was developed.

The dimensions of the rock samples used in this experiment are 1.75-in in diameter by approximately 3-in in length (4.45-cm x 7.62-cm). A detailed explanation of the preparation of the rock samples is included in Section 3.7.1.

Experiments were performed to measure the torque exerted on the bottom plate. The experiments consisted of placing the threaded rod with the bottom plate only within the acrylic cylinder. Enough water is added in the rotating cylinder at each RPM tested to cover the underside of the bottom plate only. The torque at each RPM tested was recorded and a plot was developed. Figure 3.8 shows the set-up for the end effects determination experiment.

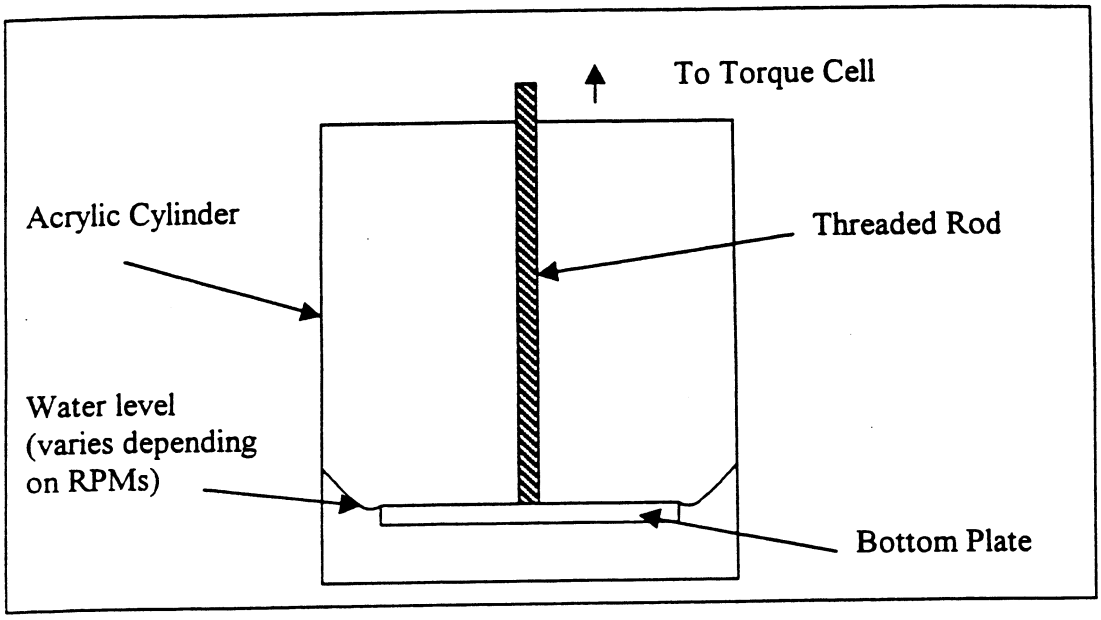

Figure 3.8. End Effects Experiment Set-up

The end effects experiments were conducted on two different dates. The results of those experiments are shown in Figure 3.9.

The results of the two end effects experiments agree. The manufacturer reported the values for the uncertainty bars shown in the figure. As will be discussed in the experimental procedures section, the torque on the bottom plate for a given RPM can be obtained from the plot. This torque is subtracted from the total torque reading. The

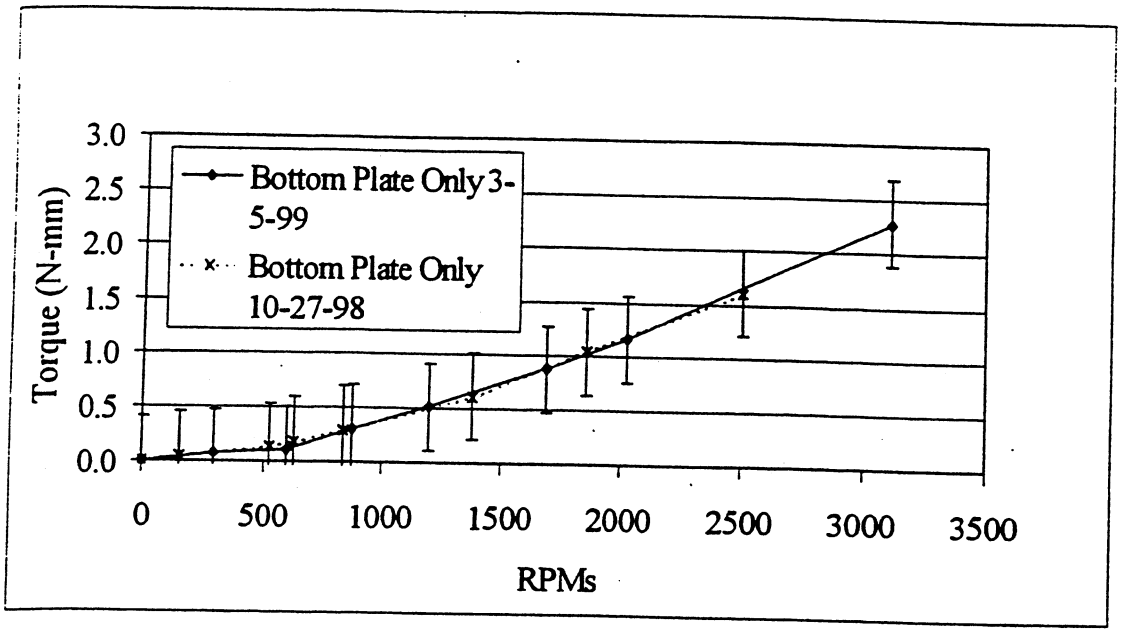

Figure 3.9. End Effects Determination

resulting torque value is that exerted on the outer surface of the sample. It should be noted that during a particular erosion test, only enough water is added to the cylinder annulus to wet the sides and not the end plate on the top of the sample. Therefore, only the end effects from the bottom plate need to be considered.

3.7 Experimental Procedures

This section describes the procedures that were used to perform the experiments. First, the sample preparation procedures are described. The experimental procedures are then described along with the calculations that are performed.

3.7.1 Sample Preparation

Samples that were tested in the rotating cylinder apparatus were collected from rock cores obtained by the FDOT. The sample was formed by drilling a horizontal solid cylinder through a vertical core. The rationale for collecting a sample from the side of a

core was based on the results of a preliminary experiment performed at the University of Florida. A sample of limestone was collected from a FDOT core and then cut into a cube. To obtain qualitative information about the anisotropy of these samples, a pressure washer was directed at each face of the sample. While this does not simulate field conditions (tangential flow over a bed), it did provide some insight into the erosion properties of the sample. It was discovered that there were differences in the rates at which various faces eroded. These differences in erosion can be attributed to the non-homogeneity and anisotropy of rock samples. It was concluded that in order to most accurately simulate the field condition, the sample face being eroded should be in the same orientation as in the field. By cutting a horizontal solid cylinder from the core, the eroding surface will be closer to that of a field situation. Figure 3.10 illustrates this point.

The samples for erosion testing were taken from 4-in (10.16-cm) nominal diameter cores collected by the FDOT. The samples were cored from the sides using a concrete wet corer with a 2-in (5.08-cm) diameter core bit. This produced a sample of 1.75-in (4.45-cm) in diameter. The ends of the sample were leveled with a concrete wet saw. This left a sample with a length of approximately 3-in (7.62-cm).

A hole must be drilled in the center of the rock material to connect the end plates as well as allow the sample to be connected to the torque cell.

In preparing the samples, it was discovered that during coring, the samples could fracture easily. Care had to be taken in the coring of the samples. To minimize the fracturing, a 3/16-in (0.48-cm) diameter hole was drilled through the center. This minimized the disturbance to the sample and kept the sample intact.

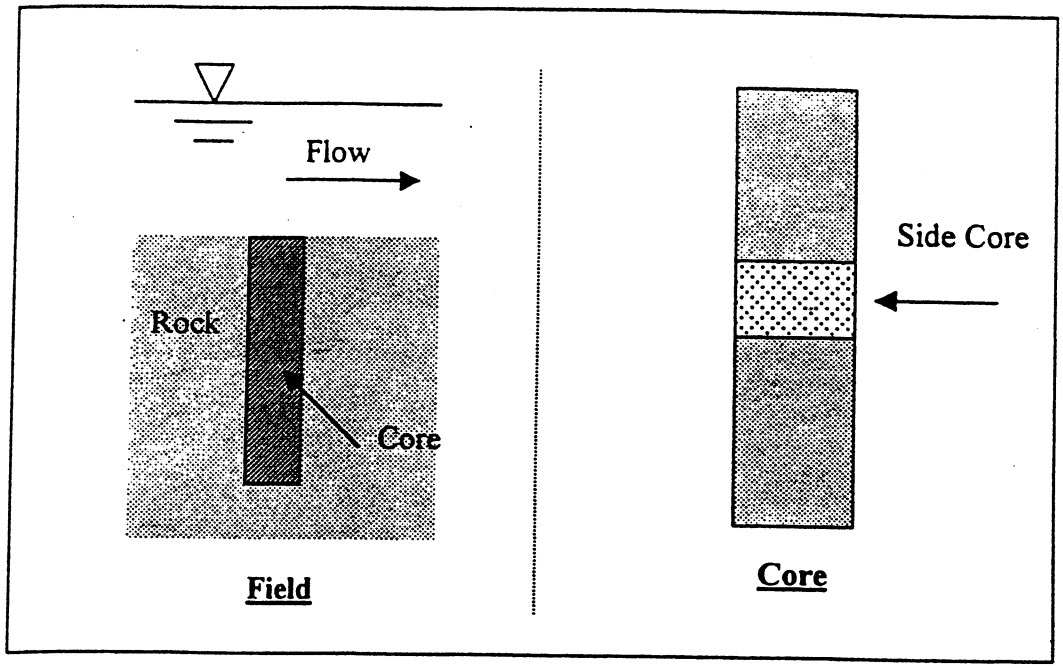

Figure 3.10. Side Coring from Rock Core

3.7.2 Erosion Testing

The procedures described herein were developed to perform the rock erosion experiments. Below is a list of equipment required for these experiments:

- rotating cylinder erosion device,
- concrete wet corer,
- 2.00-in (5.08-cm) OD/1.75-in (4.45-cm) ID wet core bit,
- 3/16-in (0.48-cm) masonry drill bit,
- drying dish,
- drying oven (Located in UF's Geotechnical Engineering Lab),
- calipers,
- Pi tape,
- mass balance (with an accuracy of ± 0.01 g),
- 1000 ml graduated cylinder,
- water,
- hand held tachometer, and
- stopwatch.

The erosion testing procedures are described in detail below.

1. Prepare the sample for erosion testing as described in Section 3.7.1 by using the concrete wet corer and masonry drill bit.
2. Record the mass of the sample with the mass balance.
3. Place the sample in the drying oven for at least 16 hours to dry. After that time, record the mass of the sample. The sample is considered dry when the mass change is less than 0.1% in a period greater than 1 hour. Record the sample dry mass.
4. Measure the diameter of the sample with the Pi Tape at a minimum of 3 locations with the calipers and record the average diameter of the sample.
5. Measure the length of the sample with the calipers.
6. Measure the volume of the sample by gently submerging the sample in a graduated cylinder and measure the volume of water displaced.
7. Compute the sample dry density from the above measurements in g/cm^3.
8. Collect the water and loose material in a drying dish. Place the drying dish in the drying oven to remove the water. Record the mass of remaining material.
9. Completely immerse the sample in water for at least 16 hours to hydrate. The sample is hydrated to simulate a saturated rock formation as may be found in a waterway bed. After that time, record the mass of the sample. The sample is considered hydrated when the mass change is less than 0.1% in a period greater than 1 hour.

Rock Erosion Test:

1. Secure sample on the threaded rod with the platens and place the sample in the rotating cylinder erosion-testing device.

2. Fill the rotating cylinder annulus with water to the proper level. It is important to note that water from the actual field site where the sample was collected should be used.
3. Place the rubber stopper on the acrylic cylinder and then attach sample to torque cell.
4. Set the offset of the torque cell with the tare switch to 0.000 mm-N.
5. Turn on the motor and increase the RPMs (as measured by the tachometer) until the desired torque is achieved.
6. Allow the test to run for a minimum of 72 hours. Record the duration of the experiment in min with the stopwatch. Periodically adjust the motor speed to keep a constant torque on the sample. Record the torque in mm-N applied to the sample.
7. Turn off the motor and allow the water within the annulus to cease motion.
8. Remove the sample from the torque cell and cylinder.
9. Empty the water out of the cylinder and clean out the eroded particles in the cylinder.
10. Place the sample in the drying oven for at least 16 hours to dry. After that time, record the mass of the sample. The sample is considered dry when the mass change is less than 0.1% in a period greater than 1 hour. Record the sample dry mass.

There are a few important items to note with regards to the experimental procedures. First, prior to beginning the actual erosion experiments, a preparation run is required. The preparation run is required to remove loose material from the surface of the

rock sample prior to measuring the erosion. The coring process disturbs the surface of the sample and this may cause an excessive amount of material to erode that may not have eroded otherwise. The preparation run was conducted after the sample dimensions were recorded but prior to the first experiment.

Also, at times, a slight amount of material would be removed from the sample during the saturation process. This material was collected and weighed (dry weight). This value was then subtracted from mass lost prior to the experiment so the change in mass would reflect the amount of material lost during the experimental run.

3.7.3 Calculations

This section explains the calculations that were made from measurements collected during the experiments. The calculations consisted of determining the mass lost during an erosion test, the shear stress acting on the surface sample and the rate of erosion. The calculations are as follows:

1. Mass lost (g) = Sample dry mass (g) - Sample dry mass after experiment (g) - mass lost from hydration (g)

2. $$\text{Shear Stress (Pa)} = \frac{\dfrac{\text{Torque (mm - N)}}{\text{Sample Radius (mm)}}}{\text{Sample Surface Area (m}^2\text{)}}$$

3. $$\text{Erosion Rate (cm / min)} = \frac{\dfrac{\text{Mass Lost (g)}}{\text{Dry Density (g / cm}^3\text{)}}}{\dfrac{\text{Sample Surface Area (cm}^2\text{)}}{\text{Experiment Duration (min)}}}$$

4. Convert to mm / hr and plot Erosion Rate (mm / hr) vs. Shear Stress (Pa)

In the calculations above, the erosion rate is expressed as mm/hr. In cohesive soil studies, this erosion rate is typically expressed as mass/area-time

(such as g/m^2-min). In this study, the erosion was converted as a length/time or an "effective" erosion rate. The purpose of this conversion was to provide an estimate of erosion in terms of a design situation. That is, how much will the bed level be lowered in a finite amount of time.

CHAPTER 4
LABORATORY RESULTS

This chapter discusses the results of the experiments that were performed to evaluate the critical stress and rates of erosion of rock materials. Erosion experiments were performed on two samples collected from rock corings at a bridge site in Florida. The conclusions that can be drawn from these experiments are presented in the next chapter.

4.1 Cemented Sand

The first experiment was conducted on a rock sample from the 17th Street Temporary Bridge in Fort Lauderdale, Florida collected on April 16, 1997. The boring log that accompanied the sample described the rock as a "Loose Cemented Sand". The sample was collected from a proposed bridge pier location at a depth interval of 27.92 m and 30.97 m (91.58 ft and 101.58 ft) below the mudline.

Experiments on this sample were conducted at the University of Florida between March 25, 1999, and April 23, 1999, in the rotating cylinder testing apparatus. The sample was tested at 4 different shear stresses. Table 4.1 presents the dimensions of the sample. Table 4.2 presents the results of the experiments. Figure 4.1 presents a plot of the erosion rate, $\dot{e}$, versus average shear stress, $\overline{\tau}$.

Table 4.1. Loose Cemented Sand Dimensions

Dry mass (g)	147.48
Diameter (cm)	4.45
Height (cm)	7.34
Volume (cm^3)	72.02
Density (g/cm^3)	2.05
Surface Area (cm^2)	102.53

Table 4.2. Loose Cemented Sand Test Results

Run No.	RPMs	Torque N-mm	$\bar{\tau}$ Pa	Duration Min	Mass lost g	Erosion rate $\dot{e}$ mm/hr
1	2280	4.4	19.3	4307.57	0.47	3.12×10^{-4}
2	1500	1.5	6.6	4389.85	0.12	7.81×10^{-5}
3	1856	2.7	11.8	4436.92	0.09	5.80×10^{-5}
4	2010	3.6	15.8	3185.07	0.35	3.14×10^{-4}

Since the amount of material being eroded was less than 1 g and the torque being measured was between 1 and 5 N-mm, uncertainty bars were assigned to the data collected. The purpose of assigning uncertainty bars in this case is to provide an understanding of the possible ranges of values especially in dealing with small quantities. The method used to estimate the uncertainty was proposed by Stein (1964). The method provides an estimate of the largest possible error that the uncertainties of individual quantities create on the final result. Stein states that the method is not entirely defensible

on statistical grounds but it represents an excellent technique for checking the general tolerances on predicted or measured values (Stein, 1964, p. 41).

The procedure consists of first determining the uncertainty for an individual measurement (ΔX for variable X). The unit error for a measurement is expressed as $\Delta X/X$. The final answer is expressed in terms of the measured variables. The logarithm is taken of each side of the equation and then the derivative of both sides is taken. It is then assumed that the unit errors are sufficiently small to substitute into the equation. That is, $\Delta X/X$ (the unit error) can be substituted for the derivative of Log X. The signs for the individual quantities are placed in the same direction. This procedure assumes that all measurement errors are combined in the most unfavorable way to result in maximum error (Stein, 1964, pp. 41-42).

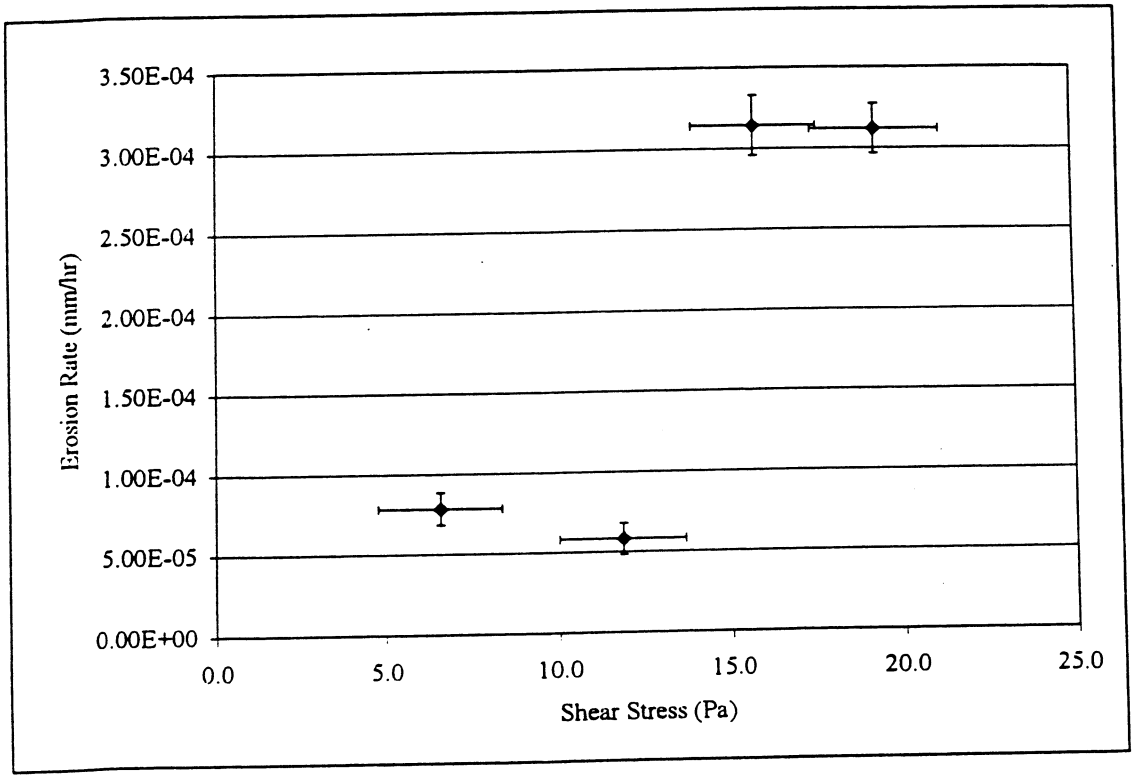

Figure 4.1. Experimental results for Loose Cemented Sand

It should be noted that the experimental run at 15.8 Pa (Run No. 4), which was the last experiment run on this sample, was performed for 53 hours as opposed to the minimum 72 hours that was described in the previous chapter. This was due to a vibration in the system that was observed. It was determined that the bearing holding the ½-in diameter shaft was showing the results of wear. The test was terminated at 53 hours as there was a concern that the vibrations may "shake" the sample within the cylinder and cause material to shake loose from the samples. This may have caused a greater erosion rate than would have occurred without the vibration.

Based on the above results, for the loose cemented sand sample, the erosion rates ranged between 5.80×10^{-5} mm/hr and 3.14×10^{-4} mm/hr for a range of shear stresses between 6.6 Pa and 19.3 Pa.

4.2 Sandstone

The second experiment was conducted on a rock sample from the 17th Street Temporary Bridge in Fort Lauderdale, Florida collected on April 14, 1997. The boring log that accompanied the sample described the rock as a "Dark Tan sandstone with Small Voids and No Shells." The sample was collected from a proposed bridge pier location at a depth interval of 29.93 m and 30.54 m (98.18 ft and 100.18 ft) below the mudline. This sample was collected at the same bridge location but different pier as the Cemented Sand sample described in Section 4.1.

Experiments on this sample were conducted at the University of Florida between April 12, 1999 and April 26, 1999 in the rotating cylinder testing apparatus. The sample was tested at one shear stress. Table 4.3 presents the dimensions of the sample. Table 4.4

presents the result of the experiment. Figure 4.2 presents a plot of the erosion rate, $\dot{e}$, versus average shear stress, $\bar{\tau}$.

Table 4.3. Dark Tan Sandstone Dimensions

Dry mass (g)	191.24
Diameter (cm)	4.47
Height (cm)	6.93
Volume (cm^3)	90.03
Density (g/cm^3)	2.12
Surface Area (cm^2)	97.19

Table 4.4. Dark Tan Sandstone Test Results

Run No.	RPMs	Torque N-mm	$\bar{\tau}$ Pa	Duration Min	Mass lost Δg	Erosion rate $\dot{e}$ mm/hr
1	2080	2.3	10.6	4334.00	0.25	1.68×10^{-4}

A second experimental run was conducted for this sample at a shear stress of 2.3 Pa (approximately 900 RPMs). This run was performed immediately after the Run No. 4 of the Loose Cemented Sand sample (at 15.8 Pa). This experimental run was unsuccessful, as excessive vibrations were visible. The sandstone sample was visibly "shaking" which most likely altered the erosion rate and thus invalidated the test.

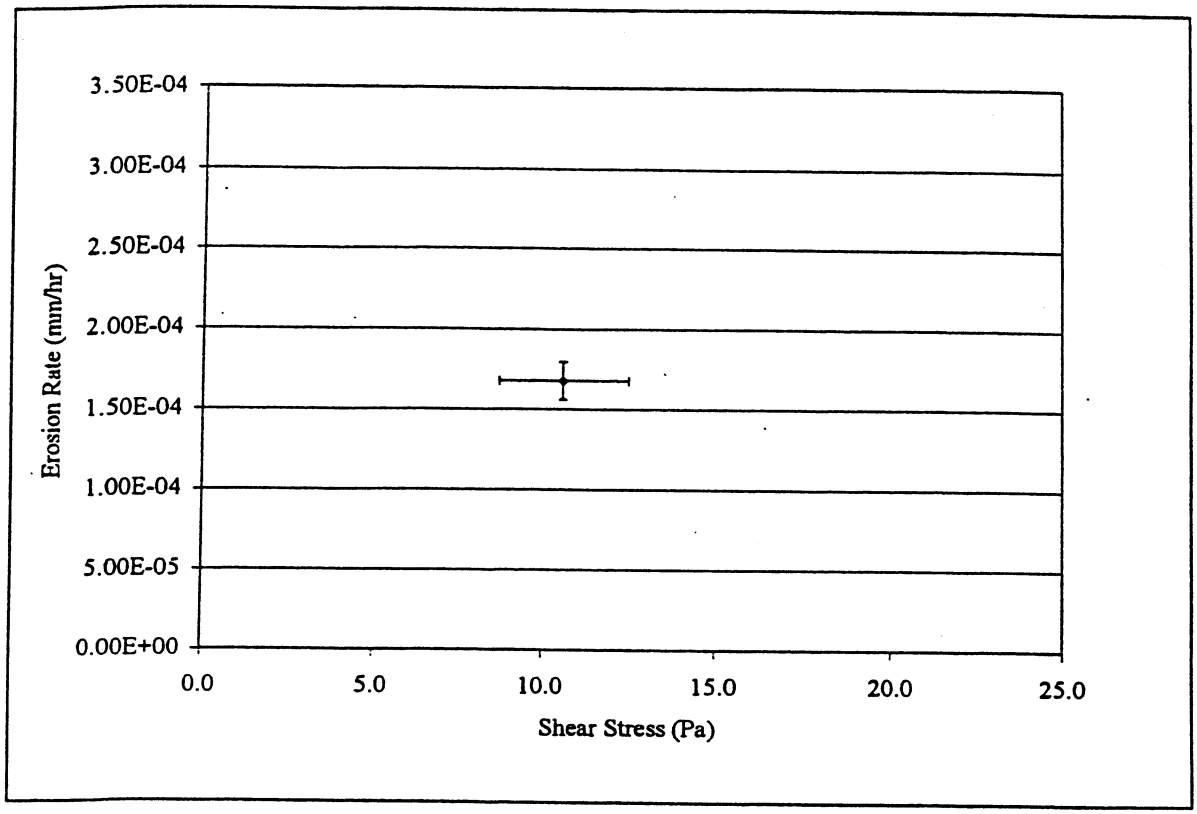

Figure 4.2. Dark Tan Sandstone

CHAPTER 5
CONCLUSIONS

This chapter discusses the conclusions that can be drawn from the data collected from the rotating cylinder apparatus. It is important to note that the data collected from the experiments should be considered preliminary as additional tests are needed at the same shear stresses and the range should be extended.

5.1 Analysis of Cemented Sand and Sandstone Tests

Figure 5.1 is a plot of both the Loose Cemented Sand and Dark Tan Sandstone erosion data A trend line was fitted through the Cemented Sand data with the Microsoft Excel software. The Cemented Sand and Sandstone samples were similar samples in appearance and texture. This linear relationship is based on only 4 data points for the Cemented Sand. Research conducted by Chapius and Gatien in the area of cohesive soil erosion found that between 6 and 10 samples were required to be tested to achieve a good evaluation of the erodibility of a clayey material for a given eroding water. The number of samples allow for a statistical determination of the critical shear stress and the mean erosion rate as a function of shear stress (Chapius and Gatien, 1986, p. 86).

As described in Chapter 2, rock is a non-homogenous and anisotropic material. It is anticipated that, similar to the results found by Chapius and Gatien, that several samples must be tested to develop the erosion relationship. Therefore, the results presented here are preliminary, as only one sample was tested. The test results have the anticipated trend

but a number of additional tests are needed before the variability of the samples and the locus of highest values can be established.

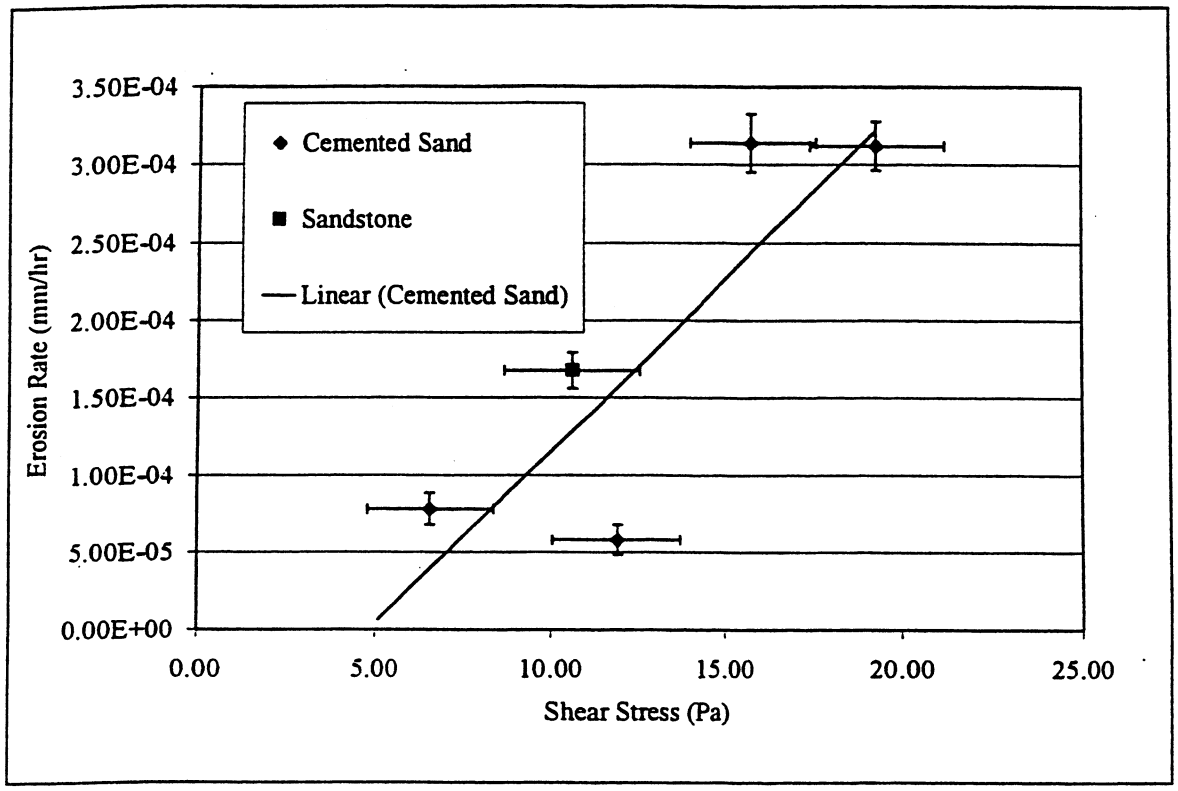

Figure 5.1. Cemented Sand and Sandstone Erosion Rate Data

To provide an estimate of the type of flow conditions that would produce the range of shear stresses tested in the apparatus, the Prandtl-von Karman formula was used. For hydraulically rough beds

$$\overline{U} = 2.5\overline{u}_* \ln\left(\frac{11.0d}{k_s}\right), \qquad \textbf{Equation 5.1}$$

where $\overline{U}$ = depth average velocity,

$\overline{u}_*$ = friction velocity,

d = water depth, and

k_s = Nikuradse Roughness Length.

The average shear stress on the bed can be calculated from

$$\overline{\tau}_0 = \overline{u}_*^2 \rho . \qquad \textbf{Equation 5.2}$$

A water depth of 7.6 m (25 ft) in freshwater and k_s = 0.20 m (0.66 ft) was used for the calculation. A shear stress of 3.6 Pa is produced for a depth averaged velocity of 0.91 m/s (3 ft/s), 6.5 for Pa for 1.22 m/s (4 ft/s), and 10.1 Pa for 1.52 m/s (5 ft/s). For example, if a bed of cemented sand (Figure 5.1) was subjected to a shear stress of 10 Pa 24 hours per day, 365 days a year, for 50 years, a total of only 5.5 cm (0.2 ft) of material would be eroded based on the preliminary test data.

Figure 5.2 is a plot of the data for the Cemented Sand sample with conceptual relationships provided. Figure 5.1 shows a linear relationship. However, researchers studying cohesive soil erosion, including Chapius and Gatien (1986), showed that the erosion rate relationship can be represented by a composite of two straight lines with different slopes. The point of intersection of the two lines is referred to as the characteristic value. The first line is followed by a second line with a larger slope, which indicates a greater erosion rate. The line with the larger slope may be extrapolated to intersect the Erosion Rate = 0 axis to determine the critical shear stress for cohesive soil erosion (Mehta, 1981, p. 124). The data collected in this study may support a similar relationship as shown on Figure 5.2.

Mehta (1981) suggested that there may be several factors that influence the location of the characteristic value in cohesive soils. These include the sampling method, grain size, salinity, temperature, pH, water content, shear strength, consolidation, and pre-

erosion contact time. In addition, the characteristic values of cohesive soils may vary between experiments. Mehta (1981) suggests that this may be a result of erosion being a stochastic phenomenon. That is, the distribution of the instantaneous bed shear stress and the spatial distribution of the orientation and of the bond strength of the surficial particles are factors that influence the rate of erosion.

Also, for design purposes where a conservative estimate is needed, the conceptual design curve shown in Figure 5.2 would be appropriate. This is a linear relationship through points on the extremes of the uncertainty bars. This relationship would provide the greatest erosion rates.

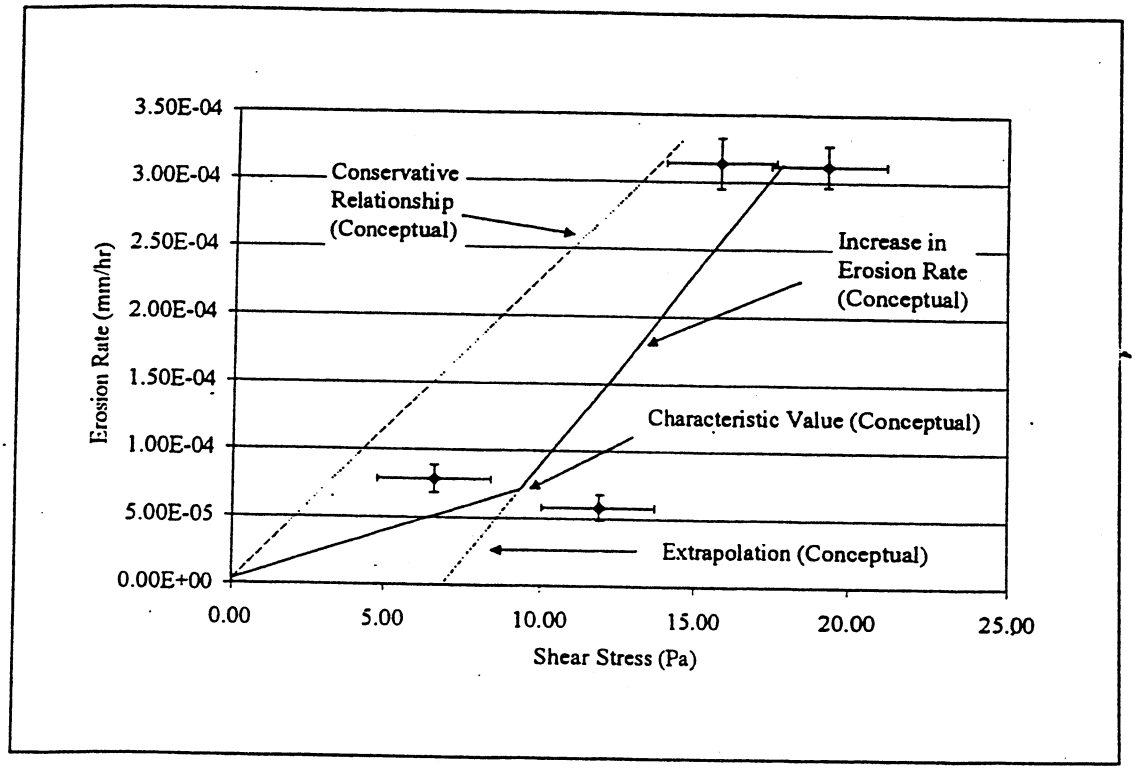

Figure 5.2. Conceptual Rock Erosion Relationships

For comparison purposes with erosion rates for other types of materials, the erosion rates for the Cemented Sand samples were converted to g/(m^2-min). The erosion rates for the Cemented Sand samples tested in this study ranged from 0.00198 - 0.011 g/(m^2-min). As described in Chapter 3, Akky and Shen (1973) tested the erodibility of cement-stabilized sandy soil under various physical and environmental conditions. Akky and Shen (1973) varied the amount of cement mixed with the sandy soil and also applied various numbers of wet-dry and freeze-thaw cycles to the samples. The erosion rates ranged from 0 – 375 g/(m^2-min) (which occurred for a sample after 12 freeze-thaw cycles). Chapius and Gatien (1986) noted that the usual range for natural clays was 0 - 30 g/(m^2-min) as compared to 0 – 100 to 1000 g/(m^2-min) for artificial clays.

5.2 Influence of Microcracks on Erosion

As described in Section 3.7 Experimental Procedures, prior to performing the experiments, a sample preparation run must be performed. The purpose of the preparation is to remove the layer of material that has been disturbed due to the coring procedure. It is likely that the stresses placed on the rock sample from may influence increases the number of microcracks in the sample and alters the stress state. It is noticed that for the same shear stress, a greater amount of material was eroded during the preparation run than an experimental run. The number of microcracks may increase the erosion rate for a sample. Microcracks were discussed in Section 2.1. Chapter 6 recommends additional research to investigate the possible influences of the state of stress and microcracks on the rate of ersoion.

5.3 Further Experiments

The experiments have shown that erosion relationships for rock may be developed. However, additional testing is required to establish definitive testing procedures. The tests that should be conducted include:

- performing multiple tests on the same sample and similar samples to evaluate the variability of the erosion properties and the repeatability of the tests,
- for a given sample, perform an experiment from the lowest shear stress to the highest shear stress and vice versa to evaluate if the magnitude and timing of the shear stress have any influence on the test results,
- measuring the calcium carbonate ($CaCO_3$) content of the eroding fluid before and after the experiments to evaluate if there is any dissolution of the sample during the test,
- varying the water chemistry parameters such as salinity to evaluate their influences on the rates of erosion, and
- adding a cohesionless sediment such as sand to the eroding fluid to evaluate if it would act as an abrading agent and influence the rates of erosion.

5.4 Design Improvements

After working with the rotating cylinder apparatus for rock erosion, there are several design improvements suggested to improve the existing device. Particularly, it was noticed during start-up activities that there was a vibration in the motor/shaft/acrylic cylinder system between 3000 and 4000 RPMs. This vibration was significant enough to preclude tests from being run between these speeds. The vibration was attributed to the difficulty in finely balancing the system for high speeds. It is suggested that the ½-in diameter shaft be replaced by a larger shaft and the top and bottom acrylic pieces of the acrylic cylinder be replaced by a larger diameter and heavier material. This would assist in damping the vibrations at high speeds. In addition, the cylinder could be supported at a

second point, near the top of the cylinder. This would provide support and help reduce vibrations at the higher speeds.

CHAPTER 6
FURTHER RESEARCH

As discussed in the conclusions presented in Chapter 5, a laboratory apparatus and testing method has been developed to estimate the rate of erosion of soft rock materials. The results can be used to estimate contraction scour depths at proposed bridge sites and may be used to estimate local scour depths. Based on the results and conclusions of this work, the following is a list of proposed research efforts:

- Evaluate rock erosion at actual bridge sites - To build a database of the erosion rates of several different types of rock materials found in the State of Florida, samples of erodable rock materials can be collected from design and construction borings being performed at actual bridge sites. The samples can be tested and the rates of erosion should be established for these rock materials. This information can be used for evaluation purposes by hydraulic engineers to assess potential erosion depths and scour severity for different types of rock materials in Florida. While it will most likely be necessary to actually test the rock materials at a specific site to assess the scour depths, estimates of scour depths based on the type of material may aid in the pre-design and conceptual design phases of the project.
- Comparison of sample orientation with the rate of erosion – It is necessary to design and construct a laboratory device that can test a rock sample from a core at different orientations. As described previously, the current laboratory device tests a sample that

is extracted from the side of a rock core. The purpose of this is to test, as best as possible, the stress plane that is parallel to the flow. However, in a case of local scour, the face or planes of the rock materials may not be oriented parallel to the flow. In addition, it would be advantageous for the FDOT to be able to test the rock cores directly from a boring as opposed to coring from the side of the sample. A modified rotating device should be constructed to be able to test the 4-in diameter rock cores. This would allow for a comparison of the results with the 1.75-in diameter cores to evaluate if there is indeed a difference between the rates of erosion and the stress plane's orientation to the flow. The preliminary tests used to gain insight into the order of magnitude of the rate of erosion indicated that the vertical planes eroded faster than the horizontal planes for the same flow conditions. If this is true in general, then using the vertical cores as samples would provide conservative results (i.e. yield higher erosion rates for the same shear stress).

- Comparison of the measurement of the rates of erosion with varying measurement devices – The rotating cylinder laboratory testing device is one type of device to estimate the rates of erosion. As described in Chapter 3, there are certain limitations to this type of device. A second type of erosion testing device is currently being designed and constructed by the University of Florida to test the erosion rates of both cohesive sediments and erodible rock materials. This device is an annular flume where the sample is raised into the flow as the material is eroded. Samples of the same rock materials can be tested in both types of devices and their respective erosion rates can be compared. This will provide an estimate as to the effects of the limitations of the rotating device on the measured rates of erosion.

- Evaluation of the Erodibility Index Method and the laboratory measurement of the rates of erosion – To evaluate the estimates of the depth of scour that can be computed using the Erodibility Index Method described in Chapter 2, rock samples can be collected and tested at a specific bridge site. The necessary geotechnical engineering properties can be collected during the boring process and the depth of scour can be computed. Then samples of the rock material from the coring can be tested in the rotating cylinder laboratory testing device to estimate the rates of erosion. Estimates and assumptions can be made to evaluate the design flow condition (500-year storm) and the depth of scour can be compared for both methods. This will provide estimates as to the difference and the degrees of conservatism, if any, between the estimates.
- Effect of dilitancy and compressibility in rates of erosion – By pre-stressing the rock samples prior to testing in the rotating cylinder laboratory testing device, the dilitancy, compressibility, and number of microcracks can be varied. The erosion rates for each of these states can be compared to evaluate the influence that they may have on the erosion rates. This may be very important in design considerations. The method of construction (such as drilled shafts or driven piles) of the bridge piers can influence the state of stress in the underlying rock materials. It may be necessary to take the method of construction into account in the estimates of the scour depths based on the measured data.

These further research items are necessary and important in continuing to provide a better understanding of not only the rock erosion process itself, but the factors that

influence the rates of erosion and the methods for estimating the depths of scour. The University of Florida is currently proceeding with the additional research in many of these areas.

REFERENCES

Akky, M.R., and Shen, C.K., 1973. "Erodibility of a Cement-Stabilized Sandy Soil." Soil Erosion: Causes and Mechanisms; Prevention and Control, Conference Workshop on Soil Erosion, Highway Research Board Special Report 135, Washington, DC, pp. 30-41.

Alizadeh, A., 1974. "Amount and Type of Clay and Pore Fluid Influences on the Critical Shear Stress and Swelling of Cohesive Soils." Ph.D. dissertation, University of California, Davis.

Anglin, C.D., Nairn, R.B., Cornett, A.M., Dunaszegi, L., Turnham, J., and Annandale, G.W., 1997. "Bridge Scour Assessment for the Northumberland Strait Crossing." Proceedings from the 1997 Canadian Coastal Conference, May 21-24, pp. 89-101.

Annandale, G.W., 1995. "Erodibility." Journal of Hydraulic Research, Vol. 33, No. 4, pp. 471-493.

Annandale, G.W., Smith, S.P., Nairn, R., and Jones, J.S., 1996. "Scour Power." Civil Engineering, American Society of Engineers, July, pp. 58-60.

Arulanandan,K., Sargunam, A., Loganathan, P., and Krone, R.B., 1973. "Application of Chemical and Electrical Parameters to Prediction of Erodibility." Soil Erosion: Causes and Mechanisms; Prevention and Control, Conference Workshop on Soil Erosion, Highway Research Board Special Report 135, Washington, DC.

Bobb, N.M., 1995. "California's Temporary Freeway Bridge." Public Roads Magazine – On-Line, Turner-Fairbank Highway Research Center, http://www.tfhrc.gov/pubrdsfall95/p95a2.htm.

Brooks, H.K., 1981a. "Geologic Map of Florida." Florida Cooperative Extension Service, Institute for Food and Agricultural Sciences (IFAS), University of Florida, Gainesville, FL.

Brooks, H.K., 1981b. "Guide to the Physiographic Divisions of Florida." Florida Cooperative Extension Service, Institute for Food and Agricultural Sciences (IFAS), University of Florida, Gainesville, FL.

Brooks, H.K., 1981c. "Physiographic Divisions of the State of Florida." Florida Cooperative Extension Service, Institute for Food and Agricultural Sciences (IFAS), University of Florida, Gainesville, FL.

Chapius, R., and Gatien, T., 1986. "An Improved Rotating Cylinder Technique for Quantitative Measurements of the Scour Resistance of Clays." Canadian Journal of Geotechnical Engineering, Vol. 23, pp. 83-87.

Cornett, A., Sigouin, N., and Davies, M., 1994. "Erosive Response of Northumberland Strait Till and Sedimentary Rock to Fluid Flow." National Research Council of Canada, Institute for Marine Dynamics, TR-1994-22, September, Ottawa, Canada, pp. 1-15, 26-27.

Cristescu, N., 1989. Rock Rheology. Kluwer Academic Publishers, Dordrecht, The Netherlands, p.1.

Froehlich, D.C., Hopkins, T.C., and Beckham, T.L., 1995. "Preliminary Assessment of Local Scour Potential at Bridge Piers Founded on Rock." Proceedings of the First International Conference Sponsored by the Water Resources Engineering Division of the American Society of Civil Engineers, Vol. 2, San Antonio, TX, pp. 976-980.

Gordon, S., 1991. "Scourability of Rock Formations." Federal Highway Administration Memorandum, July 19, Washington, DC.

Harper, S.B., 1999. Coquina, Sedimentary Rock Index, Department of Geology, Eastern Carolina University, http://index.ecu.edu/geology/harper/Sedimentary/display.cfm?ID=6.

Judson, S., Kauffman, M.E., and Leet, L.D., 1987. Physical Geology. 7th ed., Prentice-Hall, Englewood Cliffs, NJ, pp. 90-114, 465.

Jumikis, A.R., 1983. Rock Mechanics. 2nd ed., TRANS TECH Publications, Clausthal-Zellerfeld, Federal Republic of Germany, pp. 37-45, 51-53.

Lewis, G.L., 1993. "Shale Scour at BNRR Yellowstone River Bridge, MT." 1993 Proceedings of the National Conference on Hydraulic Engineering, American Society of Civil Engineers, New York, NY, pp. 2255-2257.

Mehta, A.J., 1981. "Review of Erosion Function for Cohesive Sediment Beds." Proceedings of the First Indian Conference on Ocean Engineering, Indian Institute of Technology, Madras, India, Vol. 1, pp. 122-130.

Merrington, A.C., 1949. Viscometry. Edward Arnold, London, England, p.32.

Moore, W.L. and Masch. F.D., 1962. "Experiments on the Scour Resistance of Cohesive Sediments." Journal of Geophysical Research, Vol. 67, No. 4, April, pp. 1437-1446.

Pagan-Ortiz, J.E., 1998. "Status of the Scour Evaluation of Bridges Over Waterways in the United States." Proceedings of the International Water Resources Engineering Conference, Vol. 1, Water Resources Engineering 98, American Society of Civil Engineers, Memphis, TN, p. 2.

PSI – Professional Services Industries Inc., 1996. Preliminary Geotechnical Engineering Study, U.S. 441 Bridge Over Santa Fe River, WPI No. 2110486, October 10, pp. 2-10.

Randazzo, A.F. and Jones, D.S., 1997. The Geology of Florida. University Press of Florida, Gainesville, FL.

Rektorik, R.J., and Smerdon, E.T., 1964. "Critical Shear Stress in Cohesive Soils from a Rotating Shear Stress Apparatus." Paper No. 64-216, American Society of Agricultural Engineers, June.

Richardson, E.V. and Davis, S.R., 1995. "Evaluating Scour at Bridges." 3rd ed., Hydraulic Engineering Circular No. 18, Publication No. FHWA-IP-90-017, Office of Technology Applications, HTA-22, Washington DC.

Rohan, K. and Lefebvre, G., 1991. "Hydrodynamic Aspects in the Rotating Cylinder Erosivity Test." Geotechnical Testing Journal, Vol. 14, No. 2, June, pp. 166-170.

Sargunam, A., Riley, P., Arulanandan, K., and Krone, R.B., 1973. "Effect of Physicochemical Factors on the Erosion of Cohesive Soils." Journal of the Hydraulic Divisions, Proceedings of the American Society of Civil Engineers, Vol. 99, No. HY3, March, pp. 555-558.

Shepard, J.D., and Frost, R., 1995. Failures in Civil Engineering: Structural, Foundation, and Geoenvironmental Case Studies. American Society of Civil Engineers, New York, p. 9.

Smith, S.P., 1994. "Preliminary Procedure to Predict Bridge Scour in Bedrock." Colorado Department of Transportation, Report No. CDOT-R-SD-94-14, Denver, CO, December.

Stein, P.K., 1964. Measurement Engineering. 3rd ed., Stein Engineering Services, Inc., Phoenix, AZ, 1964, pp. 41-42.

Van Dyke, M., 1982. An Album of Fluid Motion. The Parabolic Press, Stanford, CA, 1982, pp. 76-77.

Van Rijn, L.C., 1993. Principles of Sediment Transport in Rivers, Estuaries, and Coastal Seas. Aqua Publications, Amsterdam, The Netherlands, p. 4.1.

BIOGRAPHICAL SKETCH

Matthew Henderson was born in New Hartford, New York, in 1968. He grew up in Central New York and spent many summers on the shores of Lake Ontario with his family.

He received a bachelor of science degree with distinction in civil engineering from Worcester Polytechnic Institute in 1991. Upon graduation, he accepted employment with O'Brien & Gere Engineers, Inc., in Syracuse, New York, as a Civil and Environmental Engineer. He was promoted from Staff Engineer to Design Engineer in 1992 and to Project Engineer in 1994.

In 1996, he left the firm to pursue a graduate degree in Coastal & Oceanographic Engineering at the University of Florida in Gainesville, Florida. After his August 1999 graduation with a master of science degree from the University of Florida, he looks forward to a career in coastal engineering.

APPENDIX B

UFL/COEL-2000/011

PERFORMANCE REPORT ON THE SIMULATOR OF EROSION RATE FUNCTION

By

Neil K. Ganju
Kevin M. Barry
and
Ashish J. Mehta

Submitted to:

U.S. Army Engineering Research and Development Center
Waterways Experiment Station
3909 Halls Ferry Road, Vicksburg, MS 39180

Coastal and Oceanographic Engineering Program
Civil and Coastal Engineering Department
University of Florida
Gainesville, FL 32611

September, 2000

SUMMARY

Numerous rotating cylinder devices have been constructed to simulate the erosion characteristics of cohesive sediments. Typically, these devices consist of a rotating outer cylinder, which is filled with the chosen eroding fluid. A remolded or intact sample in the shape of a smaller cylinder is placed into the outer cylinder. While rotating, the outer cylinder imparts rotation to the fluid, which translates into a shear stress being uniformly imparted to the sample. The torque applied to the sample is measured and converted to the corresponding shear stress. Erosion of the sample follows, and a relation is obtained between shear stress and erosion rate. A rotating cylinder device - the Simulator of Erosion Rate Function (SERF) - was constructed and it's performance tested. SERF consists of an rotating acrylic outer cylinder filled with eroding fluid, and an inner stationary cylinder which holds the sample between brackets. A torque cell is connected to the stationary cylinder via a shaft, and measures the applied torque. A load cell connected in turn to the torque cell measures the weight of the sample.

SERF was initially tested with aluminum cylinders representing dummy samples to calibrate for shear stress, following which three commercial types of ceramic clay samples were tested. Each sample was run by step-increasing the rpm and the loss in sample mass was recorded over each time-step. A relation (erosion rate function) between erosion rate and shear stress was obtained for the sample. The erosion rate function was found to be linear or piece-wise linear, depending on the degree of uniformity of the sample. Furthermore, increasing shear strength correlated with increasing density for all three clay types.

This work was supported by funds from The U.S. Army Engineering Research and Development Center, Waterways Experiment Station, Vicksburg, MS, through contract DACW39-99-P-0238.

TABLE OF CONTENTS

LIST OF FIGURES

LIST OF TABLES

LIST OF SYMBOLS

A	surface area (m^2)
F_T	applied tangential force (kg)
R	inner cylinder radius (m)
Re	Reynolds number (-)
RPM	revolutions per minute
T	torque (kg-m, g-cm)
T_a	Taylor number (-)
U	annular peripheral velocity (m/s)
d	annular gap width (m)
g	acceleration due to gravity (m/s^2)
Δm_s	change in dry sediment mass (kg)
r	radius (m)
Δt	time interval (s)
α	empirical coefficient, Eq. 5.3 (-)
β	empirical coefficient, Eq. 5.3 (-)
χ_s	empirical coefficient, Eq. 5.2 (-)
ε	erosion rate (kg/m^2-s)
ε_N	erosion rate constant (kg/N-s)
ε_{NO}	maximum erosion rate constant (kg/N-s)
λ_s	empirical coefficient, Eq. 5.2 (-)
ρ	sediment bulk density (kg/m^3)
ρ_d	dry density (kg/m^3)

ρ_f	pore fluid density (kg/m^3)
ρ_l	fluid mud density (kg/m^3)
ρ_s	sediment granular density (kg/m^3)
τ	shear stress (Pa)
τ_b	sample shear stress (Pa)
τ_s	shear strength (Pa)
ν	kinematic viscosity (m^2/s)

PERFORMANCE REPORT ON THE SIMULATOR OF EROSION RATE FUNCTION

1. Introduction

Numerous, rotating cylinder devices have been constructed to simulate the erosion characteristics of cohesive sediment (Moore and Masch, 1962; Arulanandan et al., 1975; Croad, 1981; Chapuis and Gatien, 1986). Lee and Mehta (1994) have provided a brief summary of the underlying design-and-operation concept. Typically these devices consist of a rotating outer cylinder, which is filled with the chosen eroding fluid A remolded or intact sample in the shape of a smaller cylinder is placed into the outer cylinder. While rotating, the outer cylinder imparts rotation to the fluid, which translates into a shear stress being uniformly imparted to the sample. The torque applied to the stationary sample is measured and converted to the corresponding shear stress. Erosion of the sample follows, and a relation (erosion rate function) is obtained between erosion rate and shear stress. The device requires calibration to convert the torque into an applied shear stress, as well as some method to measure the eroded mass. For the unit developed and tested, i.e., the Simulator of Erosion Rate Function (SERF), dummy aluminum cylinders were used to calibrate for the shear stress via the attached torque cell. A load cell allowed the eroded mass to be measured without removing the sample assembly from the outer cylinder. The inclusion of the load cell is an improvement over previous devices, which required removing either the sample or fluid to measure eroded mass. Three types of commercial clays were tested to gauge the performance of the SERF.

2. SERF Characteristics

Figure 2.1 shows the schematic of the SERF, and Figs. 2.2a,b show photographic views. The clay sample is molded into a cylinder with a diameter of 7.6 cm and a height of 9.6 cm. The cylinder is impaled on a shaft which secures an upper and a lower disk of equal diameters to the

two ends of the sample. The upper end of the shaft affixes to an Omega (Stamford, CT) model TQ201-100Z torque cell, which is in turn connected to an Omega model LC601-5 load cell. When the acrylic outer cylinder is rotated, the chosen eroding fluid imparts a torque to the sample, and in turn the shaft and torque cell. The cell is connected to an Omega model DP25-S LED (light-emitting diode) display, and shows the applied torque in g-cm. The load cell is attached to the entire shaft/torque cell/sample assembly, and can be used to measure mass eroded after a given run. This unit can move vertically out of the outer cylinder for sample and water replacements.

The outer cylinder is capable of rotating at a maximum of 2,350 rpm, and a minimum of 150 rpm. The torque cell has a 1,800 g-cm capability, and the load cell can accommodate a maximum of 2.3 kg.

3. SERF Calibration

The torque cell is calibrated using an aluminum ring which affixes to the shaft of the cell. A two-point calibration is done using no load, and then with a 1,000 g weight hanging from the ring, which has a radius of 1 cm. This results in a calibration between 0 and 1,000 g-cm. The load cell is calibrated in the same two-point fashion, using a 1,000 g weight hung from the cell.

The calibration to convert torque into shear stress requires running the device with dummy samples. The SERF was run with three aluminum cylinders of varying diameter and identical height. The varying of diameters provides a relationship between the applied torque and the sample radius, considered to be necessary in instances when the radius of a sample decreases measurably during testing. For a given cylinder, the SERF was rotated from a standstill to a "reasonable" speed (up to 1,600 rpm) in time-step increments, and torque readings were taken at each rpm value, after steady-state was reached (typically within 3-5 seconds). Once at peak rpm,

the device was slowed in time-step increments and torque readings were taken again. This procedure was done three times for each cylinder, the shaft and cylinder being removed and re-installed each time in order to gauge the precision of the device after re-installment of samples. The bottom disk of the sample holder was also tested in this manner. By subtracting the bottom disk torque from the total torque, the torque applied to the sample area only can be obtained. The meniscus must be located just below the upper disk (Fig. 2.1), so the fluid is acting on the cylinder and the bottom disk. It is sometimes necessary to add or remove water to obtain an appropriate meniscus.

A trendline was plotted for the variation of torque with rpm for the disk, and the corresponding relation (Eq. 3.1) was used to determine the torque provided by only the sample area of the cylinder, by subtracting the bottom disk torque (Fig. 3.4) from the overall torque. This adjusted torque value was converted into shear stress using Eqs. 3.2 and 3.3:

$$T = 0.0086\text{RPM} - 1 \tag{3.1}$$

$$F_T = \frac{T}{r} \tag{3.2}$$

$$\tau = \frac{gF_T}{A} \tag{3.3}$$

where T is the torque reading in kg-m (g-cm for Eq. 3.1), r is the cylinder radius in m, F_T is the applied tangential force in kg, τ is the shear stress in Pa, g is the acceleration due to gravity in m/s^2, and A is the cylinder surface area in m^2. The shear stress values were then plotted versus rpm to yield calibration curves for three cylinders (Figs. 3.1, 3.2, 3.3). The spread in data is attributed to slight, inevitable changes in the alignment of the cylinders with respect to the

central axis, due to the removal and re-installment of the shaft/cylinder assembly between runs. This procedure of removal/re-installment was carried out in order to identify the degree of precision of the device. Overall, the small and large cylinders followed a power fit, and the medium cylinder ,followed a linear trend (Figs. 3.1, 3.2, 3.3). Fitting a power function to the medium cylinder resulted in overestimation of shear stress at high rpm (>1,000).

For the large, medium, and small cylinder, respectively, the following relations were obtained:

$$\tau = 4.9 \times 10^{-6}\ RPM^{1.96} \tag{3.4}$$

$$\tau = 4.7 \times 10^{-3} RPM - 1.32 \tag{3.5}$$

$$\tau = 8.0 \times 10^{-8}\ RPM^{2.63} \tag{3.6}$$

As an illustration of the differences among the above relations, note that a 10% decrease in surface area from the small cylinder to the large cylinder leads to a 67% increase in shear stress at an rpm of 1,000 for the small cylinder. This results from the decreased moment arm of the small cylinder leading to an increased tangential force and therefore increased shear stress.

4. SERF Testing

Once the relation of shear stress to rpm was determined, clay samples could be tested for their erosion rate as a function of applied shear stress. Three ceramic clays were obtained from Bennett Pottery Supply (Orlando, FL), #10, #20, and #75. The company did not provide any information concerning the compositions of these clays. In any event, each clay was molded to

two different bulk densities (both lower than initial) by adding tap water and working by hand. This procedure was repeated twice, resulting in four densities tested for each clay. A third set was prepared by molding two equal amounts of clay with water, one with tap water and another with 35 ppt salt (sodium chloride) water. Water was added in equal amounts to yield a similar density. Since the clays arrived with existing pore water, the actual salinity of the pore water was less than 35 ppt.

The first set of clays was shaped into cylinders of the same diameter as the medium cylinder, hence the medium cylinder calibration curve was used. The second set of samples was shaped into the diameter of the large cylinder, as was the third set. The volume and surface area of each sample was known, and the mass of the sample was determined by weighing the sample with the bracket and lid (Figs. 2.1, 2.2b), and weighing only the bracket and lid. This provided the density of each respective sample.

Once a sample was prepared it was lowered into the outer cylinder, and the load cell was zeroed. After 5 to 15 minutes of rotation at a given rpm, the device was stopped and allowed to rest for approximately one minute. The time-step was chosen based on observation of the erodibility of a given sample during the previous time-step. In most cases the maximum speed was 1,500 rpm. Above this speed, the possibility of mass erosion (i.e., large clasts being eroded) was present, which could have resulted in an imbalance and excessive torque, thereby damaging the torque cell. After reaching steady-state, the load cell displayed the loss in material in grams.

The load cell displayed the loss of sediment as well as the internal pore fluid which was also released. Since the load cell is measured buoyant mass, only the mass loss of solids was being displayed. If the pore fluid were assumed to be of similar density as the eroding fluid, then

the load cell displayed the loss of dry sediment mass. This value, along with the time-step and the surface area resulted in the erosion rate:

$$\varepsilon = \frac{\Delta m_s}{A \Delta t} \tag{4.2}$$

where Δm_s is the dry sediment mass loss, A is the sample area in m^2, and Δt is the time interval in seconds.

5. SERF Results

Eighteen clay samples were tested in total, and erosion rate as a function of shear stress was obtained (Figs. 5.1 through 5.6) for all but three samples (#2, 9, and 15) whose erosion was undetected by the load cell. Linear (or piece-wise linear) trendlines were fitted to each set of results with the following form:

$$\varepsilon = \varepsilon_N (\tau_b - \tau_s) \tag{5.1}$$

where ε is the erosion rate in kg/m^2-s, τ_s is the sample shear strength in Pa, ε_N is the erosion rate constant in kg/N-s (=ε when $\tau_b = 2\tau_s$), and τ_b is the shear stress, also in Pa Table 5.1).

The composite plots (Figs. 5.1 through 5.6) for each clay show a general trend towards increasing shear strength with increasing density for all three clays. For the case of saline pore fluid versus fresh pore fluid, the saline samples tended to have greater erosion rates at the same shear stress than the fresh samples, thus implying a loss of soil strength due to the addition of sodium chloride. Unfortunately, because clay compositions were not available, an explanation for this effect of sodium chloride cannot be deduced. Some of the results show a two-line trend as opposed to a single-line trend. This Type 1/Type 2 erosion phenomenon (Mehta, 1981) possibly results from the non-uniformity of the sample, whereby the erosion rates are not constant between different density zones of the sample. The hand-molding of the clay samples

likely left a surface layer of non-uniform and possibly lower density than the interior of the sample in these cases.

Table 5.1. Density, erosion rate constant, and shear strength values obtained for 15 clay samples

Sample #, type	Density, ρ (kg/m^3)	ε_N (kg/m^2-s)	τ_s (Pa)
1, 10f	1665	5.00×10^{-5}	3.14
3, 10f	1710	1.91×10^{-5}	3.38
4, 10f	1859	1.23×10^{-5}	4.49
5, 10s	1928	1.73×10^{-5}	0.60
6, 10f	1928	1.20×10^{-5}	1.67
7, 20f	1435	3.93×10^{-5}	1.93
8, 20f	1537	1.19×10^{-5}	2.81
10, 20f	1721	7.72×10^{-5}	3.02
11, 20s	1894	1.73×10^{-5}, 7.00×10^{-5}	1.58
12, 20f	1905	7.10×10^{-6}	2.00
13, 75f	1675	4.80×10^{-5}	1.39
14, 75f	1698	3.217×10^{-5}	1.73
16, 75f	1806	1.14×10^{-5}	1.76
17, 75s	1940	3.20×10^{-5}, 6.89×10^{-5}	3.27
18, 75f	1963	9.85×10^{-6}	1.88

Note: s indicates saline pore fluid, f indicates tap water pore fluid

The erosion rate constant is plotted versus shear strength (Fig. 5.7) for one set of tests with clay #75, and the trend in this case follows the fit provided by Mehta and Parchure (2000). The equation contains two empirical coefficients and is represented as

$$\varepsilon_N = \varepsilon_{NO} \exp\left(-\chi_s \tau_s^{\lambda_s}\right) \tag{5.2}$$

where ε_{NO} is selected to be 0.2 kg/N-s based on the analysis of Mehta and Parchure, and $\chi_s = 7.45$ and $\lambda_s = 0.5$ are obtained as best-fit values.

The shear strength of each sample was plotted versus the dry density, and a fit of the following form (Mehta and Parchure, 2000) was applied to each clay type (#10, #20, #75):

$$\tau_s = \alpha(\rho_d - \rho_l)^{\beta} \tag{5.3}$$

where α and β are empirical coefficients, ρ_d is the dry density in kg/m^3, and ρ_l is 64 kg/m^3 (selected to represent the dry density of fluid mud with no shear strength). The dry density was calculated from the mass balance

$$\rho_d = \frac{\rho - \rho_f}{\rho_s - \rho_f}\rho_s \tag{5.4}$$

For the #10 and #20 clays, $\alpha = 3.20 \times 10^{-3}$, and $\beta = 1$, and for #75, $\alpha = 1.30 \times 10^{-3}$, and $\beta = 1$ were obtained (Fig. 5.8).

It should be pointed out that the selected group of samples did not erode enough to significantly decrease the sample radius, and only one cylinder calibration curve was used for each sample. For example, sample #6, with a bulk density (wet) of 1928 kg/m^3, lost a total of 3 g during the entire test. This corresponds to a reduction in thickness of 0.007 cm, or 0.18% thickness lost (based on large cylinder volume).

6. Concluding Comments

A comment is in order concerning the operating speed range of SERF, the generation of Taylor vortices in the annular gap between the outer cylinder and the sample, and the development of turbulence in this gap. When a certain Reynolds number has been exceeded in the gap between two rotating concentric cylinders, vortices appear in the flow. The axes of these vortices are along the circumferences of the cylinders, and they rotate in alternately opposite

directions (Schlichting, 1968). The Taylor number is used to predict the formation of these irregularities, and is defined as

$$T_a = \frac{Ud}{\nu}\sqrt{\frac{d}{R}} \tag{6.1}$$

where U is the peripheral velocity of the cylinder, d is the gap width, R is the inner cylinder's radius, and ν is the kinematic viscosity of the fluid. Taylor vortices are formed in the range $41.3<T_a<400$, within a laminar flow regime (Schlichting, 1968). Even at the lowest operating speed of SERF, which corresponds to a peripheral velocity of 0.8 m/s (at 150 rpm), using a gap width of 0.024 m, an inner cylinder radius of 0.038 m, and water as the fluid ($\nu=10^{-6}$ m^2/s), the Taylor number is 15,000, well over the range of Taylor vortex formation.

With the characteristic Reynolds number defined as

$$Re = \frac{Ud}{\nu} \tag{6.2}$$

using a peripheral velocity of 0.8 m/s and the same fluid and gap width, Re=18,880 is obtained. The SERF is typically operated above this speed, and in these tests the lowest Re attained was 100,000 at a speed of 4.3 m/s (at 800 rpm). Operating above the Taylor vortex regime and above the laminar flow regime, one can expect a comparatively uniform distribution of shear stress over the sample surface area.

The SERF is capable of producing coherent results on the rate of sample erosion as a function of applied shear stress, even with small amounts of erosion (tenths of a gram). It should be feasible to use the apparatus to test a variety of cohesive samples, both intact from the field and remolded. The inclusion of a load cell directly attached to the apparatus considerably reduces the time necessary to obtain results, and ensures accuracy by not requiring periodic

removal and weighing of the sample assembly. The device is operated at sufficiently high Reynolds numbers (>100,000 at 800 rpm) to ensure a comparatively uniform shear stress distribution.

With regard to the clay samples tested the following conclusions can be drawn:

1. Linear and piece-wise linear erosion rate functions were observed for three types of commercial clays,
2. The clays displayed a general trend toward increasing shear strength with density,
3. The use of saline pore fluid resulted in a greater erosion rate constant than samples prepared with tap water.

A user's manual for SERF is included as Appendix.

7. References

Arulanandan, K., Loganathan, P., and Krone, R.B., 1975. Pore and eroding fluid influences on surface erosion of soil. *Journal of Geotechnical Engineering Division*, ASCE 101(1), 51-66.

Chapuis, R.P., and Gatien, T., 1986. An improved rotating cylinder technique for quantitative measurement of the scour resistance of clays. *Canadian Geotechnical Journal*, 23(1), 83-87.

Croad, R.N., 1981. Physics of erosion of cohesive soils. Ph.D. Thesis, University of Auckland, New Zealand.

Lee, S.C. and Mehta, A.J., 1994. Cohesive sediment erosion. *Report DRP-9406*, U.S. Army Engineer Waterways Experiment Station, Vicksburg, MS, 12-15.

Mehta, A.J., 1981. A review of erosion functions for cohesive sediment beds. *Proceedings of the First Indian Conference on Ocean Engineering*, Vol. 1, Madras, 122-130.

Mehta, A.J. and Parchure, T.M., 2000. Surface erosion of fine-grained sediment revisited. *Muddy Coast Dynamics and Resource Management*, B. W. Flemming, M.T. Delafontaine, and G. Liebezeit, eds., Elsevier, Oxford, UK (in press).

Moore, W.L., and Masch, F.D., Jr., 1962. Experiments on the scour resistance of cohesive sediments. *Journal of Geophysical Research*, 67(4), 1437-1449.

Schlichting, H. , 1968. *Boundary-Layer Theory*, 6th edition, McGraw-Hill, New York, 500-503.

APPENDIX—USER'S MANUAL FOR SERF

A.1 SERF Calibration

The SERF requires three calibrations: torque cell calibration, load cell calibration and shear stress calibration.

A.1.1 *Torque Cell Calibration*

Remove the torque cell by unscrewing the single hex screw which connects the torque cell to the load cell (Fig. 2.1). Use caution in handling the torque cell, which can be damaged if over-torqued. Secure the torque cell base to a horizontal surface with a vise, keeping the shaft of the torque cell aligned in the horizontal direction. Place the 1 cm radius ridged collar (provided with the apparatus) around the shaft, and tighten the collar hex nut so it secures to the shaft without rotating. Secure a loop of string to the collar; tighten it to prevent rotation. Follow the Omega-provided calibration instructions for the light-emitting diode (LED) display (Omega DP25-S), applying zero load for the 0% point, and a 1 kg mass for the 100% load. The readout will now display torque in g-cm in the range of 0-1000 g-cm. To ensure proper calibration, secure an intermediate mass to the string, and the display should show the corresponding torque (500 g load should result in a 500 g-cm torque). Remove the load, string and collar, and set the torque cell aside.

A.1.2 *Load Cell Calibration*

Remove the load cell by unscrewing the two vertical hex screws at the rear of the cell. Secure the load cell horizontally with a vise. Loop a string through the hole at the end of the cell. Securing the load to the end of the string, follow the provided calibration instructions for the LED display, applying zero load for the 0% point, and 1 kg for the

100% point. Since SERF is only concerned with small mass changes, the load cell does not have to be calibrated above 1 kg. If smaller changes in mass are anticipated, the cell can be calibrated to 500 g or less, and the decimal point can be moved for higher resolution,(0.1 gram finest resolution). Decimal point movement is explained in the LED display manual. Replace the load cell with the two hex screws, and replace the torque cell, tightening slowly.

A.1.3 *Shear Stress Calibration*

Attach the chosen aluminum cylinder to the shaft, securing it between the upper and lower disks/brackets (Fig. 2.1). The lower bracket should be flush with the shaft, and the upper bracket should tighten onto the cylinder. Screw one of the two hex nuts onto the upper portion of the shaft, so it tightens against the top of the upper bracket. Tighten with an adjustable monkey wrench. Screw the other nut onto the shaft, approximately two cm above the lower nut. Place the plastic lid (Fig. 2.2b) onto the assembly, and screw the shaft into the torque cell, twisting counter-clockwise slowly, until the shaft rests at the internal roof of the torque cell (The shaft will halt at the roof). Screw the upper nut counter-clockwise so it locks against the torque cell. DO NOT OVERTIGHTEN! The nut should be tightened until it just stops turning, no further. For maximum care, twist the torque cell by hand in the opposite (clockwise) direction to minimize the torque being applied to the cell. By keeping the LED display on, one can observe how close the cell is to being over-torqued.

Fill the outer cylinder to approximately 1/3 of it's volume with the chosen eroding fluid (e.g., fresh water). Lower the cylinder/bracket assembly into the outer cylinder by loosening the four rear-facing adjustment arms. The assembly should be brought to rest

on the square collar on the back of the post. Tighten the adjustment arms. Fill with more water until the upper bracket is just submerged.

Slowly spin the outer cylinder counter-clockwise (forward setting) at less than 400 rpm and observe the meniscus. A level meniscus is desired. Four horizontal screws (Fig. 2.2b) can be loosened to move the assembly left and right, and four vertical screws (Fig. 2.2b) can be loosened to move the assembly forward and back. Small alignment changes tend to affect the meniscus considerably. After the assembly is centered, the height of the meniscus should be adjusted so at a given rpm the meniscus is just below the upper bracket while spinning. It is ideal to start with a lower level at low rpm, and to add water as the rpm increases and the meniscus lowers.

Begin taking readings after setting the torque cell at zero rpm. Increase the speed in time-step increments, allowing the torque cell to reach steady-state before recording the torque value. Once at desired peak rpm (2,350 rpm is attainable, below 1,600 rpm is prudent), reduce the speed in increments and record torque values. Once this procedure is completed raise the assembly, loosen the shaft upper nut (clockwise), and unscrew the shaft from the torque cell (clockwise). Reattach the shaft and repeat the above procedure. Three runs in this manner are sufficient to obtain the mean trend.

To obtain the calibration for the bottom disk, remove all of the water, and repeat the above procedure, keeping only the bottom disk submerged at every rpm step. After obtaining a torque versus rpm trendline, at each selected rpm subtract the bottom disk torque from the cylinder torque. The residual torque is thus adjusted for the added stress effect of the bottom disk.

By dividing the adjusted torque readings by the radius of the cylinder, the corresponding tangential force (in kg—multiply by g for N) is obtained. Dividing this quantity by the surface area (m^2) yields the shear stress in Pa. For each cylinder tested, plot shear stress versus rpm and obtain the required calibration curves by drawing a mean trendline through the data points.

A.2. Sample Preparation

Whether using an intact field sample or a remolded sample, the sediment must be in the shape of one of the three cylinder sizes so the obtained calibration curves can be applied. In addition, the volume of the sample must be known so it's density can be measured.

Attach the selected aluminum cylinder to the bracket assembly as described in Section A.1.3, and then remove the bottom disk and the aluminum cylinder. This is necessary to place the upper bracket at the correct elevation. Impale the sample on the shaft. Screw the lower bracket to the end of the shaft, until the shaft is flush with the bottom of the disk. Plastic sheeting, cut to the height and circumference of the cylinders, is provided with the apparatus to wrap the sample and ensure the sample has the correct volume. Trim with a putty knife any extra mass before weighing. Place the plastic lid on the assembly over the top of the shaft. Weigh the entire assembly. The bracket/lid combination can be weighed later to provide the weight of only the sample. This weight divided by the volume gives the (wet) bulk density of the prepared sample.

In the same manner mentioned in Section A.1.3, secure the assembly to the torque cell.

A.3. Sample Testing

Fill the outer cylinder about 1/3 with the chosen eroding fluid. Lower the assembly into the outer cylinder to the collar level. Add water under the lid until the upper bracket is just flush with the water level. In this case the exact water level is not very important as long as the sample is fully submerged. The shear stress on the sample will be independent of the water level, as long as the entire sample is being acted on by the fluid.

Secure the black torque cell wire to the rear post using a strip of tape, so the load cell is not affected by it's movement. Zero the load cell. Wait until fluctuations are no more than 0.1 g before starting rotation.

Rotate the outer cylinder at a given rpm for a given time-step. At the end of the time-step, stop the device. The load cell usually takes one minute to reach a steady-state, and then it reads the mass lost during that time interval. Using Eqs. 4.1 and 4.2, the erosion rate can be determined. The rpm value can be converted to a shear stress via the calibration curves.

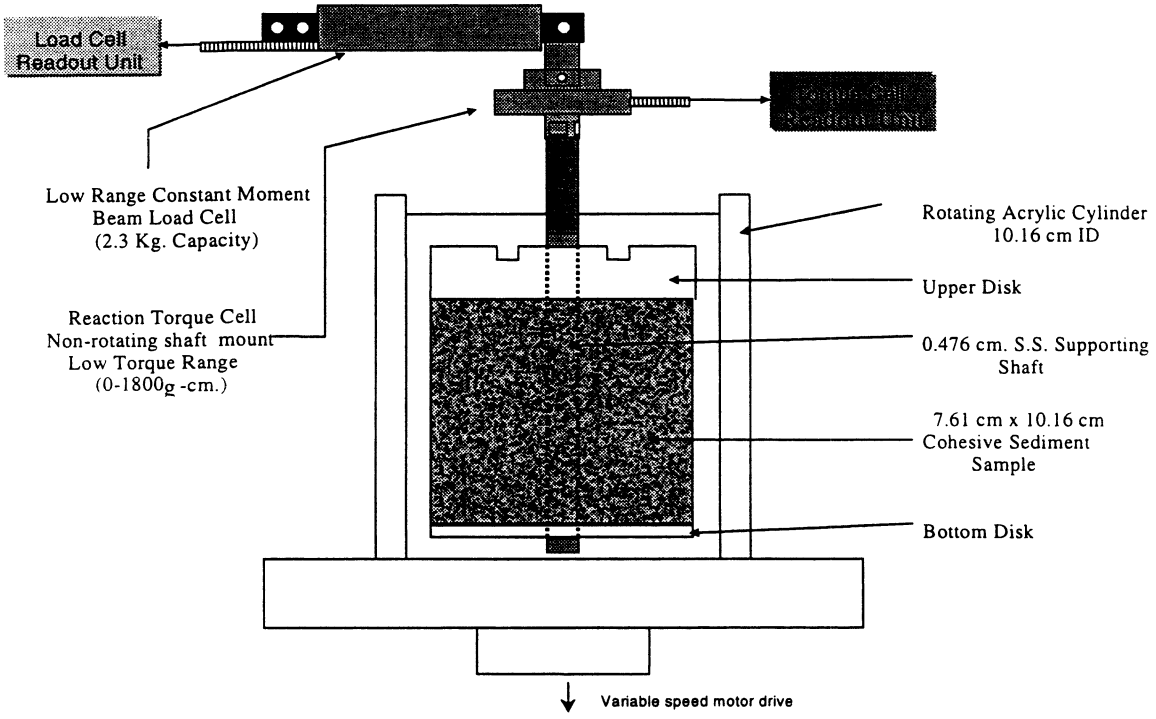

Figure 2.1. Schematic of SERF

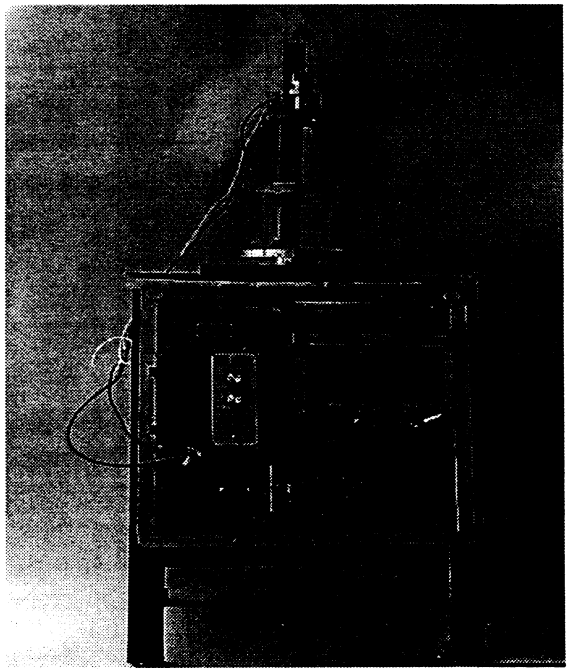

Figure 2.2a. Front-view of SERF showing the rotating cylinder assembly, speed control panel (lower left) and digital readouts (lower right) for the torque cell and the load cell

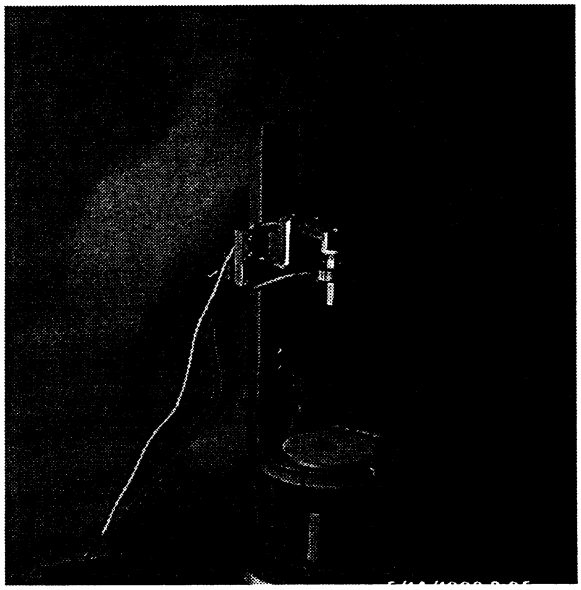

Figure 2.2b Photograph of acrylic outer cylinder and measurement cells supported by a vertical member

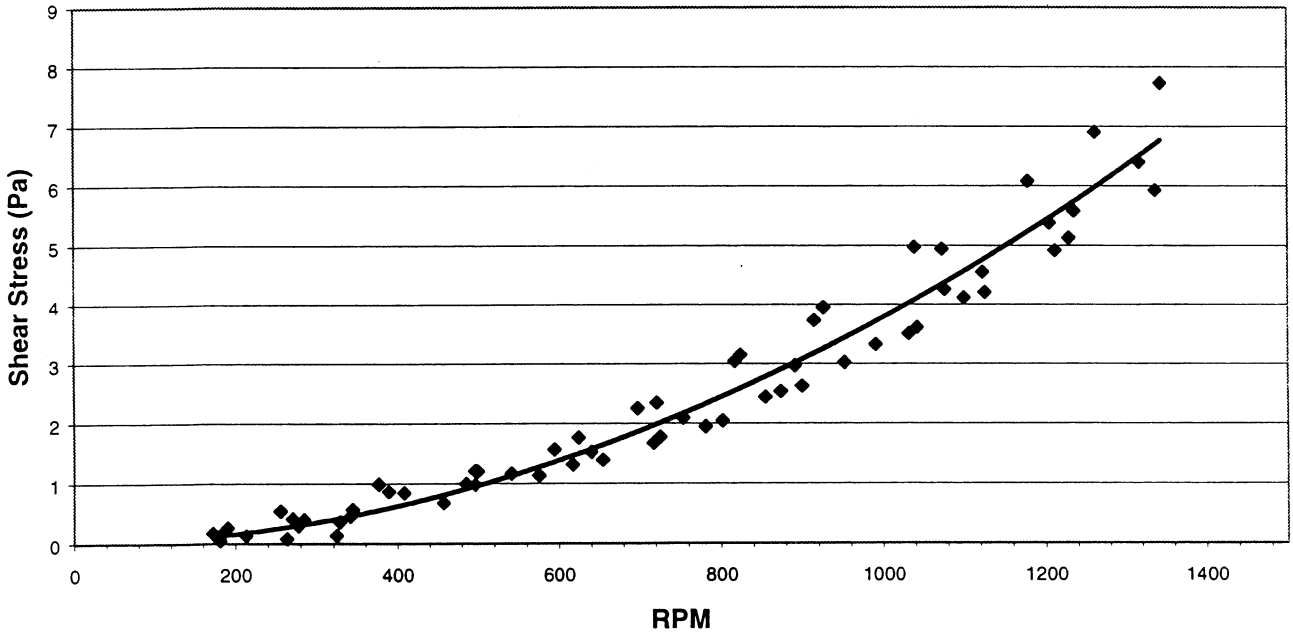

Figure 3.1. Calibration curve for large aluminum cylinder (dia.=7.6 cm)

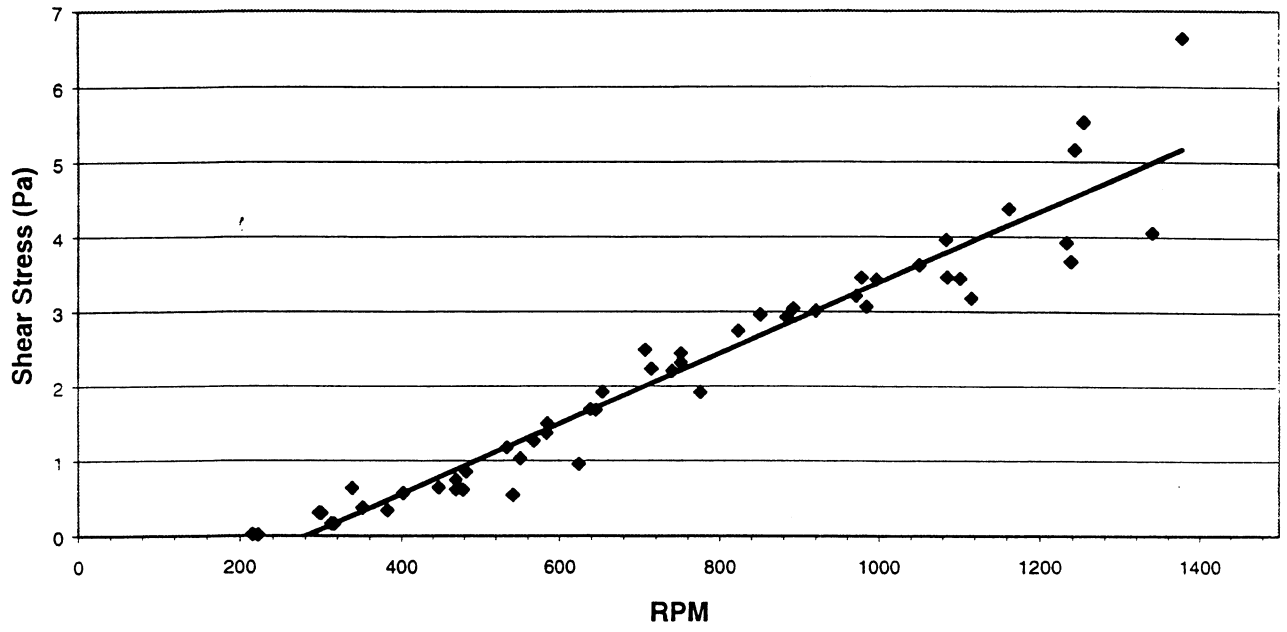

Figure 3.2. Calibration curve for medium aluminum cylinder (dia.=7.2 cm)

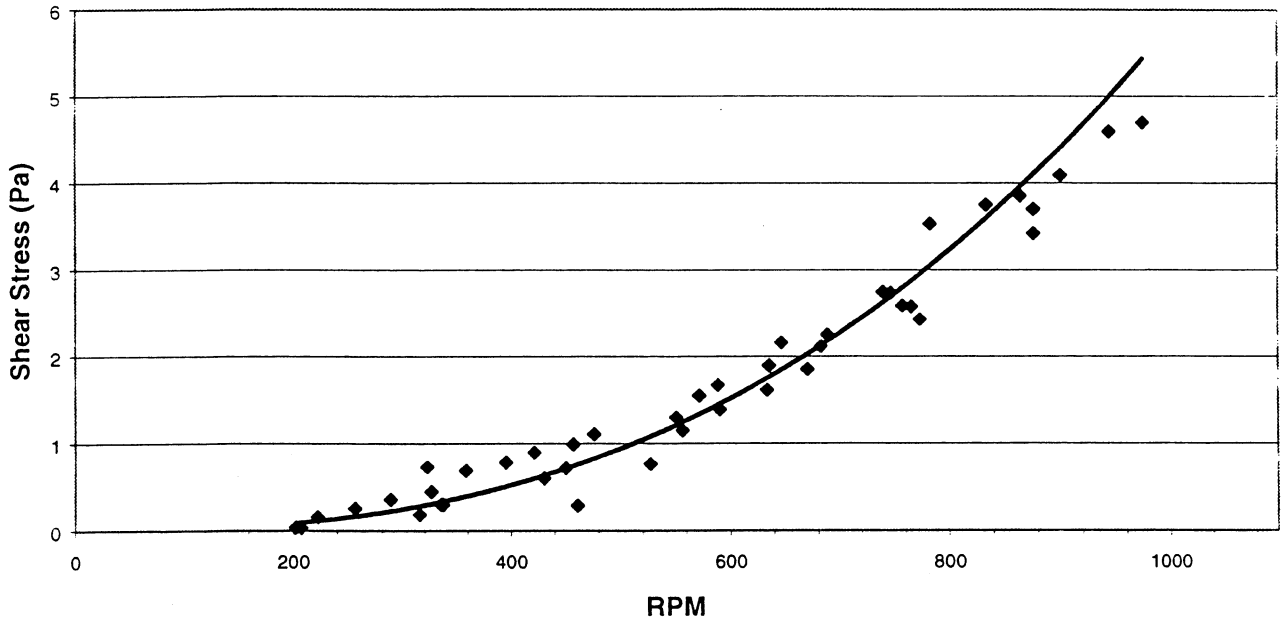

Figure 3.3. Calibration curve for small aluminum cylinder (dia.=6.8 cm)

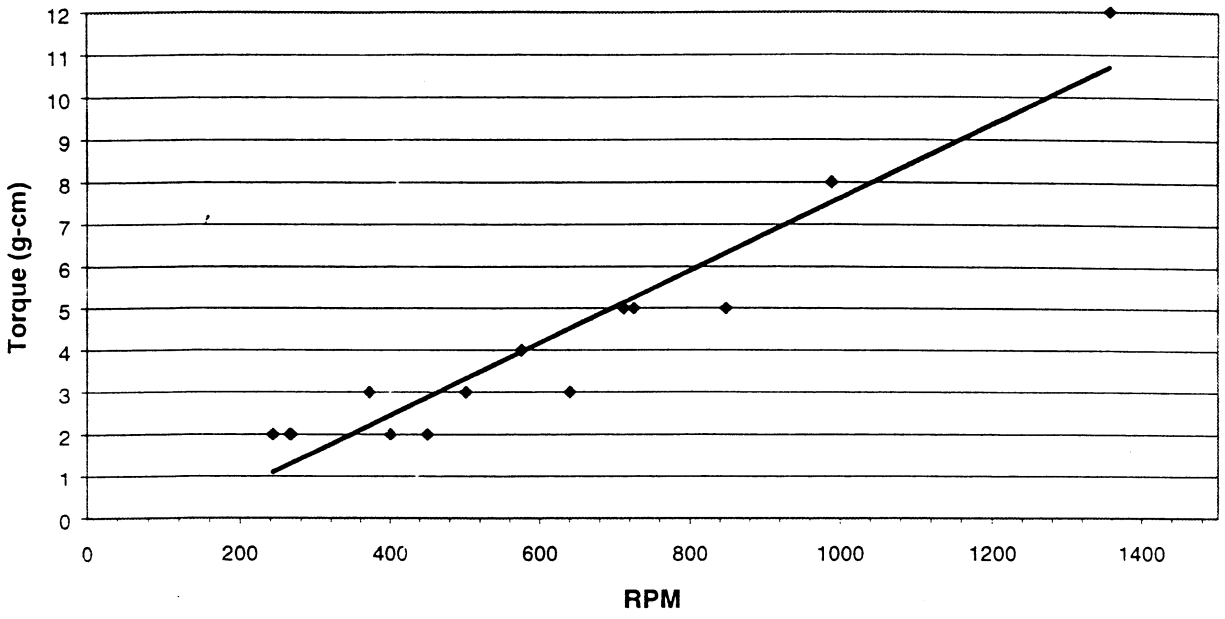

Figure 3.4. Calibration curve for bottom disk

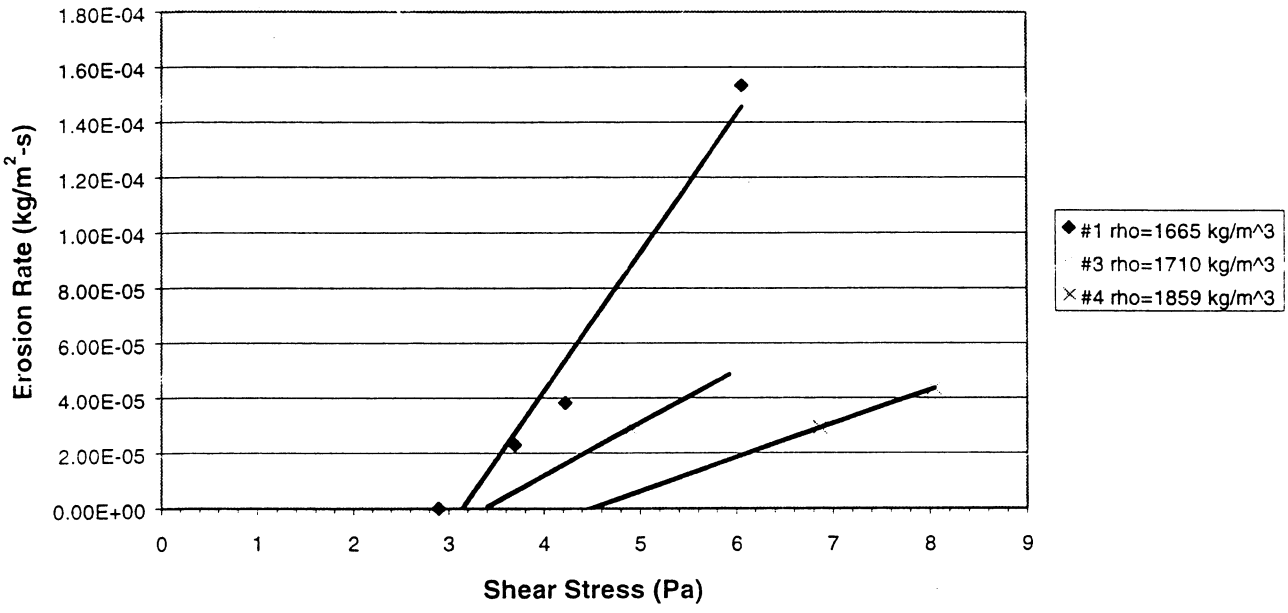

Figure 5.1. Erosion rate as a function of shear stress for clay type #10

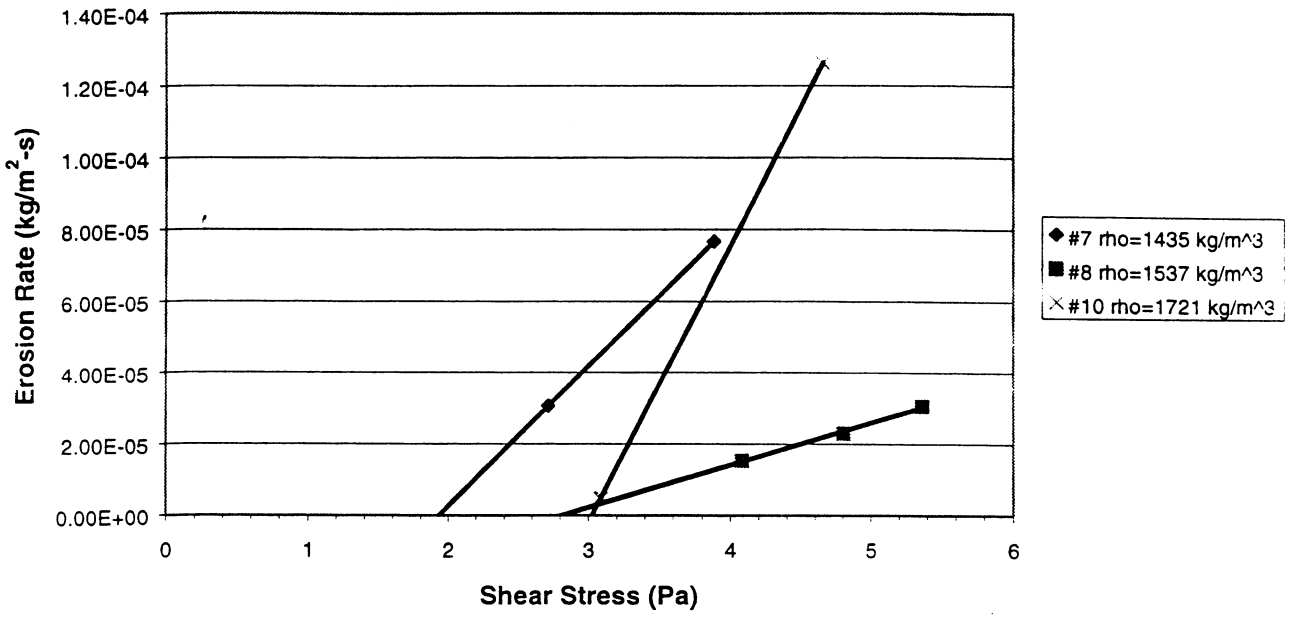

Figure 5.2. Erosion rate as a function of shear stress for clay type #20

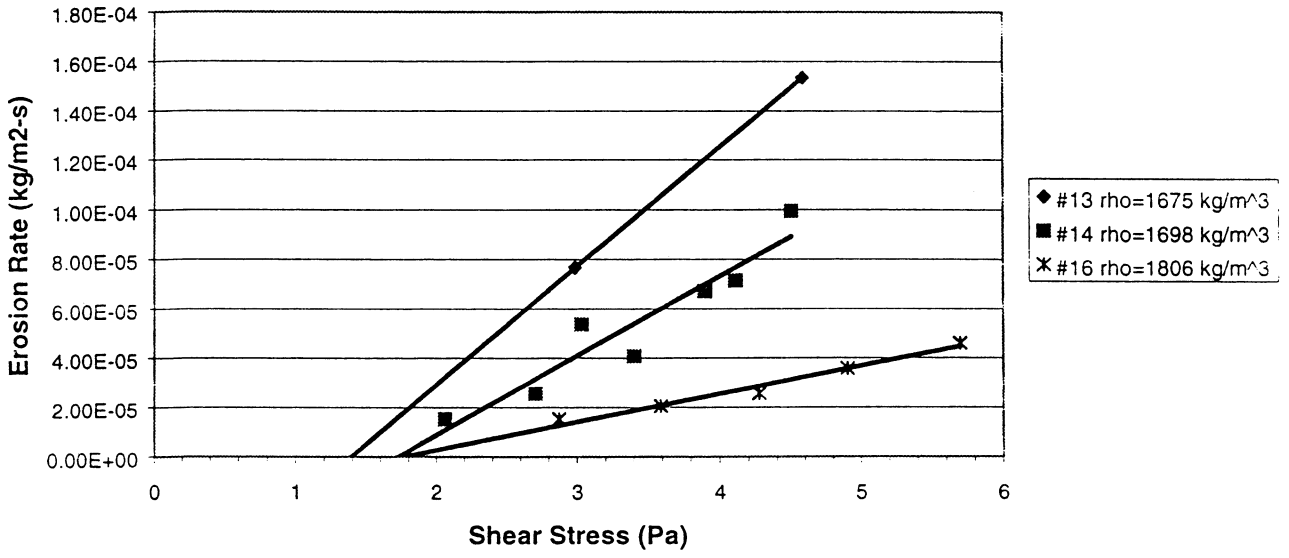

Figure 5.3. Erosion rate as a function of shear stress for clay type #75

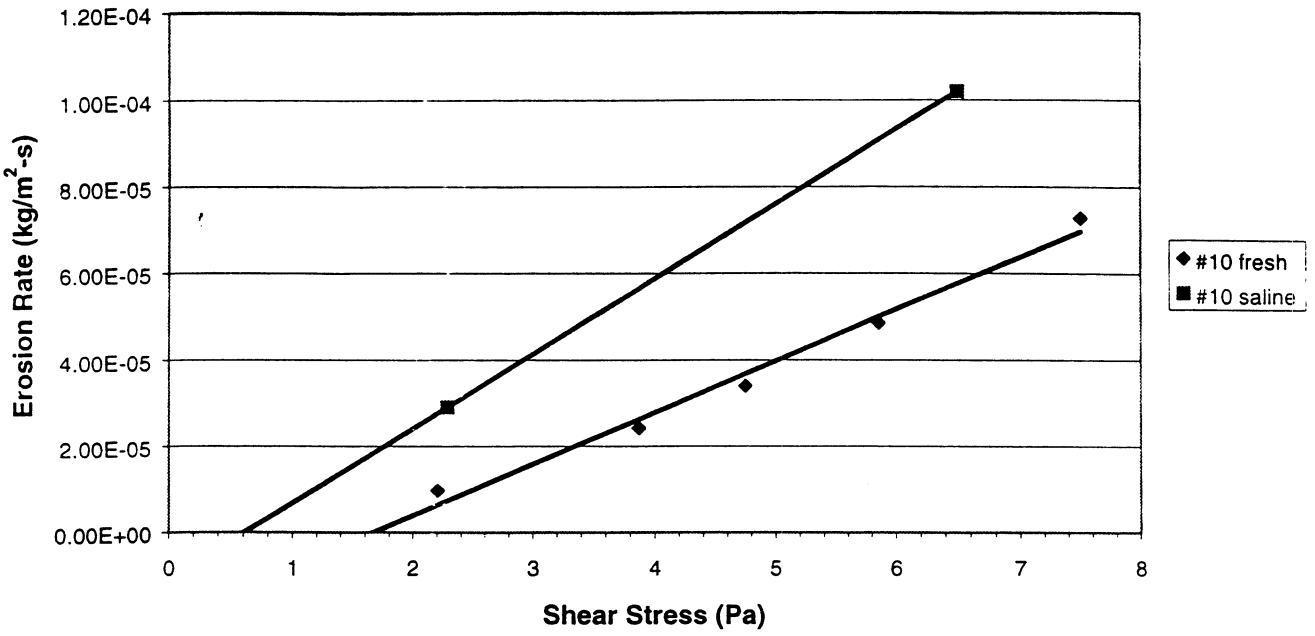

Figure 5.4. Erosion rate as a function of shear stress for clay type #10, with differing pore fluid (tap water vs. saline)

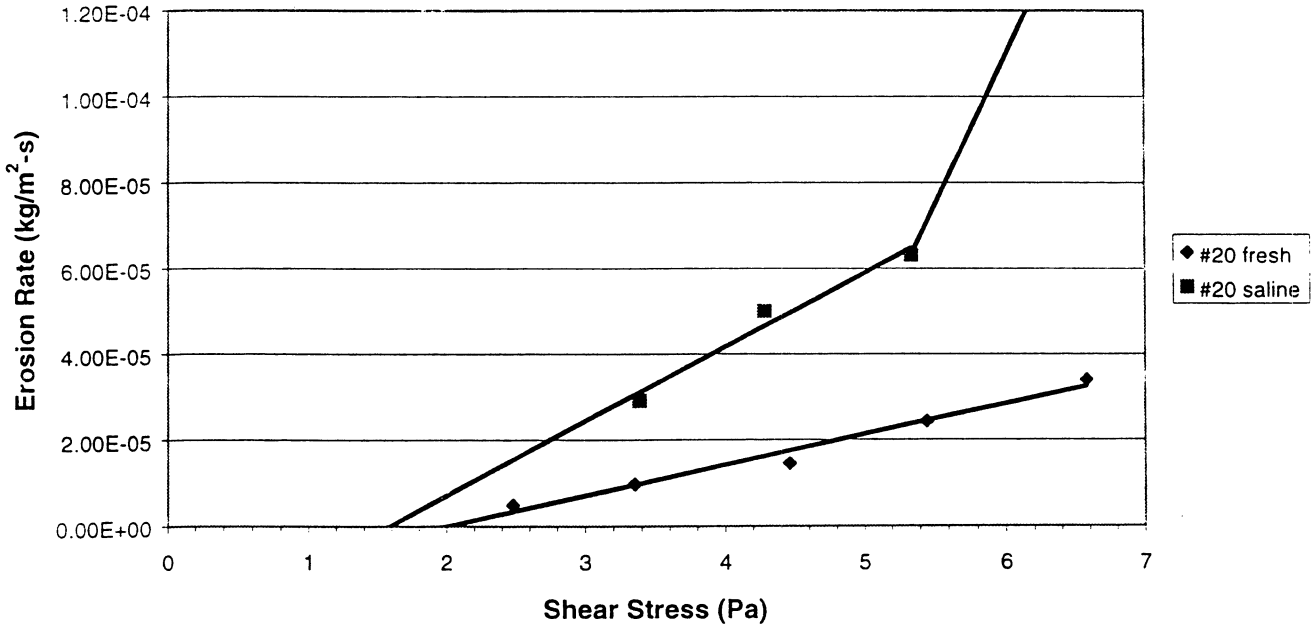

Figure 5.5. Erosion rate as a function of shear stress for clay type #20, with differing pore fluid (tap water vs. saline)

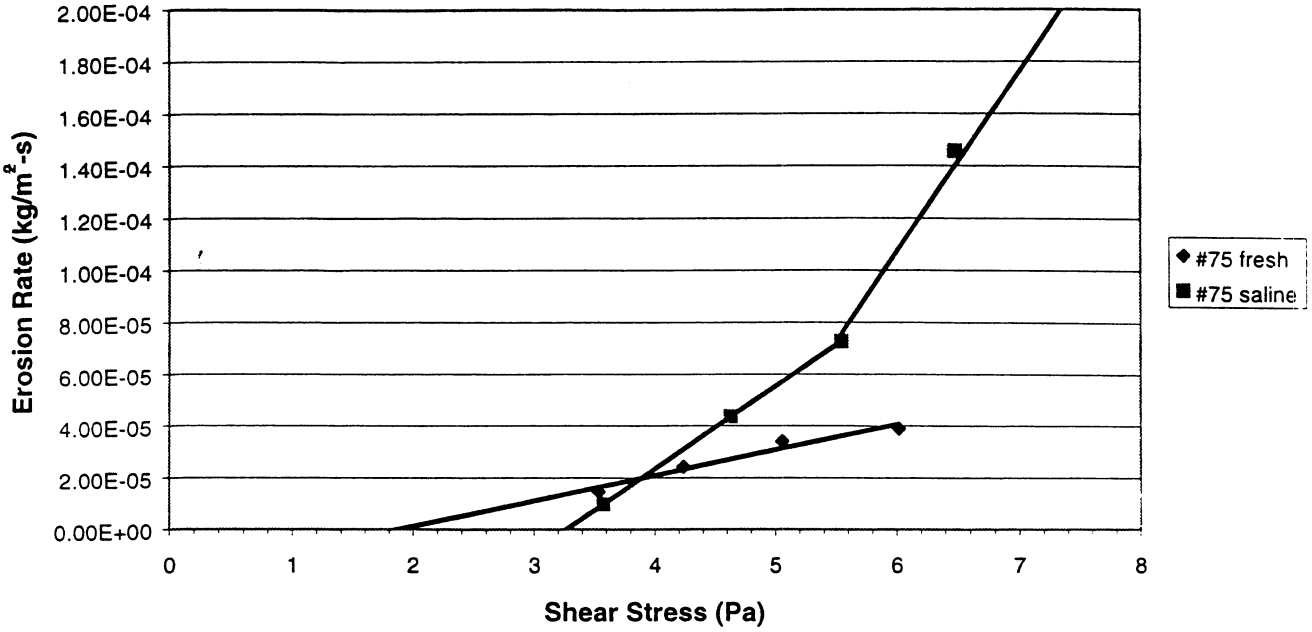

Figure 5.6. Erosion rate as a function of shear stress for clay type #75, with differing pore fluid (tap water vs. saline)

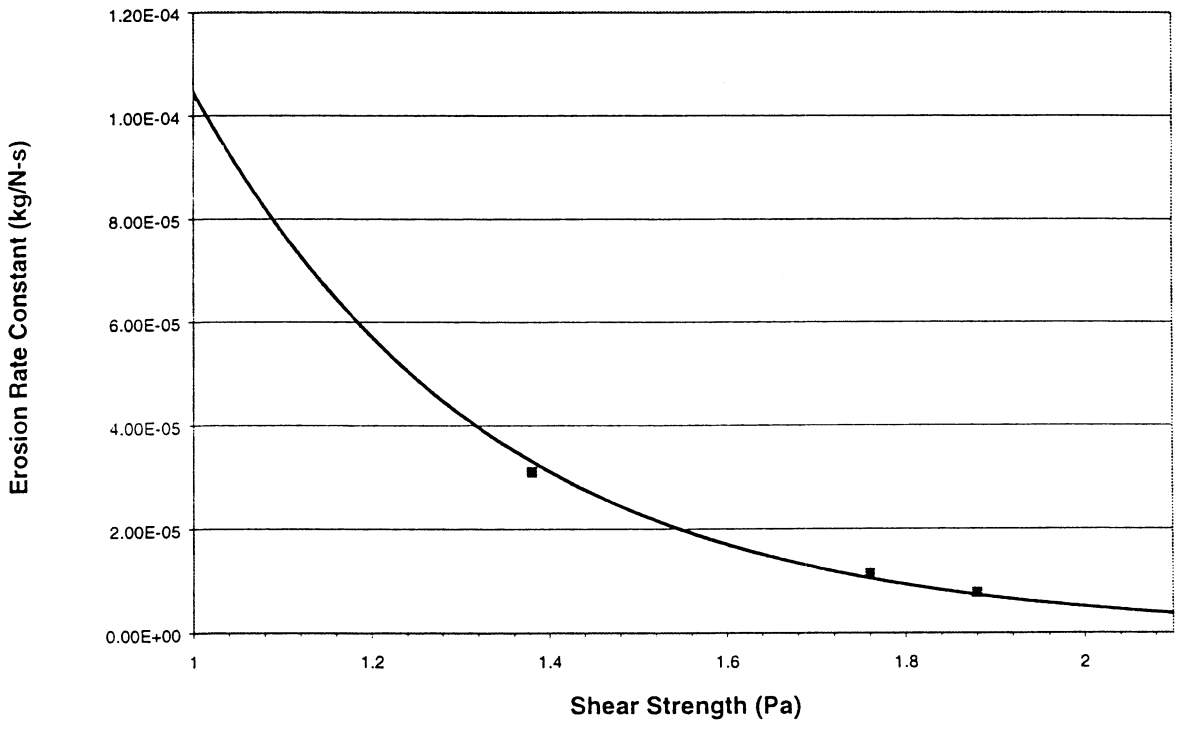

Figure 5.7. Erosion rate constant as a function of shear strength for clay type #75

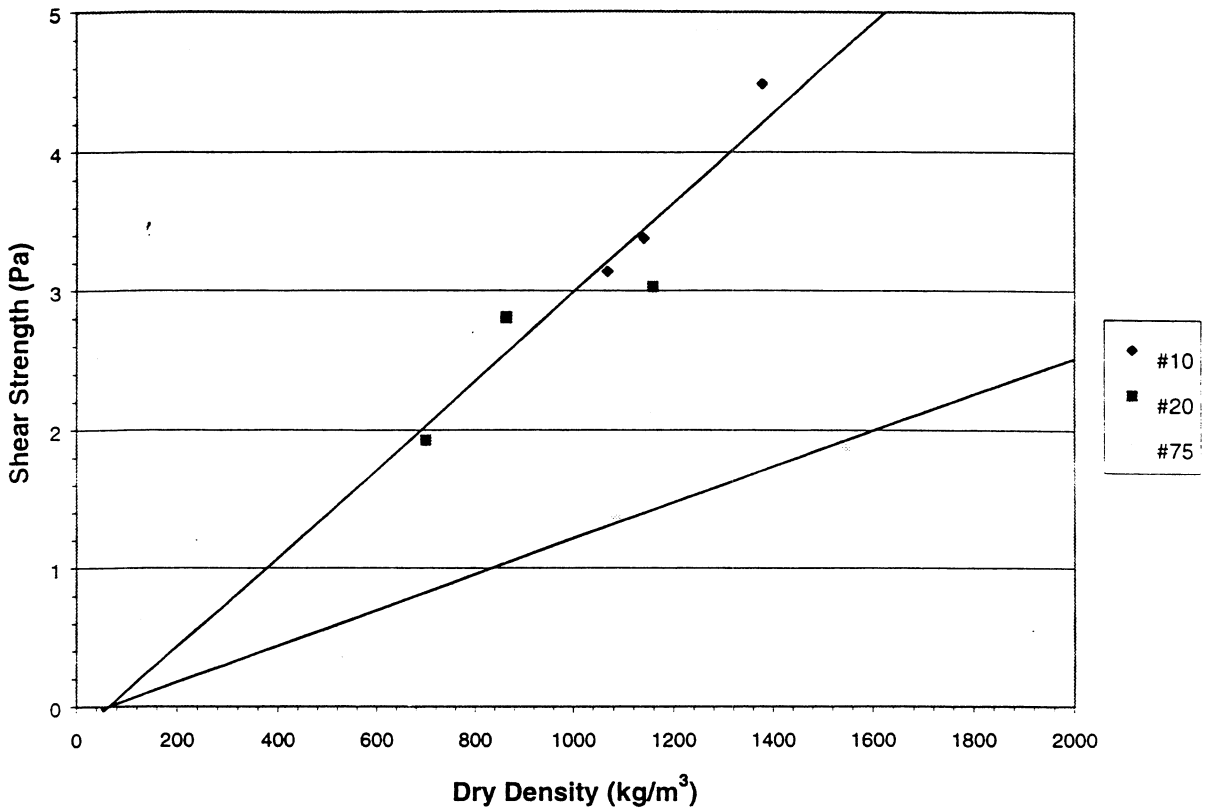

Figure 5.8. Shear strength as a function of dry density for three clays